

**UNIVERSITÀ
DEGLI STUDI
DI PADOVA**

Sede Amministrativa: Università degli Studi di Padova

Dipartimento di Ingegneria Industriale - DII

SCUOLA DI DOTTORATO DI RICERCA IN INGEGNERIA INDUSTRIALE
INDIRIZZO INGEGNERIA DELLA PRODUZIONE INDUSTRIALE
CICLO XXV

**GEOMETRICAL METROLOGY AT MICRO SCALE: NEW APPROACH
AND APPLICATION TO MICROFLUIDIC DEVICES**

Direttore della Scuola: Ch.mo Prof. Paolo Colombo

Coordinatore d'indirizzo: Ch.mo Prof. Enrico Savio

Supervisore: Ch.mo Prof. Paolo Bariani

Dottorando: Manuel Balcon

Gennaio 2013

Preface

This thesis has been prepared as one of the requirements of the Ph.D. degree. The work has been carried out from January 2010 to December 2012 at DIMEG – Dipartimento di Innovazione Meccanica e Gestionale now part of DII – Dipartimento di Ingegneria Industriale, University of Padova, Italy, under the supervision of Prof. Paolo Bariani and Prof. Enrico Savio.

From September 2011 to December 2011, about three months were spent at CPT – Centre for Precision Technology, University of Huddersfield, UK.

First of all I would like to thank my supervisors Prof. Paolo Bariani and Prof. Enrico Savio together with Dr. Simone Carmignato and Dr. Francesco Marinello for their inspiration and for their precise and accurate contribute to my work. Moreover, I would like to express my gratitude to Prof. Liam Blunt and his colleagues at CPT (Huddersfield, UK) for their collaboration. I would like also to thank Prof. Nicola Senin, from the University of Perugia (Italy), for the time spent working together in Huddersfield.

Finally I am really grateful to my Ph.D. colleagues and in particular to Dr. Anna Pierobon and Ing. Gianluca Tristo for their support and friendship.

Padova, January 2013

Manuel Balcon

Abstract

About 30 years ago, in the industry for the production of semiconductors, started the race for the reduction of the dimensions of several electronic components. The trend followed the well-known Moore's law and the dimensions of the chips halved every 18 months. The effect of reduction of the dimensions of products and components involved other scientific and technological fields. Products with micrometric dimensions, i.e. with one fundamental dimension in the range of micrometres, are presents in different domains including mechanics, biology, physics and medicine. The micro engineering concerns with the design, the realization and the industrialization of these products with micrometric dimensions. A fundamental phase of micro engineering is product/process quality control and related measurements. The metrology at micro scale is part of the manufacturing chain of micro products during the design, with the definition of the specifications, during the manufacturing, for the control of the process and in the final phase for the verification of specifications. The measurement of the dimensions and geometries at micrometric level is nowadays in evolution: several aspects, including the development of instruments and measurement techniques, need more studies.

The thesis here presented wants to contribute increasing the knowledge in the field of micro metrology and to provide useful solutions to improve the dimensional and geometrical characterization of micro products.

Although, the research has been developed to be valid in general, it is included as an integral part of the European project "CellDiaSp". The project, in collaboration with international partners, provides for the realization of a microfluidic platform for cells analysis.

The metrological activities, required by the project, are needed to characterize the dimensions and the geometry of prototypes, mould inserts, masters and finite products, in order to guarantee the respect of the specifications and the functionality of the final product.

The first phase of the research deals with the study of the state of the art of metrology and of the relevant measurement techniques that can be used at micro scale.

Successively the application of some of these techniques to the replication processes has been studied. These processes, such as micro injection moulding, are used to obtain mass production and a cost reduction. It has been considered the possibility to measure the components presents in the process of replication, that is the inserts and the replicated parts

and to evaluate the quality of the replication process through the calculation of single parameters such as parameters used in the measurement of surfaces. It resulted that this is possible only in few specific cases and that it is preferable to perform a complete three dimensional characterization of the dimensions and geometries of the product of replication.

It has been decided to focus the attention on two typologies of instruments: the scanning probe microscopes and the optical profilometers. These instruments are adapted to the measurement of the parts to be investigated within the project and, moreover, they are the best candidates to be implemented as coordinate measuring instruments, even if they were originally developed as surface measurement instruments.

The problem of “drift”, an effect that reduces the accuracy of the measurements performed through atomic force microscopes, has been treated. The causes of the phenomenon have been identified and solutions to the reduction of this error have been provided.

In order to obtain coordinate measurements from the atomic force microscopes and from the optical profilometer, a new technique for the data analysis has been developed.

The new methodology is presented applied to a case study of a microfluidic channel measured through optical profilometry. The technique is inspired by the international standards in the field of geometrical product specification and verification, with particular reference to coordinate metrology. However, these standards can't be directly applied to product with micrometric dimensions and they require new solutions for the analysis of the data. A dedicated software has been developed to treat the data, acquired through a confocal microscope, both as image and as point cloud, taking advantage of both approaches and related representation. Specific procedures of filtration and thresholding have been developed to perform the extraction of the points and the association of the geometrical features for the evaluation of dimensions and geometries of the sample. The developed software provides a semi-automatic and repeatable way for the coordinate measurement of micrometric components.

Finally, the developed technique has been validated using a case study: the measurements of microfluidic channels with cylindrical section used in the realization of peristaltic pumps.

Sommario

Circa 30 anni fa, nell'industria per la produzione di semiconduttori, iniziò la corsa alla riduzione delle dimensioni di vari componenti elettronici. L'andamento seguì la famosa legge di Moore ed è stato possibile assistere, ogni 18 mesi circa, ad un dimezzamento delle dimensioni dei chip. L'effetto di riduzione della dimensione di prodotti e componenti ha coinvolto, sebbene in modo meno evidente, anche altri campi scientifici e tecnologici. Prodotti di dimensioni micrometriche, cioè in cui una dimensione fondamentale del prodotto è mille volte inferiore rispetto ad un millimetro, sono presenti nella meccanica, nella biologia, nella fisica e in ambito medico. La microingegneria si occupa della progettazione, realizzazione e industrializzazione di questi prodotti di dimensioni micrometriche. Una fase fondamentale della microingegneria è il controllo di qualità. La metrologia in ambito micrometrico entra nella catena produttiva dei microprodotti durante la progettazione, con la definizione delle specifiche, durante la produzione, per il controllo del processo, e nella fase finale, per la verifica del rispetto delle specifiche.

La misura delle dimensioni e delle geometrie a livello micrometrico è tuttora in evoluzione: numerosi aspetti, tra cui lo sviluppo di strumenti e tecniche di misura adeguate, necessitano di approfondimento.

Il lavoro di tesi di seguito presentato vuole contribuire all'aumento delle conoscenze in ambito metrologico micrometrico e vuole fornire soluzioni utili a migliorare la caratterizzazione dimensionale e geometrica dei prodotti.

Sebbene la ricerca sia stata sviluppata per essere valida a livello generale, essa rientra nell'ambito del progetto europeo "CellDiaSp". Il progetto prevede, in collaborazione con partner internazionali, la realizzazione di una piattaforma microfluidica per l'analisi cellulare. Le attività metrologiche richieste dal progetto servono per caratterizzare le dimensioni e la geometria dei prototipi, degli inserti di stampi e dei prodotti finiti, garantendo il rispetto delle specifiche e quindi la funzionalità del prodotto finito.

La prima fase della ricerca ha riguardato lo studio dello stato dell'arte della metrologia e delle principali tecniche di misura applicabili a livello micrometrico, delle loro caratteristiche e dei loro limiti.

Successivamente è stata studiata l'applicazione di alcune di queste tecniche ai processi di replicazione. Tali processi, come ad esempio il microstampaggio ad iniezione, sono necessari

per ottenere una produzione di massa dei prodotti e ridurre quindi il costo. È stata considerata la possibilità di misurare le varie parti presenti nel processo di replicazione, ovvero gli inserti degli stampi e i prodotti replicati, e di valutare la qualità del processo tramite singoli parametri, come ad esempio parametri di misura della superficie. Dallo studio è emerso che questo è possibile solo in alcuni casi specifici e che è preferibile avere una caratterizzazione tridimensionale completa delle varie dimensioni e geometrie del prodotto replicato.

Si è quindi deciso di concentrare l'attenzione su due tipologie di strumenti: i microscopi a scansione di sonda e i profilometri ottici. Questi strumenti sono adatti alla misura dei componenti previsti dal progetto e sono inoltre i candidati migliori per essere sviluppati nell'ambito della misura a coordinate, sebbene nascano per la misura delle superfici.

È stato trattato il problema della “deriva”, un effetto che riduce l'accuratezza delle misure effettuate con microscopi a forza atomica. Sono state indagate le cause di questo fenomeno in diverse configurazioni commerciali di strumenti e sono state fornite le soluzioni per la riduzione di questo errore.

Al fine di ottenere misure a coordinate dai microscopi a forza atomica e dai profilometri ottici, è stata sviluppata una nuova tecnica di analisi dei dati di misura. La nuova metodologia viene presentata applicata al caso studio di un canale microfluidico misurato con profilometria ottica.

La tecnica prende ispirazione da quanto previsto dalle norme internazionali in ambito di metrologia a coordinate. Tali norme, tuttavia, non possono essere direttamente applicate a prodotti di dimensioni micrometriche e richiedono accorgimenti nel trattamento dei dati. È stato quindi creato un codice di calcolo, che sfruttando la natura dei dati di misura ottenuti, ad esempio da un microscopio confocale, li tratta sia come immagine sia come nuvola di punti. Sono state sviluppate procedure specifiche di filtraggio e soglia, al fine di effettuare l'estrazione dei punti e l'associazione con elementi geometrici per la valutazione delle dimensioni e della geometria del campione in oggetto. Il codice di calcolo realizzato fornisce un modo semi automatico e ripetibile per la misura di componenti micrometrici.

Infine, la tecnica sviluppata è stata utilizzata per la misura delle dimensioni di canali microfluidici a sezione cilindrica utilizzati nella realizzazione di pompe peristaltiche.

Table of contents

Preface	1
Abstract	3
Sommario	5
Table of contents	7
Chapter 1 Introduction	11
1.1 Micro engineering.....	11
1.1.1 Micro manufacturing technologies	12
1.1.2 Measurements requirements and challenges at micro scale	15
1.2 Objective of the work	17
1.3 Work structure	18
Chapter 2 Quality control at micro scale: state of the art	21
2.1 Introduction	21
2.2 Instruments for 2D metrology	22
2.2.1 Optical Microscopy and Video Systems	22
2.2.2 Electron Scanning Microscopy.....	24
2.3 Instruments for 3D metrology	25
2.3.1 Scanning Probe Microscopy	26
2.3.2 Imaging Confocal Microscopy	27
2.3.3 Coherence Scanning Interferometric Microscopy	33
2.3.4 Micro and Nano CMMs.....	36
2.4 From surface characterisation to coordinate metrology at micro scale	38
2.5 International standards.....	40
2.5.1 ISO Standards related to surface metrology	40
2.5.2 ISO Standards related to coordinate metrology.....	42
2.5.3 Other ISO standards	44
2.6 Conclusions	44
Chapter 3 Dimensional quality control of replication at the micrometre scale	47

3.1 Introduction	47
3.2 Replication analysis at the micro scale	48
3.3 Generation of simulated data sets	50
3.4 Surface characterization and comparison.....	52
3.5 Results	52
3.6 Application to real case	55
3.7 Conclusions	56
Chapter 4 Thermal drift study on Scanning Probe Microscopes	57
4.1 Errors in SPM / AFM measurements	57
4.1.1 Scaling.....	58
4.1.2 Crosstalk	59
4.1.3 Non-linearity	60
4.1.4 Other errors	62
4.1.5 Drift.....	63
4.2 Thermal drift study on SPM scanners	65
4.2.1 Scanning systems and drift distortions.....	66
4.2.2 Experimental Set up.....	68
4.2.3 Experimental plan	70
4.2.4 Results and discussion	71
4.2.5 Long and short time stability	75
4.2.6 Finite Element Method simulations	76
4.2.7 Instrument optimization	77
4.2.8 Conclusion	78
4.3 Comparison of different commercial scanning probe microscopes	79
4.3.1 Experimental set up.....	80
4.3.2 Compared instruments	81
4.3.3. Results and discussion	84
4.3.4 Conclusions.....	90

Chapter 5 3D optical microscopy for coordinate metrology measurement of microfluidic channels	91
5.1 Soft channels for push-down microfluidic valves	91
5.2 Critical geometric properties	91
5.3 Soft channel manufacturing	92
5.4 Current practice of quality inspection.....	93
5.5 Foundations of the proposed approach for the assessment of channel geometry	94
5.5.1 Micro and nano CMMs vs. 3D optical profilometers.....	94
5.6 ISO 17450-1 work flow	96
5.7 Nominal model and measurand definition.....	96
5.8 Data acquisition	97
5.9 Data analysis	99
5.9.1 Pre-processing	99
5.9.2 Void pixels.....	99
5.9.3 Artefacts	100
5.10 Levelling.....	102
5.11 Feature extraction and association.....	103
5.11.1 Extraction of the plane, association and levelling	104
5.11.2 Extraction of the cylindrical surface and association	104
5.12 Evaluation.....	105
5.12.1. Evaluation of the width of the channel	105
5.12.2 Evaluation of the depth of the channel	106
5.12.3 Results	107
5.13 Discussion.....	107
5.13.1 Measurement limitations	107
5.13.2 Sampling.....	108
5.13.3 Data processing	108
5.13.4 Traceability and Uncertainty	109
5.13.5 Application of ISO 17450-1	110

5.14 Conclusions	110
Conclusions	113
References	117

Chapter 1

Introduction

1.1 Micro engineering

Micro products are present in many fields: from mechanical to electronic industry, from chemical and physical sciences to medicine. Figure 1.1 shows some examples of micro product that are present on the worldwide market.

Even if it is not so evident, nowadays components with micro dimensions are present everywhere around us. Miniaturisation has been a major trend of manufacturing technology during the last 30 years. The phenomenon started in the field of semiconductor industry where the number of components that can be realized on a chip has been doubled every 18 months approximately, following the Moore's law. Also manufacturing technologies, related to polymers and metals, have been pushed towards the components miniaturisation.

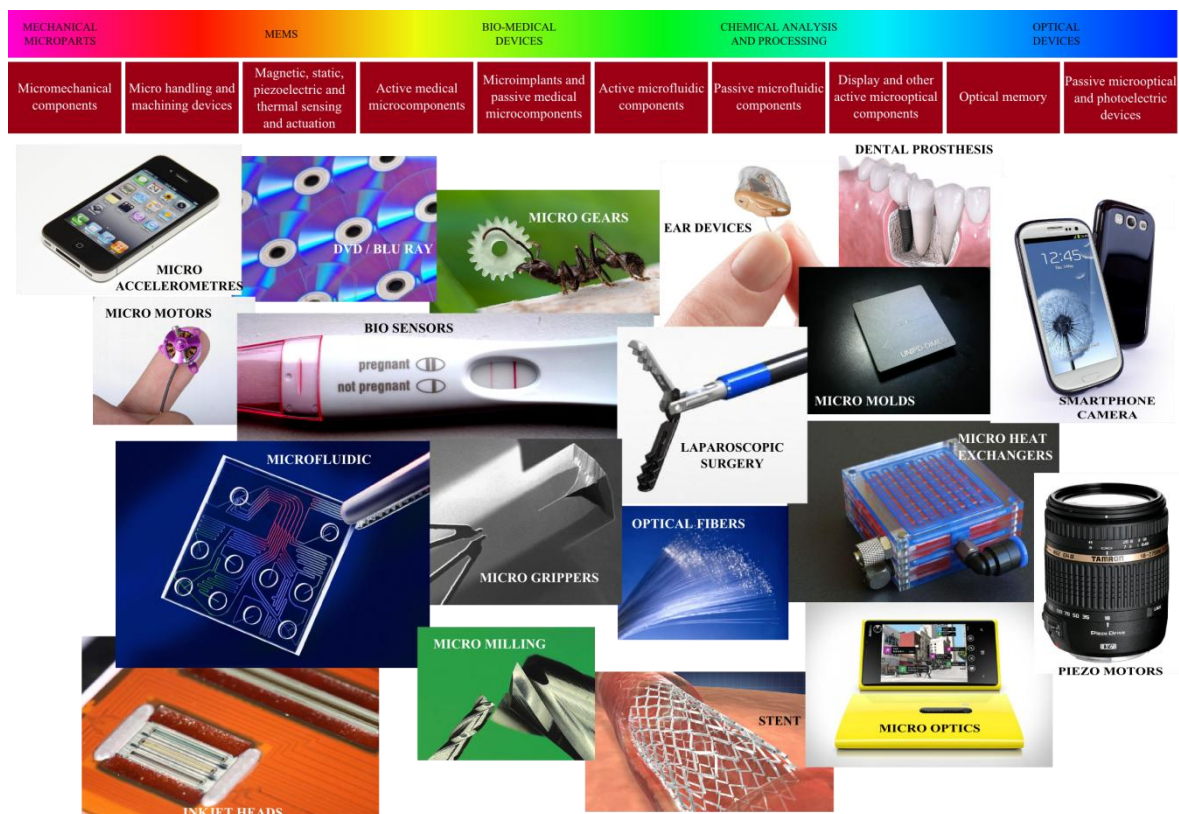


Figure 1.1: Examples of micro products present in the life of every day.

Products realized nowadays require the integration of macro and meso scale devices with micro features or micro components and sometimes with nano features. In order to satisfy these production requirements, the traditional manufacturing technologies have been adapted for the micro manufacturing and new dedicated technologies have been developed. Micro manufacturing technologies are reaching their capabilities limit in terms of minimum achievable dimension of the features and in term of accuracy. In this thesis will be considered another problem related to the production of micro features: the quality control. In particular the dimensional and geometrical quality control will be investigated. As written by K.J. Stout: *“Measurement is the most ancient of science, for if you cannot measure an object, even by the crudest means, it becomes virtually impossible to make it”*. Dimension and geometrical metrology at micro scale still presents big issues in the field of tolerancing, instruments performances, traceability and uncertainty evaluation [1, 2].

1.1.1 Micro manufacturing technologies

The term “micro engineering” indicates the whole process of development and realization of products with functional features that have at least one dimension in the order of micrometre (μm). Micro manufacturing technologies encompass all the available techniques used to produce micro products. For the realization of micro products, and their industrialization, new materials and new processes have been developed following three main paths:

- Existing manufacturing processes have been downscaled and adjusted for micro precision engineering,
- MEMS and microelectronics production technologies have been adjusted for industrial production and up scaled,
- New technologies have been developed [3].

Technologies related to MEMS and to the production of microelectronic components are the most advanced since they have been developed for many years. They are based on 2D, 2½D layer production through lithography, etching and material deposition. Integrated circuits distributed on a silicon wafer are usually produced performing these steps sequentially. In order to produce components made of materials different than silicon, LIGA technology is used. LIGA is based on X-ray lithography, electroforming and casting. The use of X-ray instead of UV-light allows to create structures with height up to 1000 μm , width of 0.2 μm , very low surface roughness ($R_a = 0.3 \text{ nm}$) and aspect ratio included between 50 and 5000.

Electroforming is performed on the silicon master, covered with resist, after lithography. Hence, the resist is etched. Silicon and the deposited material remain. The step is repeated several times, realizing several layers, in order to obtain the desired component. The component can be the final product or the mould insert for next operation of replication such as micro injection moulding. Lithography and LIGA processes require expensive instruments, they are time consuming and the production rate is low.

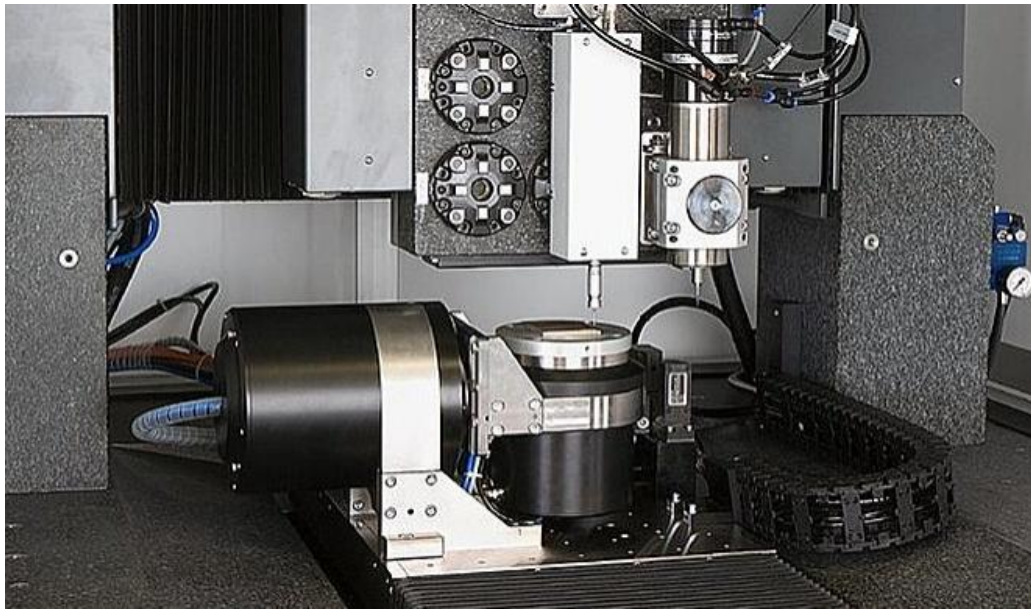


Figure 1.2: 5-axis micromilling machine including tilt-swivel unit, touch probe for workpieces measurement and mechanical machining spindle. Courtesy of Kugler GmbH.

Materials such as metals, ceramics, glass, polymers can be processed by other techniques such as laser beam machining, micro EDM machining, ion and electron beam machining and ultra-precision cutting.

Laser beam machining uses the energy of a laser light to remove, or join, the material. Even if several laser technologies are available, the minimum lateral dimension of a structure, realized through these techniques, depends on the laser wavelength, the laser energy and frequency.

Micro EDM machining derives from the technology of electro discharge machining used at meso and macro scale. The tool and the workpiece work as two electrodes: they are positioned close together separated by a dielectric and subjected to a voltage. When the voltage is sufficient to break the dielectric, sparks occur between the tool and the close

surface of the workpiece. The sparks that are generated remove the material. EDM works in different configurations such as die sinking, wire EDM, drilling and milling. EDM allows obtaining complex 3D structures. Tools are custom shaped through wire EDM, mechanical machining or LIGA.



Figure 1.3: Example of microfluidic mixer obtained through micro injection moulding. Mould insert (left) and moulded part (right).

In ion and electron beam machining, ions obtained from a plasma source are directed and focused onto the surface where they sputter away material. Fine structures and extremely fine details can be obtained. Due to the very low material removal rate, ion and electron beam machining are mainly used for surface machining.

Cutting processes for micro machining have been adapted from macro machining. Ultra-precision machines, as presented in Figure 1.2, are required for high accuracy micro cutting. One of the most critical aspect of these processes is the tool. The material of the tool must be harder than the workpiece material and no chemical interaction has to take place between tool and workpiece. Considering dimensions of the machined features, in the order of tens of microns, the desired values for the tool edge radius are in the order of hundreds of nanometres. In order to obtain sharp tool edges, the most suitable material of the tools is the monocrystalline diamond. Unfortunately, its chemical affinity with steel causes unacceptable wear. Despite some drawbacks, cutting processes are flexible. Plastics and metallic materials, as well as composite materials, can be machined and there is the possibility to machine 3D microstructures characterized by high aspect ratios and high geometric complexity.

Manufacturing processes described above can be used for the realization of the final product as for the realization of inserts for moulds used in mass replication processes. The two

pictures in Figure 1.3 show a mould insert for micro injection moulding and the replicated part. Due to the low material removal rate of the processes presented before, replication processes are frequently required to produce several parts in a more economic and fast way.

Micro injection moulding is one of the most promising technologies for the replication at micro scale allowing producing micro products at relatively low price. The polymer material is melted and injected into the mould cavity. Differences, respect to the traditional process of injection moulding, include elevated moulding temperatures, highest injection speed, and final product handling.

It is possible to realize microstructures with wall thicknesses of 20 μm , structural details in the range of 0.2 μm and surface roughness $R_z < 0.5 \mu\text{m}$. Aspect ratios exceeding 20 are obtainable. Micro products made in polymers are used for micro optics, micro fluidics and biological and medical technology [4].

1.1.2 Measurements requirements and challenges at micro scale

The term “dimensional metrology” indicates the measurement of dimensions and geometries based on distance measurements. Dimensional micro metrology can be defined as the measurement of the geometries and dimensions of objects in which at least one critical dimension or functional feature is in the micrometre range. Table 1.1 indicates generic measurement tasks at micro scale.

Table 1.1: Generic measurement tasks at micro scale.

Surface Topography assessment	- surface roughness - characterisation of structured surfaces
2D measurements	- measurement of the position of micro features on a plan
2½D measurements	- measurement of step height, channel height and width in microfluidic devices or MEMS
3D measurements	- assessment of a micro component that is not laying on a surface and measurement of form
Multi-scale measurements	- measurements of micro feature distributed in a large area (microfluidic devices)

The difficulty, in performing metrology at micro scale level, is due to the fact that metrology

has been developed mainly at macro scale. Instruments and measurement technologies, but also international standards, have been developed in order to solve metrology challenges at macro scale level. Considering for example the performances of a conventional CMM (Coordinate Measuring Machine), measurements of distance of hundreds of millimetres can be performed with uncertainty of few microns. Hence, the uncertainty of the measurement is thousands or more times lower than the measured dimensions. Applying the same consideration at the micro scale level, the measurement uncertainty should be in the order of nanometres. Three main gaps have to be covered in order to perform measurements at micro scale with an approach that can be compared to the metrology at macro scale:

- a gap in the measurement definition and tolerancing,
- a gap in the traceability and uncertainty assessment,
- a gap in the instrument performances.

Designing a product in macro world, the geometry and dimensions are defined considering the functionality of the product and the main functionality of a product at macro scale is to be assembled with other components. ISO GPS standards have been developed to assist the production from the design, to the manufacturing and quality control. Unfortunately, ISO GPS standards can't be directly applied to micro dimensions. For examples, tolerances grades are not defined for nominal size below 3 mm. It is sufficient consider the definition of the surface roughness. Surface roughness assessment is quite far from the "standard dimensional metrology" and it is more close to micro metrology. Beneath this consideration, the smallest probe size for surface profile measurement is set as 2 μm and the smallest considered feature has dimensions of about 2.5 μm .

A different point of view is necessary in order to develop a tolerancing system in the field of micro and nano world. It is necessary to start considering the aspect of a micro component. A micro part can be a standalone part that is assembled to other components. In this case the main functionality of the part is the possibility to be assembled, so the dimensional and geometrical features of the part have to be controlled. This case, similar to what happens at macro scale, is defined as *Hetero Integration*. Micro components can be fixed positioned on a substrate realizing a micro system. In this case, defined as *Hybrid Integration*, it is important to evaluate the position of the parts on the substrate. *Monolithic Integration* considers the case in which the micro features are realized from the substrate and no mating is required. In this case the functionality of the micro system is the main characteristic and dimensional

measurements are less important. So a functional approach has to be used when designing tolerances for a micro component [1]. GPS approach can be used, too, but with some adaptation. For example Weckenmann et al. [5] presented a top down approach. Beneath these problems on different points of view in the tolerancing, the main problem when performing measurements at micro scale is the evaluation of the measurement uncertainty.

In fact, the second gap that needs to be covered in the field of micro metrology is the need of calibrated instruments, traceable measurements and the uncertainty estimation. Standards samples for calibration already in use are step heights, scales, 2D scales and structured surfaces. These standards are sufficient when performing surface measurements. For 3D coordinate measurement, similar to what is performed at the macro scale, a micro ball plate or a micro step gauge should be used. No fully 3D calibration standards exist. There is a need of developing new physical standards and there is the need to achieve uncertainty evaluation. Considering also the fact that at micro and nano scale the interaction between the workpieces and the probes doesn't follow standard physical rules, the uncertainty evaluation is a big task.

The third gap considers the developing of instruments able to perform measurement at micro scale. Instruments measuring object with accuracy in the order of micrometres are available, but instruments measuring objects with dimensions in the field of the micrometre need an accuracy at least in the field of nanometre. The development of new instruments is a challenge. Several aspects have to be considered such as the measurement range, the measurement resolution, the measurement speed, the easiness of use and so on. Typical instruments that can be used for metrology at micro scale are described in chapter 2. The present work of research is focused mainly on giving hints for covering this third gap.

1.2 Objective of the work

This thesis presents the main results of the research carried out during the Ph.D. period in the field of dimensional and geometrical metrology applied to components which present features with dimension in the micrometre range. In particular, microfluidic devices have been considered as reference case study. The research activity is mainly included in wireframe of the European project CellDiaSp - "Cell-Diagnostic Sample-Preparation Polymer BioMEMS". The project is realized in collaboration with international partners and deals with the realization of microfluidic platforms for cells analysis. Metrology activities are required, within the project, in order to characterize the dimensions and geometries of masters, mould

inserts and replicated parts. Measurement results are necessary to provide fundamental information for the development of the manufacturing processes. Hence, the problem at the base of the research activity is, in a more generic and wide meaning, the geometric and dimensional characterisation of components at micro scale. Metrology at micro scale is still at an embryonic stage. The work presented in this thesis is focused on increasing the knowledge in the field of micro metrology with application to the specific case of microfluidic devices.

The objective of the work can be summarised in the following points:

- identification of the main techniques for dimensional measurements at micro scale,
- study of these techniques in order to identify the main limits,
- improvement of some measurement techniques considering both instruments and data analysis,
- application of the obtained results to a real case such as a microfluidic channel.

1.3 Work structure

The Ph.D. thesis is structured in the following way.

A first part is related to the study of the state of the art of the main metrological measurement techniques at micro scale. Optical microscopy and video sensors, electron scanning microscopy, the use of dedicated coordinate measuring machines (NanoCMM), scanning probe microscopy and optical profilometry (confocal/interferometry) resulted to be the most suitable technologies. Chapter 2 presents a review of these techniques.

In Chapter 3 the use of these techniques for the quality control of parts realized through replication has been studied. The study considered the possibility to measure the surfaces of the parts present in a replication process (mould inserts and replicated parts) and to calculate a single parameter, able to describe and to map the quality of the replication process, both in structured and unstructured surfaces. It resulted that, especially in the case of structured surfaces, a single parameter is not sufficient to characterize the quality of the replication process and that a geometrical and dimensional characterisation, typical of the coordinate metrology, is preferred.

Successively, it has been decided to concentrate the research activities on the study of two categories of instruments: the scanning probe microscopes and the optical profilometers.

The reason of this choice is that the characteristics of these instruments result to meet the measurement needs of the components for the realization of the microfluidic devices

considered within the European project CellDiaSP. Moreover, these two categories of instruments are the candidate to the development of a 3D measurement technique at micro scale.

Scanning probe microscopes and optical profilometers were developed for the surface roughness characterisation. The adaptation of these instruments for 3D coordinate measurement is recent and the research in this way is the objective leading the research activity presented in the thesis.

In Chapter 4, the problem of “drift” reducing the accuracy of the measurement performed with the atomic force microscopes has been considered. The sources of this error have been investigated in several commercial atomic force microscopes and solutions to reduce and control it have been presented.

Chapter 5 concerns with the use of the optical profilometry as technique for coordinate metrology. Considering measurement results that are obtained using the optical profilometers in the conventional way, a new approach for the data analysis have been developed in order to perform three dimensional coordinate measurements. The micro dimensions of the geometrical features and the measurement technique requires some adaptations in order to apply the methodologies developed for coordinate metrology at macro scale that are well described in the international standards. The result of the research is a calculation code that takes advantage of the double nature of the data, point cloud and image, and allows to perform procedures as image filtering and thresholding combined with the points extraction and the association of geometrical features. The developed approach can be used also for measurement data obtained through scanning probe microscopy.

Finally the developed technique has been applied to the case study of a microfluidic peristaltic valve with cylindrical section for the measurement of the main dimensions and geometries.

Chapter 2

Quality control at micro scale: state of the art

2.1 Introduction

Different instruments are available in order to perform measurement of features with dimensions of micrometres. The instruments considered in the diagram are well known instruments. In fact, no special purpose or dedicated instruments have already been developed for the task of dimensional and geometrical measurements at micro scale. Existent instruments are adapted and used. Two approaches are followed: the use of instruments developed for surface texture measurements and the miniaturization of coordinate measurement machines.

Figure 2.1 represents the state of the art of the metrology at micro scale. The instruments in the diagram are classified following two measurement properties of the instrument. In the vertical axis it is represented the dimensional range of measurement while in the horizontal axis it is represented the geometrical complexity achievable.

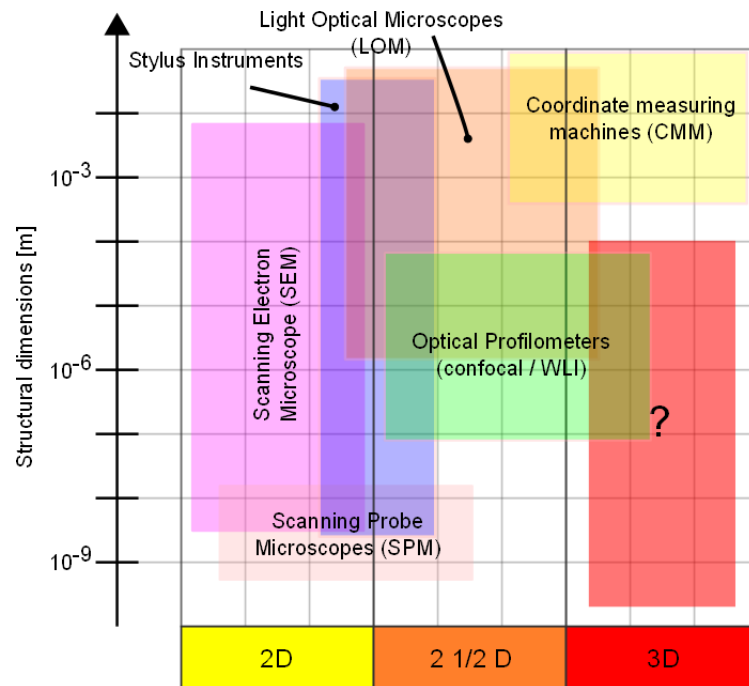


Figure 2.1: Diagram representing some categories of instruments, available at the state of the art, for measurements at micro scale. On the vertical axis it is represented the dimension of the feature that can be measured and on the horizontal axis it is represented the achievable measurement complexity.

This kind of classification is useful in order to point out the real capabilities of the instruments and to identify where more effort should be put in research. For example measurement of microstructures with submicron and nano dimensions can be performed considering two dimensional measurements, while three dimensional measurements are still a challenge as represented by the red box.

A review of the main measurement techniques for metrology will be given in this chapter considering instruments designed mainly for 2D measurements and instruments designed for 2½D and 3D measurements. Stylus profilometers will not be considered in the review. In these instruments the tips geometry have an aperture angle of sixty degrees or more and the minimum radius is 2 µm. Small features can be measured only in one direction, high aspect ratio features, such as deep grooves, vertical sidewalls and undercuts cannot be measured. An evolution of the stylus profilometers for micro scale metrology can be considered the Scanning Probe Microscopes [6, 7].

2.2 Instruments for 2D metrology

2.2.1 Optical Microscopy and Video Systems

Optical microscopes are the most used instruments in laboratories. They are the main instruments used to image samples with high magnification. They are used in many fields of science: biology, chemistry, material analysis and quality control. In quality control they can be used as simple instrument for inspection, but calibrating the field of view of the objectives they can be used as measurement instruments. The evolution of the optical microscopes is the video systems. These instruments are dedicated to measurements and are designed in order to perform two dimensional measurements using an optical magnification and a video sensor as probe. These instruments are equipped with software for image processing (for examples edge detection) in order to identify geometrical features. The shape of the most advanced video systems is the shape of a CMM with an optical probe.

Main advantages of video systems are:

- the possibility to obtain accurate measurements in thin, soft, brittle or elastic parts thanks to the non-contact technique,
- the possibility to measure components and features that normally cannot be accessed by conventional contact measurement systems,

- the possibility to integrate these instruments in the manufacturing process due to the high measurement speed.

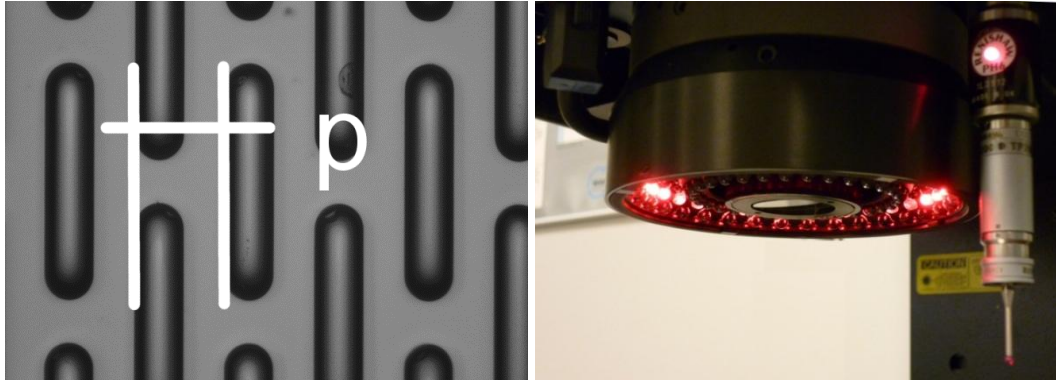


Figure 2.2: Example of measurement with video sensor on a silicon wafer where the visible structures have been obtained by x-ray lithography $p = 100 \mu\text{m}$ (left). Video Sensor Probe on a multi-sensor CMM Werth Video Check IP 400 (right).

Measurement systems basically consist of optical and electronic components in order to perform image formation and acquisition, image processing and communication.

An illumination system is used to illuminate the sample. The sample can be illuminated in different way with light with different colours coming from different directions (lateral light, direct light, back light). The illumination of the sample is the most critical part of the measurement because it influences the quality of the data.

The illuminated sample is imaged, through an optical system, into a sensor, usually a CCD or CMOS sensor. Once the image is digitally acquired by the sensor, a computer is required to capture the image and process it through computer vision functions and algorithms. The operator can interact with the instrument identifying edges and features on the image in order to perform measurements. An example of measurement is given in Figure 2.2.

The main limitations of these instruments are:

- the resolution limited by the Abbe principles,
- the influence of the illumination and of the optical properties of the sample on the results.

Other error sources are the quality of the optical components, the presence of optical distortions or aberration [8]. The evaluation of the measurement uncertainty when using optical probes results difficult. CMM International standard describing calibration, performance verification and acceptance tests for conventional CMM with contact probe, are

available (see for example ISO 10360 series). These standards are not directly applicable to non-contact measurement systems and the ISO Working Group on CMMs (the ISO/TC 213/WG10) is working to the development of a series of standards dedicated to optical CMMs. VDI/VDE 2617 is a German guideline developed since the mid-1980s and has received the most international use prior to the release of the ISO 10360 standard [9].

2.2.2 Electron Scanning Microscopy

Scanning electron microscopy (SEM) exists since several decades and is extensively used for imaging structures with dimensions in the field of micrometre. A beam of electrons is used to scan the specimen as a raster of parallel contiguous lines. Electrons are backscattered and other electrons are emitted (secondary electrons) from the test surface. Different emissions can be detected and used to characterize physical and chemical properties of the sample under investigation. Emitted electrons are collected by detectors in order to reconstruct an image of the sample. The image resembles that seen through an optical lens but at a much higher resolution. A typical SEM image is presented in Figure 2.3.

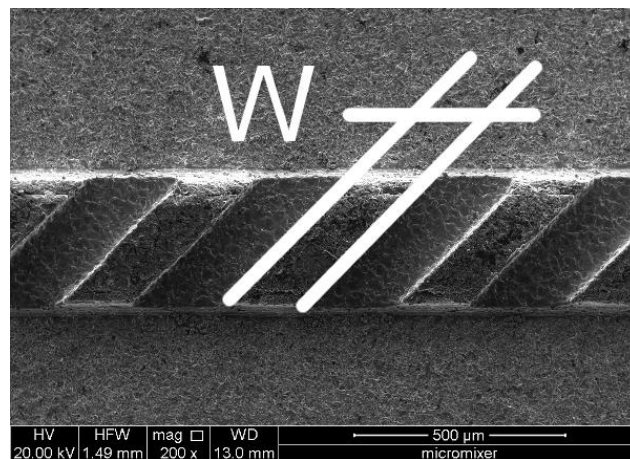


Figure 2.3: Typical image obtained through scanning electron microscope. The image shows some micro features ($w \sim 160 \mu\text{m}$) realized on a mould. The mould is the same presented in chapter 1. It is interesting to notice that the resolution of the image allows seeing the structure of the surface.

SEM presents properties that, combined together, are not reached by any other technique. Magnification levels vary from 100x to 200.000x, the resolution reach 2 nm (for highest magnification). SEM presents large depth of field and long working distance (allowing

multiple positioning measurement strategies), elemental analysis capability and minimum diffraction effects [1].

Unfortunately, some disadvantages are present when working with SEM.

The sample must be placed in a vacuum chamber. In addition, the surface must be conducting (or at least be semiconducting). SEM photographs are still inherently 2D, and no height information can be extracted directly from the images. Furthermore calibration of scales and uncertainty estimation is a prerequisite for the use of SEM pictures for quantitative evaluations. To gain three-dimensional images using an electron microscope, the sample can be tilted to a number of angles and geometrical relationships used to calculate three-dimensional images [10, 11]. Nevertheless, 3D SEM metrology is not a consolidated technique.

2.3 Instruments for 3D metrology

Thinking about instruments for 3D measurement at macro scale it is immediate to think about coordinate measurement machines. In fact CMM are the main used instruments for measurement and characterization of components with dimensions from millimetres to metre with accuracy in the order of few microns. CMM are so diffused that the metrology, and in particular the coordinate metrology have been developed focusing on these machines. For example ISO standards have been developed considering CMM. The whole concept of metrology is based on the working principle of coordinate measurement machines.

Standard CMM cannot be used in the world of micro components, so different instruments have to be developed. The approach to the development of instruments able to perform 3D measurements at micro scale is based essentially on:

- downscaling of existing CMM,
- adaptation of instruments used for surface metrology.

In the first case the so called NanoCMM have been developed, while in the second case atomic force microscopes and optical profilometers have been considered as promising technologies. Optical profilometry (OP) is a technology, still in development, for surface metrology. Several techniques of optical profilometry are available such as chromatic and imaging confocal microscopy, point autofocus instruments, focus variation instruments, digital holography, phase shifting and coherence scanning interferometry.

In this review will be presented, as instruments for 3D coordinate metrology, the NanoCMMs,

the Scanning Probe Microscopes (SPMs), the Imaging Confocal Microscopes, and the Coherence Scanning Interferometry Microscopes. In fact SPMs, and OPs are not 3D measurement instruments. They can be defined as 2½D measurement instruments. The object of the research work is to study the possibility to use these instruments as 3D instruments.

2.3.1 Scanning Probe Microscopy

SPMs or scanning probe microscopes are measurement instruments that use a nano probe to scan the surface of the sample in a similar manner to a stylus instrument. Atomic Force Microscopes (AFMs) are scanning probe microscopes where the physical interaction between tip and surface is based on atomic forces. While the probe scans the surface, the signal of the interaction is acquired and is usually used to control the distance between the probe and the sample surface through a feedback mechanism. The surface topography is reconstructed considering signals from the feedback loop. An example of the working principle of an AFM is given in Figure 2.4.

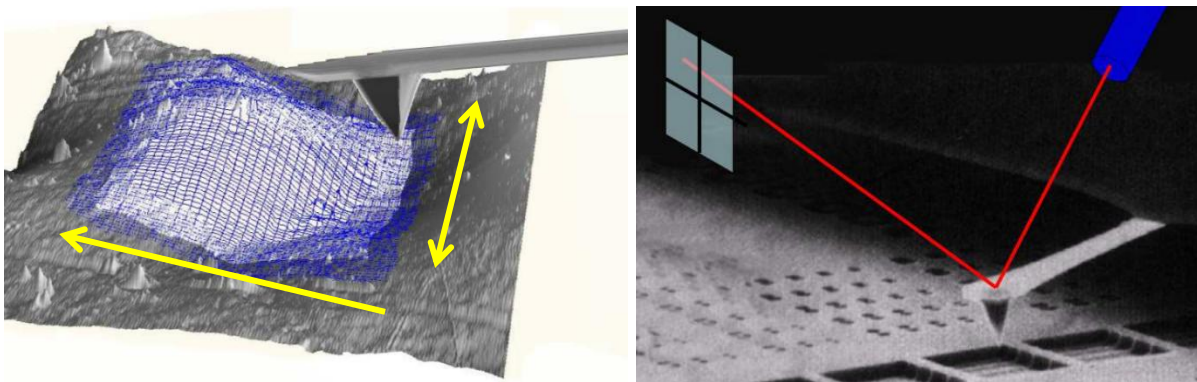


Figure 2.4: Representation of the AFMs scanning principle. The tip scans the surface in a raster fashion acquiring consecutive profiles (left). Representation of the optical lever for the calculation of the tip deflection and the determination of the topography [12].

The movement of the tip or the movement of the sample is performed through a piezoelectric mechanism. For this reason the measurement range of these instruments is limited to 100 μm or 200 μm in the lateral directions and 20 μm in the vertical direction. The contact between the surface and a tip with radius of 10 nm and the use of the piezo technology allow these instruments to image all types of surface with potentially sub-nanometre vertical resolution

and nanometre lateral resolution. The measurement range can be increased to several millimetres using an AFM as probe in a coordinate measuring machine. AFM scanning is relatively slow and even over 100 μm by 100 μm the scan time can be measured in minutes.

In conclusion, AFMs can be used for measuring planar structures or surface texture with dimensions in the order of tenth of microns. Advances are required for them to be able to measure the high aspect ratio and high slope angle structures. Chapter 4 of this thesis is dedicated to AFMs.

2.3.2 Imaging Confocal Microscopy

The confocal microscopy principle has been invented by Marvin Minsky about 60 years ago. The confocal microscopy differs only slightly from the conventional microscopy. Due to the fact that images are generated electronically, the method became practical after the computer reached the necessary power for image processing. Images produced through confocal microscopy are “optically sectioned”, so only the region of the sample within the focal plane is detected. A commercially available confocal microscope is presented in Figure 2.5.



Figure 2.5: Commercial Imaging Confocal Microscope Sensofar PluNeox.

Optically sectioned image are produced restricting the illuminated regions on the sample through a structured illumination pattern and observing the reflected or backscattered light through a second pattern identical to the illumination pattern. Light coming from the regions of the surface out of the focal plane of the microscope's objective is blocked. The illumination and detection patterns can be:

- a single pinhole placed on the optical axis
- a set of pinholes, slits, parallel slits
- any other pattern that effectively reduces the size of the illuminated and detection regions

Independent of the geometry of the patterns, an in-plane scanning of such patterns is needed in order to produce a complete optically sectioned image. Different in-plane scanning techniques, for generating the illumination and detection patterns, and for detection are available. Most confocal microscopes can be divided in three categories:

- laser scanning,
- disc scanning,
- programmable array scanning.

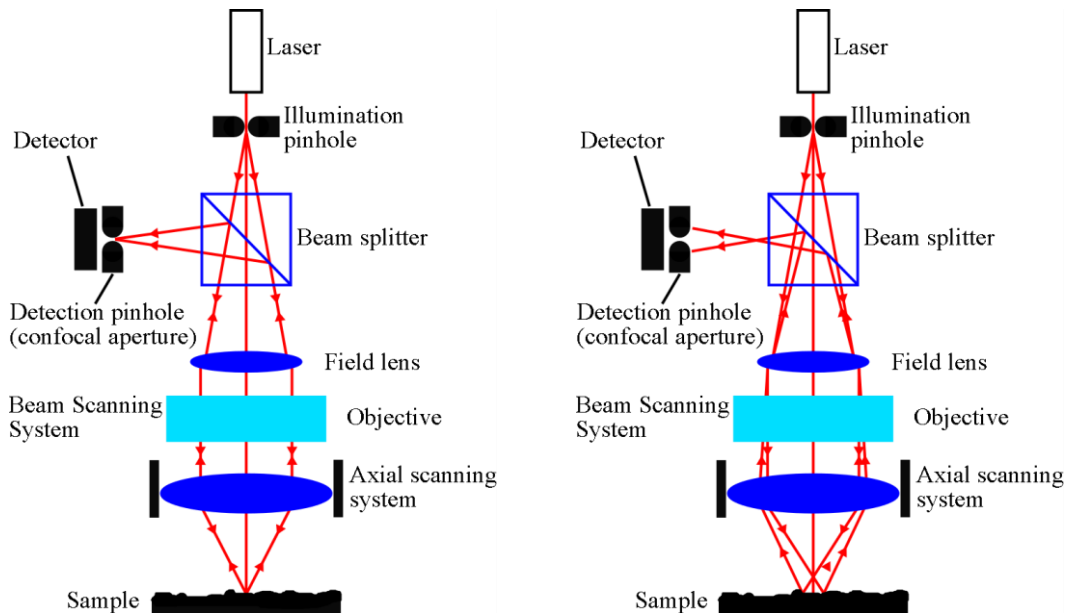


Figure 2.6: Laser scanning confocal microscope working principle when the sample is in focus (left) and when the sample is out of focus position (right).

The simplest confocal microscope is a laser scanning microscope. Light coming from a laser source passes through the illumination pinhole, through the microscope objective and reach

the surface of the sample. The reflected light passes back through the objective and is reflected, by a beam splitter, into the detection pinhole. A photo detector is placed behind the detection pinhole in order to detect the reflected light signal. As shown in Figure 2.6, if the surface is placed in the focal plane of the microscope, the reflected light passes through the detection pinhole and the light signal intensity on the detector is high. If the surface of the sample is out of the focal plane of the instrument, the reflected light is projected out of the detection pinhole and recorder signal on the detector is low.

Considering a Cartesian coordinate reference system; x , y are the axis on the surface of the sample plane and z is the axis perpendicular to the surface of the sample plane, so the optical axis of the instrument.

The laser spot is moved scanning the sample surface in the x , y plane. Only the regions of the sample that are in the focal plane of the instrument are detected. In Figure 2.7 the phenomenon of isolation of regions that are in focus is shown. In this case the instrument is not a laser scanning confocal microscope, but a programmable array confocal microscope. The working system is a little bit different, but the result is the same.

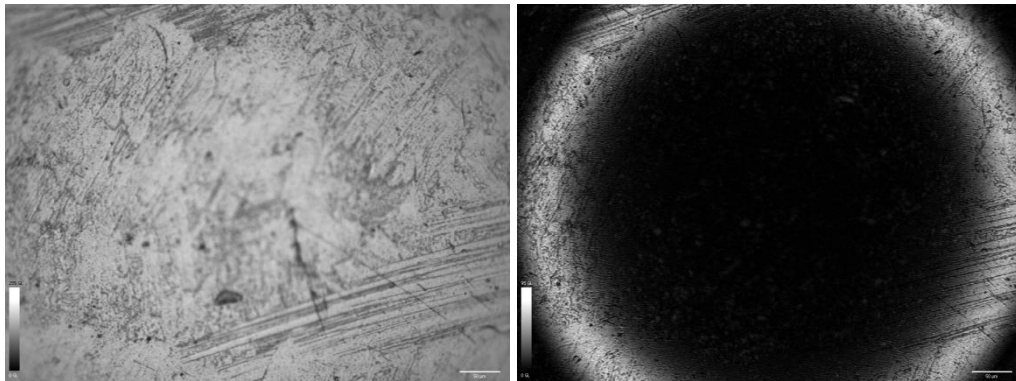


Figure 2.7: Bright field (left) and confocal (right) images of a spherical surface obtained at through a confocal scanning microscope. Images are captured at the same height.

An optically sectioned image is a grey level image where the pixel intensity is related to the position of the surface respect to the focal plane. Black regions are out of focus while white regions are in focus (see Figure 2.7).

The scanning along x , y plane is performed at different z levels. The vertical position of the instrument is controlled. The result is a series of grey scale confocal images associated to different z values as presented in Figure 2.8. Considering the same pixel in the series of images taken during the vertical scanning, the grey value change with the z value.

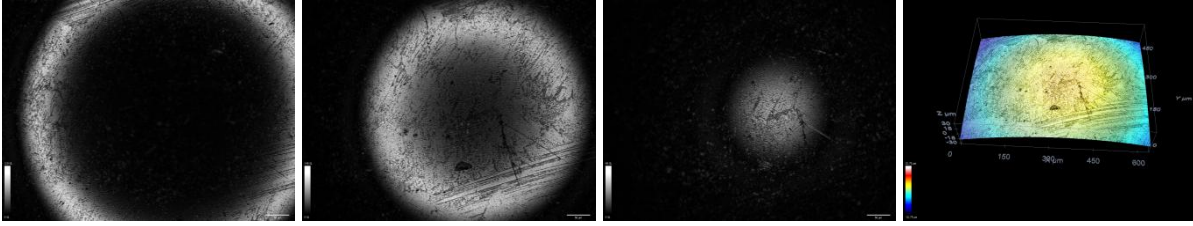


Figure 2.8: Sequence of grey scale confocal images captured at different z level during the scan from the lowest position (left) to the highest position. Image on the right is the resulting measured topography.

Each pixel has an “axial signal”. The grey value is maximized when the point on the sample surface, corresponding to the considered pixel, is on the focal plane of the instrument. Considering the “axial signal” it is possible to calculate the vertical position of a pixel that is to quantify the vertical position of the points of the surface. Performing this operation for any pixel the surface topography is acquired. Laser scanning confocal microscopes require a plane scanning and a vertical scanning, so the time necessary to acquire the surface topography is long. Disc and programmable array scanning microscopes are faster. They can acquire topography with vertical range of hundreds of microns in less than one minute. There are different way to calculate the z position of the surface. The easiest and fast method is to assign the value of the discrete position of the scanner. The smallest typical step for a confocal microscope is in the order of $0.05 \mu\text{m}$.

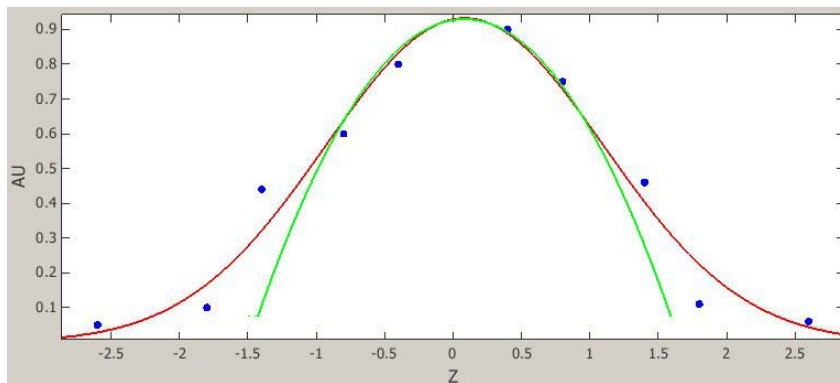


Figure 2.9: The axial signal is represented on a diagram. Z values [μm] are on the horizontal axis, normalized grey level is on the vertical axis. For the calculation of the vertical position of the pixel the axial signal can be fitted with a Gaussian function (red). Eventually, to increase the calculation speed, only a central subsample of points is fitted with a paraboloid.

Paraboloid fitting consider some points around the maximum of the axial signal. The points are fitted through a second order curve (green curve in Figure 2.9). The maximum of the

curve is calculated and the z value is considered as the z value of the point. This method is fast and allows reaching a resolution that is about $1/100$ of the step of the vertical scanning.

A more advanced algorithm considers fitting the “axial signal” using a Gaussian curve (red curve in Figure 2.9) and calculating the maximum. This algorithm is more accurate but requires more computational power or computational time.

A scheme representing a programmable array scanning confocal microscope (PACMs) is shown in Figure 2.10.

PACMs use a light source (usually LEDs) that is parallel, so an entire region of the surface is illuminated with the same intensity. In this way only the vertical scan is required and the topography acquisition results faster than in laser confocal microscopy where only a point of the surface is illuminated and horizontal scan is required. Light passes through the illumination pattern that is generated inside the micro display. The pattern is constituted by regions where the light is blocked (OFF) and regions where the light can pass (ON). The light signal reflected from the surface is projected in the CCD detector. The elements of the CCD detector are synchronized with the pixels of the display, so only the pixels corresponding to the ON region of the display acquire the light signal. A confocal image is reconstructed from a sequence of recorded images on the CCD camera correlated by shifting the ON elements on the micro-display.

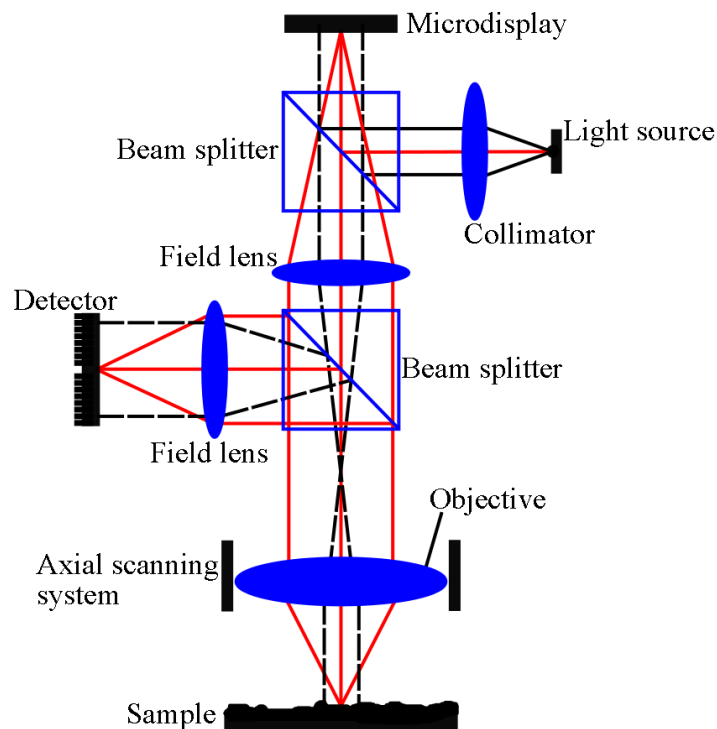


Figure 2.10: Scheme of a programmable array scanning confocal microscope.

The functioning of the confocal microscopes is influenced by the objectives used in the measurements. Objectives for metallography are commonly used operating in air. Two main characteristics should be taken into account during the choice of the objective appropriate for the measurement task: the magnification and the numerical aperture.

The magnification influences the measurement range and the lateral resolution.

For example it is necessary to measure a surface of 300 μm x 300 μm . A 20x objective with field of view of 636 μm x 477 μm can be used. Considering a CCD with resolution of 577 pixels x 768 pixels, the spatial sampling is 0.83 μm in both x, y directions. The same measurement can be performed using a 100x objectives with the field of view of 127 μm x 95 μm . Lateral spatial sampling result in 0.17 μm , but the stitching of several topographies is required. Using a 100x objective more detailed images are acquired, but the stitching is necessary resulting in a long acquisition time. Moreover, the topography is affected by stitching errors.

The numerical aperture of the instrument affects the maximum detectable slope. Maximum detectable slope is one of the main limits of the optical confocal microscopes. The numerical (or angular) aperture A_N determines the largest slope angle on the surface that can be measured and affects the optical resolution. The numerical aperture of an objective is given by:

$$A_N = n \cdot \sin \alpha \tag{2.1}$$

where α is the angle indicated in Figure 2.11 and n is a coefficient equal to 1 when working in air.

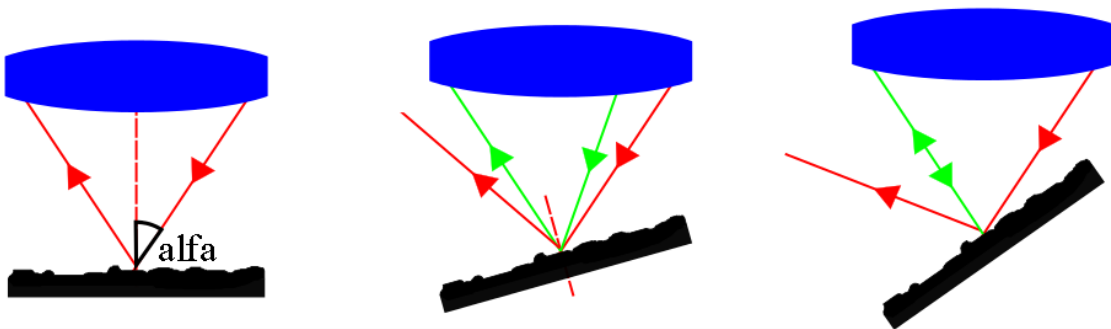


Figure 2.11: Tilting the surface the quantity of light reflected in the objective decreases resulting in a bad or null signal.

An example of objectives with associated numerical aperture and maximum detectable slope is indicated in the Table 2.1. The indicated maximum detectable slope is the theoretical value calculated through equation 2.1. The real value of maximum detectable slope depends also by the surface properties such as reflectivity, roughness, colour, etc.

Table 2.1: Maximum detectable angle calculated for objectives with different magnification, different numerical aperture

Objective	Numerical Aperture	Theoretical Max. Detect. Angle
20x	0.45	26.74°
100x	0.9	64.16°

2.3.3 Coherence Scanning Interferometric Microscopy

Coherence Scanning Interferometry (CSI) is another non-contact measurement technique.

CSI can be indicated also as Vertical Scanning Interferometry (VSI) or White Light Interferometry (WLI). Several other names can be found indicating CSI technology.

The working principle of these instruments combines vertical (z-axis) scanning techniques with optical interferometry techniques in order to reconstruct a three-dimensional surface topography. Interferometry consists of superposing two or more waves, in this case light waves, to create an output wave that differs from the input waves.

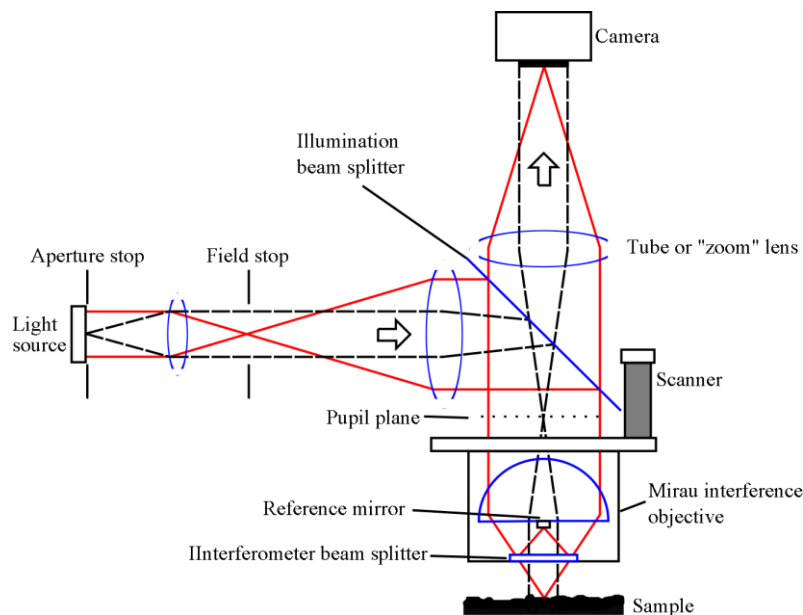


Figure 2.12: Scheme of the geometry of an optical interference microscope for CSI with Mirau objective.

Two waves with the same frequency, phase and amplitude will add constructively while two waves that are out of phase by 180° will add destructively and cancel each other. This phenomenon is known as superposition and results in a set of dark and light bands called fringes. In Figure 2.12 it is represented a typical CSI design. A light source projects light waves. Light is divided in two paths. In the reference paths the light is reflected by a reference mirror. The length of the reference path is known and do not change during the measurement. In the second path the light is reflected by the sample. The length of this path is different from the length of the reference path, so the two waves result different. When the two waves are combined together, so superimposed, fringes appear where the two paths have the same length. In this way it is possible to know the vertical position of the points of the image where fringes appear. CSI are usually equipped with a tilting table with several degrees of tilt adjustment around the x and y axes. Tilt adjustment will be necessary for fringe pattern optimization. The fine scanning movement of the objective in the vertical direction (tens of nanometres to hundreds of micrometres) is achieved using piezo-electric actuators (PZTs). The vertical range varies from tens of nanometre to hundreds of micrometres with vertical resolution that can be lower than $0.1 \mu\text{m}$ (working in phase shifting mode). The most important part of a CSI is the objective. The objective is the responsible of the physical phenomenon of superposing of waves. Different designs of objectives can be used for a CSI instrument, but the two most common are the Mirau and the Michelson objectives.

A Mirau objective is basically a microscope objective lens with the addition of a reference surface and a semi-transparent optic (beam-splitter). These elements are configured as shown in the Figure 2.13.

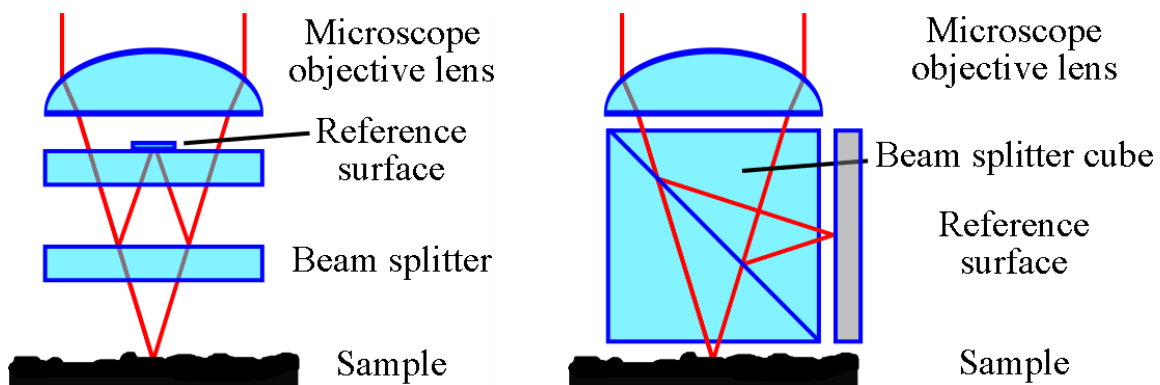


Figure 2.13: Schematic of a Mirau objective (left) and of a Michelson objective (right).

From the light source to the detector there are two waves in two paths.

The light wave following the reference path reflects from the top surface of the beam-splitter into the reference mirror. Then it is reflected back on the beam splitter and finally in the digital image sensor.

The second light wave goes through the beam splitter, to the sample surface. It is reflected back by the surface of the sample and goes again through the beam splitter into the detector after being combined with the wave following the reference path.

A Michelson objective is similar to a Mirau objective but the reference mirror is in a difference position as represented in Figure 2.13. The Michelson configuration is normally used for low magnification lenses (less than $5\times$) because the reference mirror will result too large to be placed in the same position of the Mirau objective.

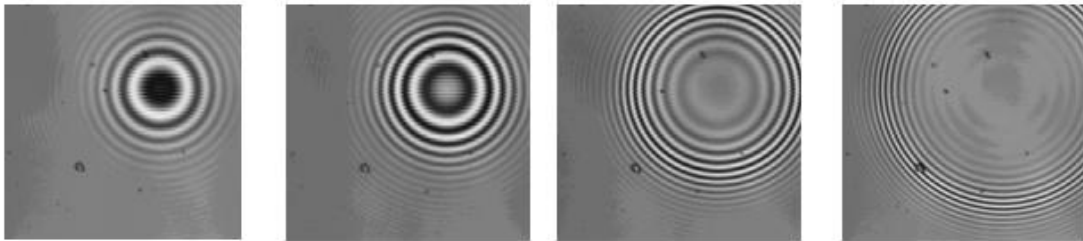


Figure 2.14: Sequence of scanning with a CSI operated in vertical scanning model. The images show fringes appearing when scanning a spherical surface.

In the Figure 2.14 are represented the images appearing on the screen of a CSI during the scanning of a spherical surface.

Each image is associated to a vertical position of the objective. Considering a single pixel of the images its value changes from black to white as it meet the conditions for constructive and destructive interference. In Figure 2.15 it is represented the changing of value of a pixel during the vertical scanning. The intensity of the light changes on the basis of the vertical position of the instruments, so on the basis of the interference. The interference diagram can be enveloped with a function and the position of maximum constructive interference can be calculated, determining the vertical position of the points of the surface corresponding to the pixel.

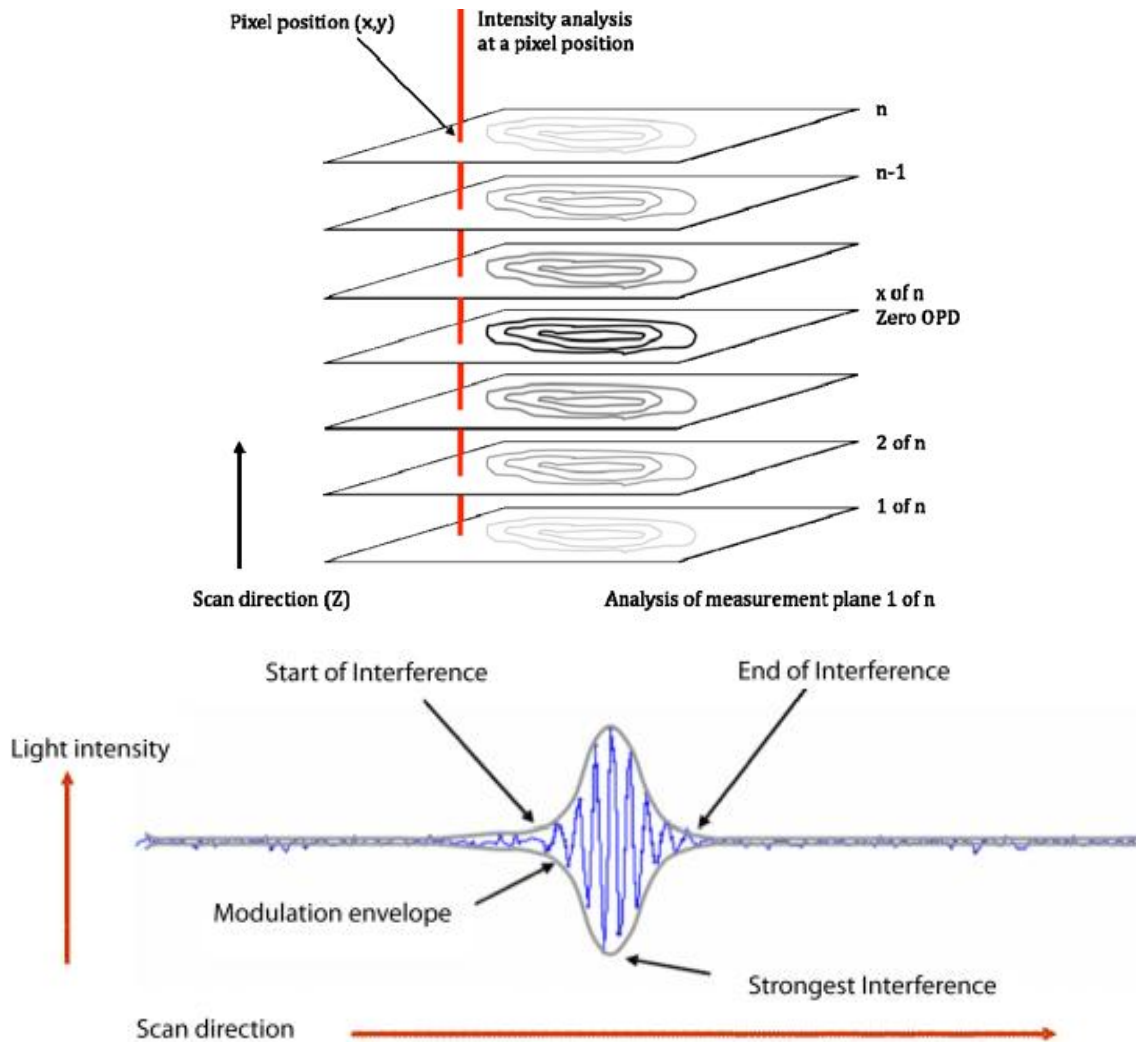


Figure 2.15: Analysis of the intensity on a pixel (top) and representation of the pixel intensity as function of scan direction (bottom).

2.3.4 Micro and Nano CMMs

The last instruments considered in this short review are the Micro and Nano Coordinate Measuring Machines. They have been developed from the CMMs used in conventional metrology and can be considered the only complete three dimensional measurement instruments available at the state of the art. Geometrical elements are measured acquiring a set of points, each one defined by three coordinates. Points are then fitted with the defined geometrical feature. Conventional high accuracy CMMs allows measurement uncertainty in the order of few micrometres. Tactile probes are too big, relative to the dimensions of parts realized by micro technology manufacturing processes. Hence, the use of conventional CMMs for dimensional and geometric characterization of micro components is therefore limited by the machine accuracy and the size of the probes (diameter of 0.2 mm). Recently, few groups

have developed coordinate metrology machines for dimensional metrology of micro components. The target accuracy was below 100 nm.



Figure 2.16: ISARA 400 NanoCMM developed by IBS.

The development was not a simply adjustment of conventional CMMs. The design has been characterized by several working principles different respect to the usual systems present in the CMM. For example displacement sensors, based on heterodyne interferometry or grating encoders replace, in such high accuracy machines, the traditional optical encoders.

Micro and Nano CMM have been designed in order to overcome problems related to temperature variations and deformations and the presence of noise and vibrations.

Contextually new miniaturized probing systems have been developed. The development of miniature touch probes has been difficult. In order to measure features with micrometric dimensions using a contact probes it is necessary that the probe is small enough. Also the forces applied during the contact have to be small. Even small contact forces result in high contact pressure because of the small area of application, causing damages of the surfaces of the probe and of the sample. Sticking between probe and sample can be in the order of contact forces resulting in large measurement errors. So, the developing of new probes resulted in the development of a complete new scan system.

An example of NanoCMM is the ISARA 400 (Figure 2.16) developed by IBS Precision

Engineering in the context of the project NanoCMM. The specifications are:

- measurement range of 400 mm X 400 mm X 100 mm;
- measurement uncertainty $U_1= 45$ nm, $U_3= 100$ nm;
- workpiece weight max 32 kg
- moving speed 20 mm/s

Isara has been designed reducing the error due to the violation of the Abbe principle. Three interferometers, aligned with the probe, measure the position of the table in which the sample is positioned. The instruments structure is made of granite and silicon carbide in order to have a long thermal stability and a stiff structure with relative low mass.

Even if NanoCMMs seem to be the best solution for three dimensional measurements at micro scale they are affected by several limitations and their use for quality control results not applicable. Limitations are related to their performance as presented, but there are also limitations that are not immediately evident.

The measurement with a nanoCMM follows the measurement procedures of a conventional CMM. Acquisition points are defined on the sample and the probe path is programmed. In conventional CMM it is possible to check the points acquisition procedure just watching the probe. In nanoCMM this is not possible because of the small dimensions of probe and features and it is necessary to rely on the CMM software. Moreover a wrong contact between sample and tip can occur resulting in a damage of probe or sample. For example, ISARA 400 is designed in order to prevent probe damage and when an emergency trigger occurs, the machine motion stop within 10 micrometres. In conclusion the measurements through nanoCMMs result to be complicated and full of risk. Even if three dimensional measurements can be performed, the process is not robust, so this kind of machine is not diffused.

2.4 From surface characterisation to coordinate metrology at micro scale

The first step in the field of the metrology at micro scale was done with the development of the surface metrology. In fact, surface metrology is the science of measuring small-scale geometrical features on surfaces: the topography of the surface. One of the first serious instruments for quantitative assessment of surface topography was developed in USA from Abbott et al. (1938). There was the feeling that the quality of the surface influenced the functionality of the surface. The instruments evolved with the possibility to filter, through analogic filters, the acquired profiles in order to describe the form, the waviness or the

roughness of the surfaces. Having the instruments able to measure the surfaces, the capability to quantify the measurement through numbers was needed, but representing the surface texture with a parameter, which number should be calculated? A profile represents a surface providing too much data, but using a single parameter there is the risk to give a not sufficient representation of the surface. Actually, the early analogue instruments had limited capability to provide numerical parameters. The average roughness value Ra and slope were possible.

Around 1970, taking advantage from the computing technologies, first digital commercial instruments appeared on the market. The possibility to have and manipulate the profile data led to a proliferation of parameters to describe the profiles and so the surfaces.

A further step in the surface texture measurement was made with the advent, in 1980s, of computers able to handle large amount of data and making areal measurement more practical. Commercial areal surface instruments gradually became available in the early 1990s. The problem was again how to use the data in order to describe the surface. Which parameters should be calculated? Which are significant? Initially, the approach for areal surface characterisation was similar to the approach used for the characterisation of surfaces through profiles. The surface is considered composed by three components: form, waviness and roughness, now called scale limited surfaces. Surfaces are described through statistical parameters.

The nanotechnology age required our ability to measure and to qualify micro and nanometre scale manufactured components. For example ultra-precision surfaces can be considered surfaces with micro and nano characteristics. In fact they are incredibly smooth, and the specifications of surface geometries are near atomic magnitude. Moreover, textures and features realized on surfaces can be considered as micro components. The need to measure and quantify geometric products at micrometre level, nanometre and atomic is leading the evolution of the surface metrology from: profile to areal characterization; stochastic to structured surfaces; and simple shapes to complex freeform geometries.

The available instrumentation adopt a wide range of principles including contacting stylus, phase-shifting interferometry, white-light interferometry, confocal microscopy, chromatic probe microscopy, structured light techniques, scanning electron microscopy, scanning tunnelling microscopy and atomic force microscopy.

The areal method wants to characterize the fundamental and functional topographical features of the surface, including assessment of texture shape and direction, estimation of feature

geometrical characteristics and differentiation between connected and isolated features. Nevertheless, areal methods are still connected to the concept of surface roughness. Surfaces are measured and evaluated through parameters giving a summary description of the surface, such as the number of peaks, the maximum peak height, etc.

The next step is to use the possibility to have measurements of area to obtain information on the dimensions and geometries presents on the surface, such as the height of holes, the width of a channels or the radius of spheres. This means apply the measurement techniques used in surface metrology in order to perform coordinate metrology.

2.5 International standards

In this paragraph, a review of the available international standards related to dimensional and geometric metrology is presented.

The ISO committee published several series of standard titled “Geometrical product specification (GPS)”. These standards contain useful information necessary to perform a quality control of a manufactured product. Standards cover the aspect of measurement from the definition of tolerances to the verification including the description of measuring instruments and procedures. Even if more than eighty standards are available and more than twenty are under development, there are no standards related to the measurement in the field of micro technology. So, no rules have been defined for metrology at micro scale, but general rule and guidelines developed for conventional metrology can be used with adaptations.

2.5.1 ISO Standards related to surface metrology

Standard series regarding the surface metrology, in particular ISO 4287:1997 and ISO 4288:1996 can be used for the assessment of the roughness value, even in micro features. These standards have been developed more than ten years ago. They have been based on the assessment of surface roughness through the use of stylus profilometers. As said before, these measurement instruments cannot be applied to the measurement of micro features, but principle defined in ISO 4287 and ISO 4288 should be taken into account and applied to the surface measurement through other instruments. Fortunately, ISO is publishing a new series of standards related to the assessment of surface texture. The series is the ISO 25178 and consider the assessment of surface texture through areal methods considering also instruments

for metrology and surface assessment at micro scale. The standard published at the moment are ISO 25178 Geometrical product specifications (GPS)- Surface texture: Areal:

- Part 2:2012 Terms, definitions and surface texture parameters;
- Part 3:2012 Specification operators;
- Part 6:2010 Classification of methods for measuring surface texture;
- Part 601:2010 Nominal characteristics of contact (stylus) instruments;
- Part 602:2010 Nominal characteristics of non-contact (confocal chromatic probe) instruments;
- Part 701:2010 Calibration and measurement standards for contact (stylus) instruments;
- Part 71:2012 Software measurement standards.

This is the first series considering the assessment of surface topography through the areal method. General principles included in parts 2, 3 and 6 can be applied to any instrument measuring the surface topography scanning an area, included Atomic Force Microscopes, for example. Part 601 consider again the stylus instruments. Part 602 consider the non-contact instruments for the topography acquisition. This series of standards, even if at the beginning of their evolution, represent a big breakthrough in the field of surface metrology. It is interesting to notice that many drafts are going to be published as standard in the near future. Parts 603, 604, and 605 regard the use of other non-contact instruments for surface metrology. The standards under development are:

- ISO/DIS 25178-1 Geometrical product specifications (GPS) - Surface texture: Areal - Part 1: Indication of surface texture;
- ISO/NP 25178-603 Geometrical product specifications (GPS) - Surface texture: Areal - Part 603: Nominal characteristics of non-contact (phase-shifting interferometric microscopy) instruments;
- ISO/DIS 25178-604 Geometrical product specifications (GPS) - Surface texture: Areal - Part 604: Nominal characteristics of non-contact (coherence scanning interferometry) instruments;
- ISO/DIS 25178-605 Geometrical product specifications (GPS) -- Surface texture: Areal -- Part 605: Nominal characteristics of non-contact (point autofocus probe) instruments;
- ISO/CD 25178-72 Geometrical product specifications (GPS) - Surface texture: Areal - Part 72: XML file format x3p;

2.5.2 ISO Standards related to coordinate metrology

ISO 17450-1:2011 Geometrical product specifications (GPS) -- General concepts -- Part 1: Model for geometrical specification and verification, has been considered as reference in this research work. The standard defines the general concept for specification and verification of workpieces. Concepts expressed in the standard have been used as reference in chapter 5.

The methodology presented in ISO 17450-1 is here resumed.

A process of design of a workpiece is considered. A workpiece is designed focusing on the functional requirements and defining the specification necessary to meet the requirements.

The designer first specifies a “workpiece” with a perfect form and dimensions necessary to meet the functional requirements. This is called the “nominal model”. Nominal model contains nominal features with nominal dimensions and form that are impossible to produce or inspect.

From the nominal model, the designer imagines how could be the real workpiece and which variations could be expected on the real surface of the workpiece. A second model, representing the imperfect geometry of the real workpiece is defined. This is called the “non-ideal surface model” or “skin model”. On the “skin model”, the designer define the geometrical specification. The geometrical specification is the design step where the permissible deviations of a set of characteristics of a workpiece is stated. Moreover, using the skin model, the designer defines the steps for the verification of specifications. The steps are:

- partition: it is used to identify a portion of a geometrical feature;
- extraction: it is used to identify a finite number of points from a non-ideal feature;
- filtration: it is used to distinguish between roughness, waviness, structure and form;
- association: it is used to fit ideal features to non-ideal features;
- collection: it is used to identify and consider some features together;
- construction: it is used to build ideal features from other features;
- evaluation: it is used to identify either the value of a characteristic or its nominal value and its limit or limits;
- verification: it is the provision of objective evidence that the workpiece fulfils the specification.

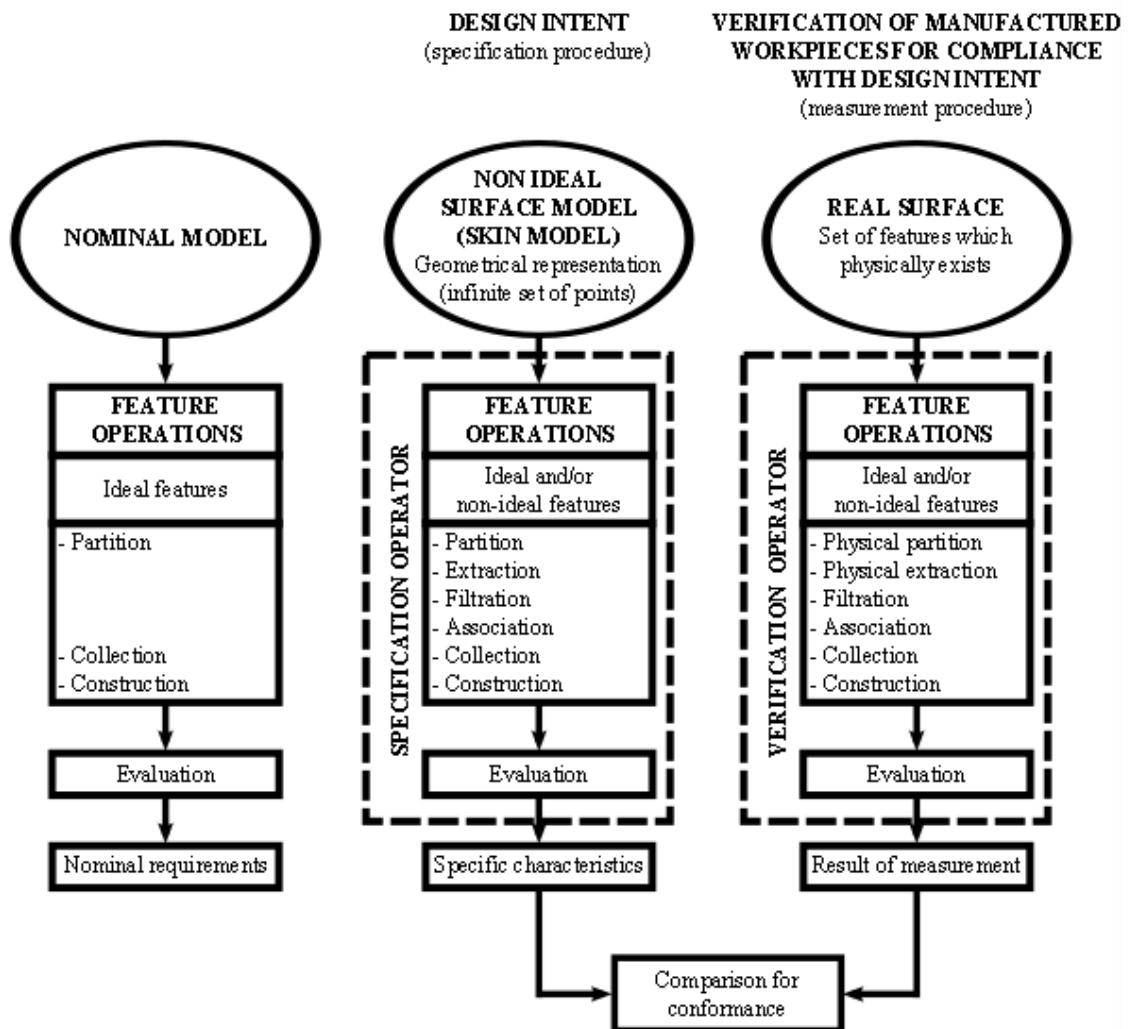


Figure 2.17: Scheme of the model for geometrical specification and verification. Nominal model and design intent procedures are presented with the comparison between specification and measurement procedures [13].

In Figure 2.17 the process of workpiece design, geometrical specification and verification is represented. It is interesting to notice that the operations of measurements should be defined during the design together with tolerances. Then, measurement procedure should be physically performed on the real workpiece. The results of the measurements are compared with the specification in order to characterise the quality of the workpiece.

The method here presented is the basis of any dimensional and geometrical verification and could be applied in any case. Unfortunately, as will be presented in chapter 5, some adjustments are necessary in the case of metrology at micro scale.

2.5.3 Other ISO standards

Other ISO standards fundamental for the metrology are the standards related to the uncertainty evaluation and in particular:

- ISO 13005:1999 Guide to the expression of uncertainty in measurements;
- ISO 14253-1:1998 Geometrical Product Specifications (GPS) - Inspection by measurement of workpieces and measuring equipment - Part 1: Decision rules for proving conformance or non-conformance with specifications;
- ISO 14253-2:2011 Geometrical product specifications (GPS) - Inspection by measurement of workpieces and measuring equipment - Part 2: Guidance for the estimation of uncertainty in GPS measurement, in calibration of measuring equipment and in product verification;
- ISO 14253-3:2011 Geometrical product specifications (GPS) - Inspection by measurement of workpieces and measuring equipment - Part 3: Guidelines for achieving agreements on measurement uncertainty statements;

Considering metrology at micro scale, the main issue regarding the uncertainty assessment is related to the traceability of the measurements. Calibrated physical standards for instruments such as atomic force microscopes, confocal microscopes and white light interferometers have not been yet developed. Calibration grids and steps realized in silicon are available, but a method to give traceability, especially in non-contact measurement is not ready available.

So, even if ISO standards define general rules for uncertainty assessment they can't be easily applied because of the lack of traceability for measurements at micro scale.

NanoCMMs can take advantage from the old the consolidated knowledge of CMM. Moreover, ISO 10360 and ISO 15530 series gives some specific hints for the performance verifications and uncertainty evaluation when working with CMM. Furthermore, different error sources are present when measuring at micro scale because of the influence of physical phenomena that are not considered when working in conventional CMM. These error sources must be taken into account in the uncertainty evaluation. But, as said before the application of NanoCMMs to the measurement of micro components is not so easy, it is time consuming and the advantages do not justify the big effort that has to be put for the measurement.

2.6 Conclusions

A review of instruments available at the state of the art to perform metrology at micro scale has been presented. Instruments for 2D and for 3D metrology have been considered.

Each instrument presents different characteristics. It is not possible to identify a key technology for the dimensional and geometrical characterization of micro components. Different technologies have to be combined in order to give a full characterisation of samples. Two technologies have been identified as promising: the atomic force microscopy and the optical profilometry. Atomic force microscopy is the measurement technology that allows obtaining the highest resolution; the resolution is near to the atomic scale. Optical profilometry allow a big range of measurements. Measurements are fast and allow integrating the technology in a manufacturing chain. The research work has been concentrated mainly on these two technologies. Finally, a review of the international standards shows that there are not specific standards related to the metrology at micro scale. Standards used in conventional metrology can be used with adaptation.

Chapter 3

Dimensional quality control of replication at the micrometre scale

3.1 Introduction

Replication is extensively used in micro manufacturing. Large majority of processes available for precision and micro-material removal are relatively slow: creating and replicating a master is often the only profitable way for mass production. Another aspect of replication processes is connected to material selection: manufacturing technologies exploit their best performance only when applied to specific materials (e.g. electro discharge machining is not suited for polymer machining, milling is difficultly applied to brittle materials, or diamond cutting is not adequate for iron alloys). In all of these cases, making the workpiece using a first material optimized for the specific chosen technique and then replicating the geometry with a second material which better answers to the workpiece functionality requirements is a way to optimize the manufacturing process.

Hence, replication processes are involved at different levels of the production chains, from manufacturing to final products. The main drawback for implementation of replication in a process chain is the unavoidable loss of accuracy which is intrinsic to each replication step. Indeed, in any replication, there is loss of information during the shape transfer from the master to the copy [3]. Usually the geometry is reproduced only within a certain level of accuracy, and surfaces topography is not correctly replicated. The problem is evidently amplified whenever more than one replication step is introduced within the process chain as represented in Figure 3.1. Therefore, in order to optimize the quality of the manufacturing process chain it is important to properly monitor replication steps: minimizing the difference between the master and copies allows assuring that the final product conforms to quality specifications [14, 15]. A study on the quality control of replicated surfaces is presented. The work is based on simulated data sets, resembling different surfaces, and in particular:

- master data sets resembling a surface with cylindrical and rectangular micrometric features (here on referred to as *structured surfaces*),
- master data sets resembling a generally planar surface with roughness and/or waviness contribution presenting no systematic distribution (here on referred to as *unstructured*

surfaces),

- data sets of replicas simulated on both structured and unstructured surfaces (here on referred to as *replicas*),
- data sets resembling the output of different measuring instruments on both structured and unstructured surfaces or on replicas (here on referred to as *measurements*).

Techniques such as roughness analysis and cross correlation were applied to study the effect of the replications on the surface. Obtained results are discussed in order to identify instruments and analysis techniques that are sensitive to the replication process providing a reliable instrument for the quality control in the production of parts through replication processes.

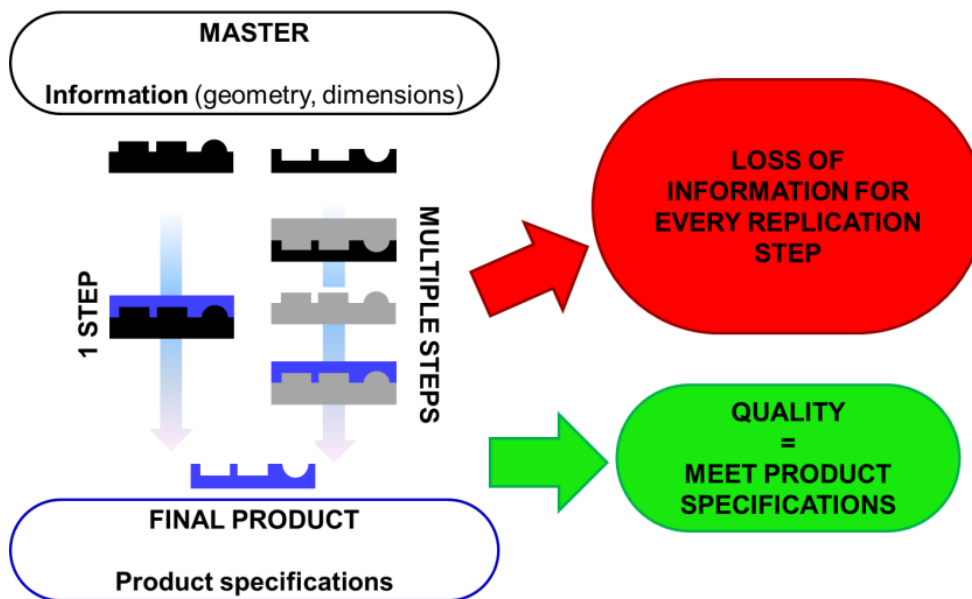


Figure 3.1: Schematic representation of a manufacturing process through replication.

3.2 Replication analysis at the micro scale

Geometrical features must be reproduced accurately within tolerances. Surface characteristics and parameters, as for instance roughness or micro-geometry, influence in different ways functionality: tribological and mechanical behaviour, optical properties, appearance and tactile sensations transmitted by the surface. A correct replication eventually allows obtaining the desired surface properties in the final product. In order to control the replication quality, mould and replication surfaces must be analysed and compared.

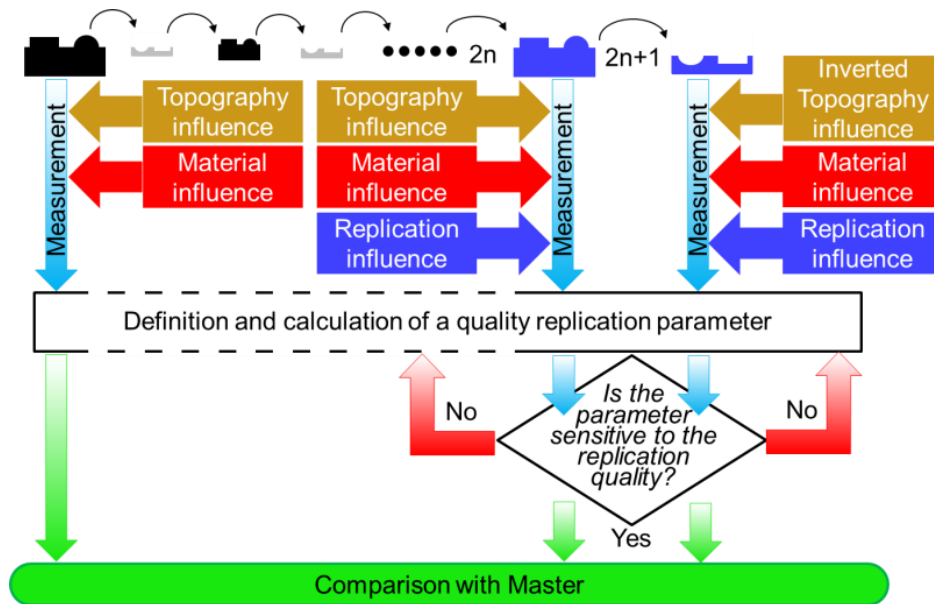


Figure 3.2: Proposed approach for the study of the quality of replication considering factors influencing the process.

Different strategies for analysis and control of micro geometrical features surface replication are documented in literature, such as evaluation of roughness parameters, geometrical parameters, cross correlation, Fourier transform, etc. The choice of the analysis strategy depends on the product functionality that has to be controlled and, strictly related, there is the choice of the measurement instrument. Therefore the definition of an appropriate parameter to monitor a given replication process is the result of an optimal definition of the couple instrument-functionality. In fact as shown in Figure 3.2, performing measurements at different level of the replication chain, results can be influenced by different factors. Measurement results can be influenced by the material that is different from master to replica. Results are influenced by the topography that is change from the master to the final product. In particular there is an inversion of the topography every step of replication. Finally, measurement results are influenced by the quality of replication. The aim of this study is to understand if it is possible to identify a set of parameter that are sensitive only to the replication in order to monitor the whole process through the measurement of some parameters without perform a full characterisation of the workpiece.

Many metrological systems are available for dimensional and geometrical characterizations at the micro scale. Scanning probe microscopes (SPMs) consent to perform measurements with sub-nanometre accuracy providing 3D information about surfaces topography. Of particular

interest are those instruments that can perform non-destructive measurements even on high aspect ratio structures such as 3D optical profilometers (OPs) that produce fast non-contact measurements but are limited by the difficulty in achieving good reflection signal from surfaces that present high local slope or are reflective or transparent to the light source. Scanning electron microscopy (SEM) measurements allow resolutions on the nanometre scale, but must be used measuring conductive materials. Their major limitation is that, without additional measurement data and specific software tools, they perform only 2D measurements [1, 16].

3.3 Generation of simulated data sets

Data sets of both structured and unstructured surfaces (as defined in paragraph 3.1) were generated for preliminary investigations. Two different data sets were developed with lateral dimensions of $65.1 \times 74.7 \mu\text{m}$ and maximum vertical size of $2 \mu\text{m}$ (see Figure 3.3). The structured surface is characterized by the presence of well-defined geometrical features: 5 positive and 5 negative rectangular features with constant depth ($1 \mu\text{m}$) and varying width (from $10 \mu\text{m}$ to $1 \mu\text{m}$) and 6 circular features (3 positive and 3 negative, height $1 \mu\text{m}$ and diameter $5 \mu\text{m}$).

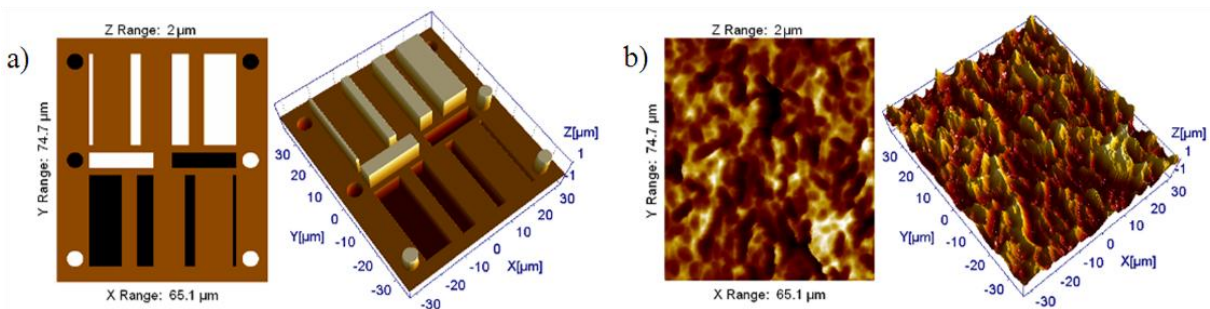


Figure 3.3: Data sets developed for the study: a) structured topography and b) unstructured topography.

Rectangular features are placed at a constant distance in order to realize a periodical structure. Periodical structures can be studied through a Fourier analysis. The width of the features is different in order to highlight the performance of different instruments when dealing with narrow and large structures (tip convolution for SPMs, reflection or shadowing for optical

profilometers, and shadowing for SEMs). These kinds of structures allow amplifying replication artefacts as for instance the filling of channels during a polymer injection process. The unstructured surface has an average roughness $S_a = 698$ nm. Such surface is a particularly interesting benchmark for SPMs and optical profilometers tests, providing a good base for tests with roughness parameters, cross correlation and Fourier transform. Data sets were generated to simulate both master and replicas. Replicas (namely from 1 to 5): simulated different degrees of replication accuracy, being *replica 1* a high accuracy replication and *replica 5* a low quality replication. In order to simulate an actual replication, the five grades of accuracy were artificially generated considering different levels of cavity filling, smoothing of edges and air inclusions. Additionally in the case of unstructured surface, simulated replicas where exhibiting also a lateral distortion, as it may happen when during the demoulding process, excessively high forces can cause a sample stretching distortion.

Furthermore, three categories of measuring instruments were simulated:

- optical profilometers (OPs),
- scanning probe microscopes (SPMs),
- scanning electron microscopes (SEMs).

Table 3.1: Simulated measurement artefacts and distortions for any specific instruments.

OP	SPM	SEM
Void pixels / poor reflection	Tip convolution	Shadowing
Void Pixels / high slope region	Thermal drift	Edge Bloom
Noise	Creep	Noise
Spikes	Noise	
	Overshoots	

Measurements with the different instruments were simulated including artefacts and distortions typical of the specific instruments as described in Table 3.1.

All data sets were generated by means of a commercial software (SPIP™, by Image Metrology A/S, Denmark); replica and instrument simulations and cross correlation analysis

were carried out taking advantage of specific routines developed and implemented in the software by one of the authors [12].

3.4 Surface characterization and comparison

Different data analysis approaches can be used in order to extrapolate quantitative information from the simulated topographies. Specific analyses have to be defined on the basis of the specific functionality relevant for the workpiece. Most important analysis, considered within the present work, is:

- 1) Roughness parameters or areal statistical parameters, which give a description of the surface texture and allow comparing two or more surfaces. These parameters, together with the Abbott-Firestone curve, describe the distribution of peaks and valleys on the topography. Because of the statistical nature of the parameters, the use of this technique is normally helpful when describing an unstructured surface, but it is less useful whenever well-defined isolated geometrical features are present on the surface. In this work the parameters considered were S_a , S_q , S_v , S_p , S_{pk} , S_k , S_{vk} as defined in ISO 25178-2 [17, 18].
- 2) Cross correlation index, applied to compare pairs of data sets. This index indicates how much two surfaces are overlapping, but it does not allow identifying where differences between master and replication surfaces are actually located [19].
- 3) Fourier related parameters. Such analysis gives information about the presence of periodic distributions and surface orientation. In particular, the comparison of the Fourier analysis between the master and the replication allows to control that the periodicity of the structure has been preserved during the replication process.

3.5 Results

Results related to unstructured surfaces are reported in Figure 3.4 (first line). Values for replicas are reported as a percentage of the same value estimated in the master that is considered the reference surface.

For an unstructured surface, the use of statistical roughness parameters is normally recommendable for analyses. These parameters are sensitive to the loss of surface quality from master to replica, but their variations result small. The main differences between master and replicas are in correspondence of highest peaks and deepest valleys, therefore only in a

small portion of the total area: for these reasons they have only a negligible influence on parameters which are estimated in the whole areas, such as average roughness S_a . On the contrary, graphs show that cross correlation provide a useful index well describing distortions occurring from the master to the replica. Furthermore, roughness parameters are not sensitive to simulated horizontal distortions and present the same value obtained without distortions. This is a well-known phenomenon, due to the fact that amplitude parameters are estimated only computing vertical elevation, and they are therefore insensitive to horizontal variations. On the other hand, cross correlation index and the wavelength of the surface calculated through Fourier analysis presented relevant variations (Figure 3.4). As a general statement, the use of cross correlation method is recommended to describe replication accuracy when single or coupled horizontal and vertical distortions occur. Fourier analysis is also apt to detect and monitor lateral distortions, also in case of non-periodical surface distributions, but on the other hand its behaviour is not influenced by vertical distortions, as clearly evidenced by the tests on structured surfaces.

The use of areal statistical parameters is normally not recommended whenever structured surfaces and isolated features have to be analysed. However, parameters related to the Abbott-Firestone Curve are representative of the bearing area regardless peaks and valleys distribution. Considering SPM simulations, the statistical parameters calculated in the master surface and in the replication surface, Spk , Sk and Svk are those that have shown the largest variations (see Figure 3.4, second line). In particular Spk and Svk values decrease while decreasing the quality of the replicas. Conversely, Sk is increasing from replica 1 to replica 5. This behaviour is different from the expected. Usually Sk decrease while the bearing surface increase, but this is true only for unstructured surfaces. Considering structured surfaces, the poor replication of the highest peaks and the lowest valleys causes the modification of the into an “unstructured surface”. This step happens before the surface become flat, so Sk increase before to decrease. Hence, low performance features replication generates a surface that can be monitored through Svk and Spk decrease and Sk increase. Other roughness parameters are less sensitive to the flattening of the surface. The variation of S_a , for example, is negligible. When calculating S_a , high local surface differences between master and replications (peaks and valleys), are considered distributed in the whole surface causing a small variation of the parameter even if the quality of replicas is low.

On the other hand, the same analysis performed on an optical profilometer didn't give the

same results. This is mainly due to the fact that when measurements are carried on through an optical profilometer, surface regions locally overcoming maximum detectable slope (typically 30-40 degrees) are giving only a noise signal (or a so called “void pixels” portion, meaning a lack of data). Therefore in the case of optical profilometers, mainly flat regions are recognised: i.e. mainly top and bottom plateaux (when not shadowed) of the geometric structures and the mean plane. Therefore it is clear that, while a slight correlation with replication quality is still present when Spk and also Svk values are analysed, a lower correlation is noticed from Sk or Sa parameter analyses.

Interesting results were given by the cross-correlation index calculated between master and replicas. Significant variations were recognized with SPM (up to 48%), OP and SEM. The simulation however didn't consider the difficulty in relocating exactly the same surface portion (in master and in replicas), which is a factor particularly relevant and influent in cross-correlation computation.

Fourier analysis correctly gave only negligible variations (<1%, comparable with pixel resolution) on detected wavelengths of periodical structures for all of the three instruments (in Figure 3.4, for readability reason, results are reported only in the case of SEM simulation).

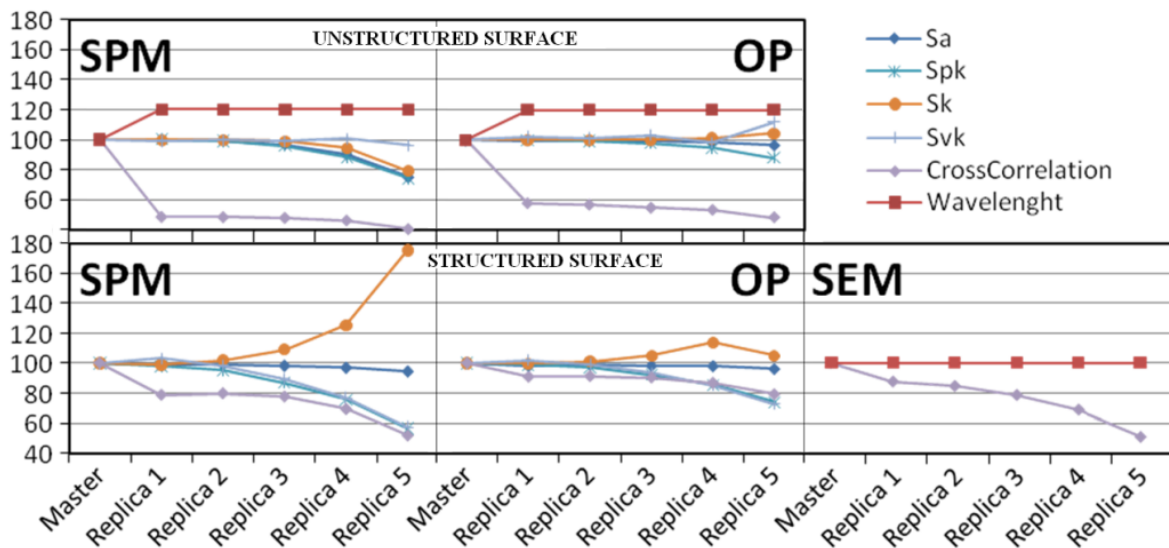


Figure 3.4: Parameters variations analysing different replicas in case of unstructured surface (first line) and structured surface (second line). Variations for different parameters (y-axis) are expressed as a percentage of the same parameter estimated in the master.

3.6 Application to real case

The replication process analysis explained before has been applied to a real case. The considered surface is a structured surface, a pattern of channels presented in Figure 3.5. The nominal spacing is 8 μm and the nominal dimensions of the grooves are width 5 μm and height 20 μm . The nominal model of the surface has been considered as a soft gauge master. The measurement of the master through an optical profilometer has been simulated following the procedure explained in the paragraph 3.2. Replications with three level of quality (good, medium, bad) have been considered and their measurement through an OP has been simulated. Results are reported in Table 3.2.

Measurements using an optical profilometer have been performed on actual surfaces of master and replica. Only one replication was available for measurement. S_a and S_q were not considered because, following the previous considerations, they are not indicative of the quality of replication when considering structured surfaces. S_k , S_{pk} and S_{vk} have been considered as indicator of the replication quality.

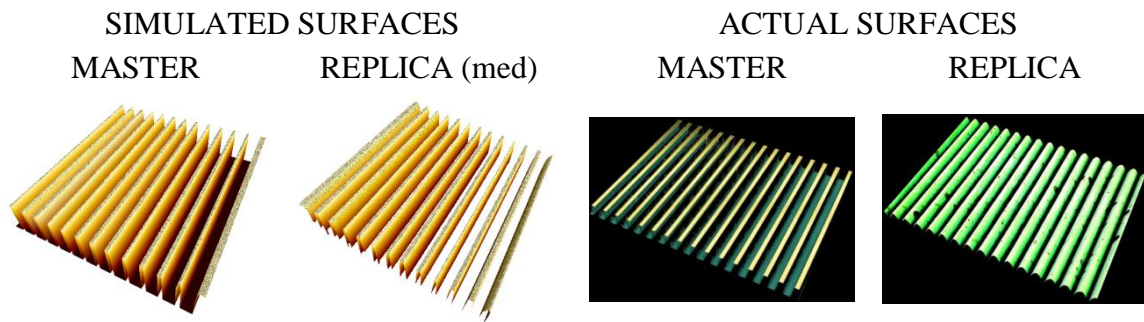


Figure 3.5: Image topographies of the surfaces considered as real case.

Analysing the results obtained through the simulation we can reach the following considerations.

The values between master and the good replica measurement simulation are quite similar except the values of S_{pk} and S_{vk} that result inverted. This mean that the results are sensible to the step of replication (in this case is an odd step). Also the surface structure is influencing the results. In fact, the surface of the master is described by S_{pk} and S_k , while the value of S_{vk} is near 0. Considering replications with decreasing quality it is reasonable think that S_{pk} (S_{vk} in replications) will decrease. S_k will increase. S_{vk} (S_{pk} in replications) will increase because of

the transition between “structured” and “unstructured” surface, as described in the previous paragraph for the parameter Sk. Simulation results follow the expectation.

Considering the real measurements on actual surfaces of master and replica, Svk and Spk follow the behaviour described through the simulations indicating that the quality of replication is poor. Sk is not following the expected behaviour, but as already stated, this is due to the fact that the optical profilometers are limited in the acquisition of tilted surfaces. This effect can be simulated only partially and the indication given by Sk should be considered with attention.

Table 3.2: Results of simulated measurement of master and replica and results of measurements on actual master and replica.

	SIMULATED SURFACES				ACTUAL SURFACES	
	MASTER	REPLICA (good)	REPLICA (med)	REPLICA (bad)	MASTER	REPLICA
Spk	31166 nm	48 nm	41 nm	4966 nm	46204 nm	357 nm
Sk	1262 nm	1174 nm	1932 nm	14268 nm	453 nm	151 nm
Svk	76 nm	12915 nm	12018 nm	1915 nm	79 nm	206 nm

3.7 Conclusions

In this work artificial data sets were used to simulate replicated surfaces and to test their measurements through different instruments. The results were analysed in order to compare the quality of surface replication from the master to the final part leading the following conclusions.

Simulations of replication can help to select the correct instrument and measurement settings.

The behaviour of the roughness parameters related to the Abbot-Firestone curve can monitor the quality of a replica if the part presents isolated features extended along a direction perpendicular to the surface.

Cross correlation index provides a description of the similarity between master and replications. When it is combined with a Fourier analysis can also highlight the presence of distortions during demoulding. However, the cross correlation is limited by the necessity to obtain two measurements of the same portion of the surface in the master and the replica.

When analysing surfaces obtained through replication it is necessary to pay attention to the replication step. Results can be influenced by an odd or even step of replication.

Chapter 4

Thermal drift study on Scanning Probe Microscopes

In this chapter are presented some studies related to the thermal drift distortion in scanning probe microscopy and in particular in atomic force microscopy. Thermal drift affect in particular high resolution measurements (typically slow). The relation between temperature, drift and scan parameters have been analysed in order to find solution to improve the quality of measurements. A comparison between some commercial scanning probe microscopes has been performed in order to study the

4.1 Errors in SPM / AFM measurements

A classification of the main distortions occurring during AFM imaging is here presented. In the atomic force microscopes there are four main sources of distortion: the “scanning system, the probing system, the environment, and the image processing. Table 4.1 reports a classification of the main error sources. Some of the most influencing errors are discussed and modelled in the following paragraphs.

Table 4.1: Main AFM distortions [12].

SOURCE	DISTORTION
scanning system	scaling crosstalk non linearity overshoot mode switching
probing system	convolution unsampled parts tip artefacts
environment	drift noise
data processing	filtering leveling

4.1.1 Scaling

AFM working principle is based on a scanner providing lateral movement to the probing system. The lateral movement, usually performed through piezo actuators, is electronically controlled. A certain voltage step is applied to the piezo causing a relative displacement of the probe. The position of the tip is extrapolated knowing the characteristic of the actuating system. Open-loop system rely on this information and the x, y coordinates of the scanned systems are defined by the supplied voltage. Closed-loop systems are provided with a feedback control in the horizontal x, y plane, and tip position is monitored and adjusted. In both cases the measured position doesn't correspond to actual tip position leading to a distortion generally proportional to the scanned measured range (see Figure 4.1), and that can be described as a linear scaling of scanned topographies.

Calibration operations are used in order to quantify and correct systematic deviations of the measuring device, providing traceability to the SI-unit of length. Calibrated standards consisting of dimensional gratings with various arrangements of structures, allowing for lateral and vertical calibration are used. A mathematical model can be introduced in order to describe the scaling problem. It is assumed that the fast scanning direction coincides with the x axis. It is assumed that the process leads only to linearly distorted images, the correct tip position is given by:

$$\begin{bmatrix} x \\ y \\ z \end{bmatrix} = \begin{bmatrix} c_{xx'} & 0 & 0 \\ 0 & c_{yy'} & 0 \\ 0 & 0 & c_{zz'} \end{bmatrix} \cdot \begin{bmatrix} x' \\ y' \\ z' \end{bmatrix} \quad (4.1)$$

and using the compact notation:

$$M_{xyz} = C_{xyz} \cdot M'_{xyz} \quad (4.2)$$

M'_{xyz} is the vector of the measured coordinates of the tip. Measured coordinates are noted with an apostrophe.

C_{xyz} is the calibration matrix where the terms on the principal diagonal represent the scaling factors:

$$c_{xx'} = \frac{\partial x}{\partial x'} ; c_{yy'} = \frac{\partial y}{\partial y'} ; c_{zz'} = \frac{\partial z}{\partial z'} \quad (4.3)$$

M_{xyz} is the vector of the corrected coordinates of the tip.

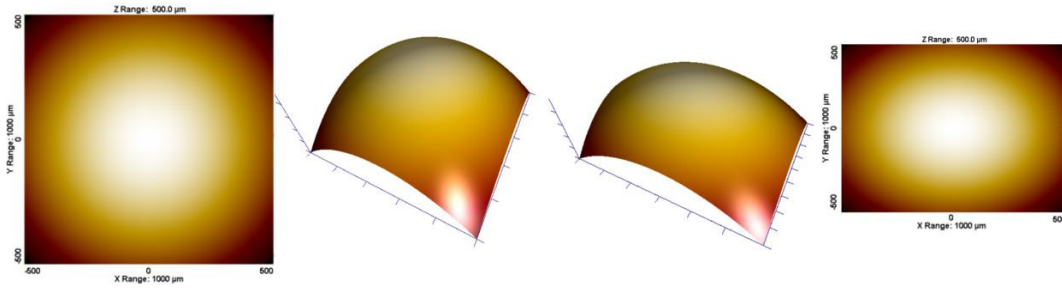


Figure 4.1: Scaling occurring to a spherical structure

4.1.2 Crosstalk

The crosstalk (Figure 4.2) is the presence of deviations from orthogonally between the axes. This distortion occurs when the movements of the tip along one direction generate uncontrolled shifts along the other directions. The problem can be resembled as an angular misalignment between instrument and the ideal reference coordinate axes system. Open-loop AFMs suffers of this distortion. Closed-loop and instruments suffer in a minor way.

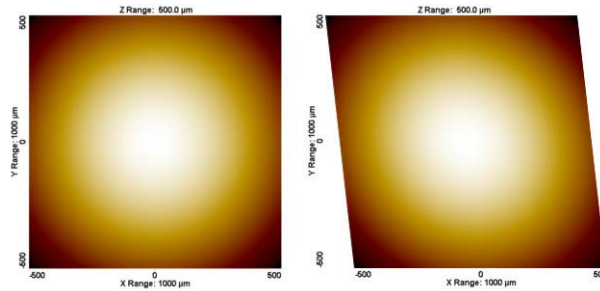


Figure 4.2: Representation of crosstalk distortion.

It is assumed that the imaging process leads only to first order squareness distortions. following the notation used previously the correct tip position is now given by:

$$\begin{bmatrix} x \\ y \\ z \end{bmatrix} = \begin{bmatrix} 1 & c_{xy'} & c_{xz'} \\ 0 & 1 & c_{yz'} \\ 0 & 0 & 1 \end{bmatrix} \cdot \begin{bmatrix} x' \\ y' \\ z' \end{bmatrix} \quad (4.4)$$

The terms lying over the diagonal represent the crosstalk correction factors. They can be evaluated as follows:

$$c_{xy'} = \frac{\partial x}{\partial y'}; c_{xz'} = \frac{\partial x}{\partial z'}; c_{yz'} = \frac{\partial y}{\partial z'} \quad (4.5)$$

4.1.3 Non-linearity

The linear model discussed in paragraph 4.1.1 is in practice applicable only to closed loop AFM scanners, whose non linearity is in the order of 0.01% or less. Open loop AFM scanners, provide not linear distortion in images. Scanners based on piezoelectric actuation, the most diffused systems, suffer from not linear distortion as hysteresis and creep.

Because of differences in the material properties and dimensions of each piezoelectric element, AFM scanners respond differently to different applied voltage. This response can be measured as the ratio between the piezo movement and the piezo voltage. The ratio is not constant or linear. Piezo scanners are more sensitive (i.e. a larger movement per volt) at the end of the scan line than at the beginning. The forward and reverse scan directions behave differently and display hysteresis between the two scan directions. An example of these effects on AFM images is simulated by the waffle image in the Figure 4.3 a):

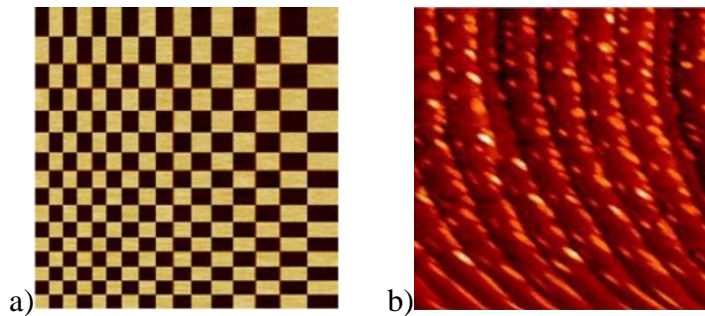


Figure 4.3: a) representation of hysteresis distortion; b) 60 nm STM image of the Au(11,12,12) surface representing creep distortion. At the bottom of the image, the steps are not straight and Co islands are elongated due to creep of the piezoelectric ceramics.

Creep can be seen as the drift of the piezoelectric actuator after an offset voltage is applied usually occurring when large changes are imposed in x or y direction. When a large offset voltage is applied, the answer of the scanner is not immediate. The majority of the offset distance is moved quickly, and then slowly moves over the remainder. Creep causes a change of the scan scale and of the position of the scan centre. It appears in the image as an elongation and stretching of features in the direction of the offset for a short period of time

after the offset. An example of creep is shown in the image of a dimensional calibration standard (Figure 4.3 b)). The tip was scanning from the bottom to the top of the image. Creep decreases logarithmically, settling out by the end of the scan. What operators usually do in order to avoid creep effects into quantitative measurements is to cut the affected zones out and perform calculations over zones where creep effect is negligible. Alternatively it can be reduced by offsetting beyond the desired point and then offsetting back to the desired initial measuring point.

A combination of non-linearity associated with coupling between the vertical axis and the x-y directions is frequent, known as bow distortion (Figure 4.4.). This is a non-linear image artefact that has the appearance of a false curvature superimposed to the actual specimen topography. This kind of artefact is not due to hysteresis phenomena, but to the particular probe movement, associated with tube scanner architectures. In fact the tip raster scan pattern is achieved by lateral bending of the piezo-tube: this movement is not horizontal but follows a curved trajectory with a radius of curvature generally in the order of some tens of millimetres. The influence of bow is negligible when measurements are performed in reduced scan ranges, but gets more severe as the scanning range increases.

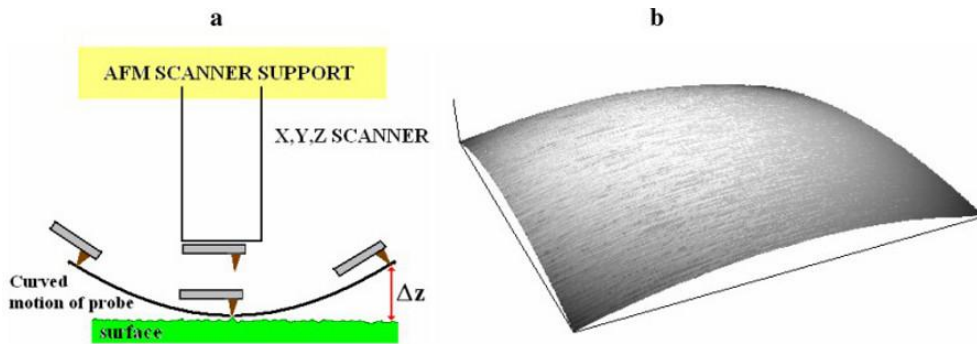


Figure 4.4: A representation is given of the spherical/paraboloidal movement (depending on the scanner architecture) causing bow

Assuming that the imaging process is already compensated for first order distortions, the correct tip position is now given by (4.6):

$$\begin{aligned}
 \begin{bmatrix} x \\ y \\ z \end{bmatrix} &= \begin{bmatrix} x' \\ y' \\ z' \end{bmatrix} + \begin{bmatrix} C_{xx'^2} & C_{xy'^2} & C_{xz'^2} & C_{xx'y'} & C_{xx'z'} & C_{xy'z'} \\ C_{yx'^2} & C_{yy'^2} & C_{yz'^2} & C_{yx'y'} & C_{yx'z'} & C_{yy'z'} \\ C_{zx'^2} & C_{zy'^2} & C_{zz'^2} & C_{zx'y'} & C_{zx'z'} & C_{zy'z'} \end{bmatrix} \cdot \begin{bmatrix} x'^2 \\ y'^2 \\ z'^2 \\ x'y' \\ x'z' \\ y'z' \end{bmatrix} + \\
 &+ \begin{bmatrix} C_{xx'^3} & C_{xy'^3} & C_{xz'^3} & C_{xx'^2y'} & C_{xx'^2z'} & C_{xx'y'^2} & C_{xx'y'z'} \\ C_{yx'^3} & C_{yy'^3} & C_{yz'^3} & C_{yx'^2y'} & C_{yx'^2z'} & C_{yx'y'^2} & C_{yx'y'z'} \\ C_{zx'^3} & C_{zy'^3} & C_{zz'^3} & C_{zx'^2y'} & C_{zx'^2z'} & C_{zx'y'^2} & C_{zx'y'z'} \end{bmatrix} \cdot \begin{bmatrix} x'^3 \\ y'^3 \\ z'^3 \\ x'^2y' \\ x'^2z' \\ x'y'^2 \\ x'z'^2 \\ x'y'z' \end{bmatrix} + \sigma \begin{bmatrix} x'^3 \\ y'^3 \\ z'^3 \\ x'^2y' \\ x'^2z' \\ x'y'^2 \\ x'z'^2 \\ x'y'z' \end{bmatrix} \quad (4.6)
 \end{aligned}$$

or using the compact notation:

$$M_{xyz} = C_{xyz}^{(1)} \cdot M'_{xyz} + C_{xyz}^{(2)} \cdot M'_{xyz} + C_{xyz}^{(3)} \cdot M'_{xyz} + \sigma(M'_{xyz}) \quad (4.7)$$

Where:

- $C_{xx'^2}$; $C_{xx'^3}$; $C_{yy'^2}$; $C_{yy'^3}$, $C_{zz'^2}$; $C_{zz'^3}$ represent second and third order non-linearities along the three coordinate axes;
- all the other coefficients describe second and third order non-linear coupled interaction (i.e. cross correlation between axes);
- $C_{zx'^2}$; $C_{zy'^2}$; $C_{zx'^3}$; $C_{zy'^3}$, represent the second and third order parameters of the paraboloid that best fits the bow deformation.

Not all of the coefficients in (4.6) have the same importance and influence for the instrument characterization.

4.1.4 Other errors

The main errors occurring during AFM measurement have been mathematically modelled in the previous paragraphs. The remain errors, listed in Table 4.1, have minor influence on the measurement results. They are here summarized. More details are reported in [12].

Overshoot is a bad compensation of hysteresis and creep in the piezoelectric ceramic that moves the cantilever

in the motion perpendicular to the surface, the vertical motion. The problem is often observed when measuring micro-fabricated structures such as step-patterns of silicon wafers. The result is an over-extension of the step in the proximity of the edge.

Mode switching distortion appears when recording images with an AFM using the intermittent mode. Artefacts appears as unexpected height shifts when the mode switch between contact and no contact mode.

AFM measurements are the result of scanning over a surface using a mechanical probe of finite dimensions, and the resulting topography includes features of both the measurand and the probe shape. This interaction is normally known as convolution effect and introduces distortions that are particularly evident whenever structures with sharp details are measured in the nanometre range.

Unsampled parts are the result of the fact that the Atomic Force Microscope is an instrument measuring “from above”. This, combined with the finite dimensions of the probing tip, produces inconsistent values in proximity of steep slopes, narrow cavities, undercuts or hidden parts.

Errors introduced by filtering and levelling can be considered separated from the errors occurring during the topography acquisition.

4.1.5 Drift

Drift is the gradual uncontrolled movement of the system over time. Drift distortions are often regarded as temperature dependent phenomena, associated to temperature gradients and transients that occur in the instrument parts and in the measuring volume. However, up to now in the literature there is no experimental evidence of such dependency. It is not clear if the causes of drift are referable only to temperature or if also other factors like humidity, construction of the instrument and thermal expansion coefficients play a role [20]. This distortion is almost insignificant for a measurement carried out in a range of some micrometres: in fact in this case the error is in the order of 1 % or less. Conversely drift results heavily distorting when high resolution imaging is achieved by taking many profiles (i.e. a long scan operation) in the nanometre scale: in this case errors in the order of some percent can indeed affect measurement. This is of concern also in closed loop scanners, whereas tip position is controlled.

Considering the equation (4.7) drift is usually included in the term of highest order, but it's

influence must be taken into account when performing long measurement, with a small measurement range and with high resolution. In the following paragraphs further studies on drift analysis and quantification are reported.

Drift effects should be conveniently described by considering both short term and long term effects. Thermal drift determines distortion in the single image as presented in Figure 4.5. Drift is continuously affecting scan operation, but it is somehow discretized during the measurement process: in fact when the tip is positioned for beginning scan of the n -th profile, a positioning error occurs, given by the whole amount of drift accumulated during trace and retrace of the $(n-1)$ -th profile. Recognizing horizontal drift distortions within single profiles is very difficult, often impossible; therefore it has to be considered as a stochastic error affecting single pixels position. A mathematical model can be introduced for describing drift assuming that the imaging process leads only to constant velocity drift deformations, and considering that drift velocities are known to be free of rotational components, the following equation can be written:

$$\begin{bmatrix} x \\ y \\ z \end{bmatrix} = \begin{bmatrix} x' \\ y' \\ z' \end{bmatrix} - \begin{bmatrix} d_x \cdot t \\ d_y \cdot t \\ d_z \cdot t \end{bmatrix} \quad (4.8)$$

where t is the time elapsed from the beginning of the scan to the measurement of the pixel lying in the position (x, y) . By indicating the scanning velocity as v_x (in the fast scan direction), the number of pixels with $(N_x = N_y = N)$, the scanned range with L_x and L_y , the time interval can be also expressed through:

$$t = \frac{2 \cdot L_x \cdot y \cdot (N-1)}{L_y \cdot v_x} + \frac{x}{v_x} = \frac{2 \cdot L_x \cdot y \cdot (N-1) + L_y \cdot x}{L_y \cdot v_x} \quad (4.9)$$

As already stated this model doesn't consider deviation of drift velocity from the mean value: these deviations will be therefore considered as contributes of the uncertainty affecting x, y, z positioning.

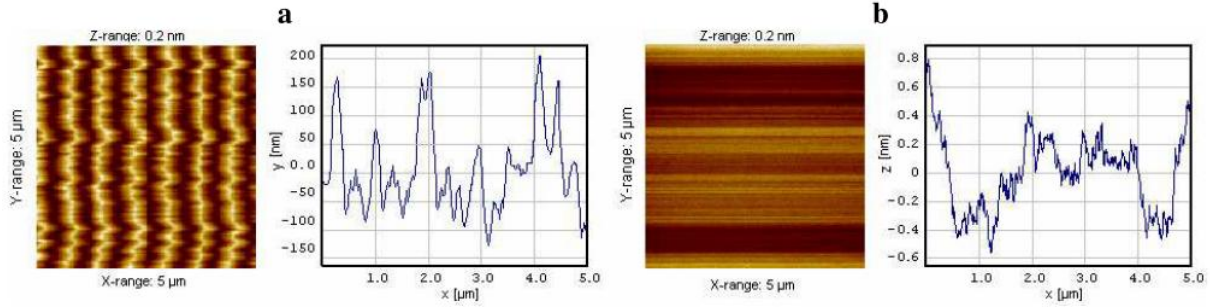


Figure 4.5: Surface topographies affected by horizontal a) and vertical b) drift: in the graphs relative shifts respectively in the y and z direction are reported. In case of drift-free scanning, graphs would report a straight line.

4.2 Thermal drift study on SPM scanners

Scanning Probe Microscopes (SPMs), such as AFMs (Atomic Force Microscope), SNOMs (Scanning Nearfield Optical Microscope) or KPMs (Kelvin Probe Microscope), are instruments commonly implemented in characterization of surface topography and other properties (optical, electrical, tribological, etc.) [21]. SPMs can provide measurements in a range of a few tens of micrometres, with sub-nanometre lateral and vertical resolutions [22, 23]. Different fields of research and, to some extent, of industrial production benefit from implementation of SPMs, such as micro electro mechanical and bio-medical systems, data storage and micro-optics devices. The working principle is based on the interaction between a sharp tip (with a tip radius normally smaller than 10-15 nm) and a sample. The surface is scanned in a raster fashion and the topography is reconstructed sequentially, as a collection of consecutive profiles. As described in Paragraph 4.1.5, scanning probe microscopy (SPM) imaging process is inherently slow, and commonly suffers from instrumental drift. Drift is an uncontrolled time dependent movement of the tip relatively to the sample surface, which limits the accurate correspondence between acquired points and real surface. Drift influences measurement results obtained using the instruments for long periods of time, e.g. when high resolution imaging is performed by taking many profiles. Evaluation and control of actuator drift is an important issue for high accuracy measurements and quantitative metrology. In particular, a better probe positioning can be obtained through characterization of the scanning system's metrological performance, and distinguishing systematic and stochastic behaviour components. Proper modelling and quantification of drift is important in precision positioning and measuring systems: finding strategies to avoid, control or partially compensate it, allows

improvement of the actuation quality and eventually reduction of measurement uncertainty [24–30].

The study here presented has been run to correlate thermal phenomena to SPMs drift distortions.

A new approach is proposed to study long term thermal phenomena, correlating them to SPM scanner drift distortions evaluated using calibrated reference samples. Long term drift evaluation is then cross-correlated to thermal analyses carried out in parallel by means of an infrared-camera. Drift estimation is then cross-correlated to thermal analyses parallelly carried out by means of a thermo-camera opportunely positioned.

Eventually, it is discussed how the study can help proper instrument set up and optimization allowing reduction of distortions

4.2.1 Scanning systems and drift distortions

The scanner is a fundamental component of an SPM: it is responsible for controlling and changing the position of the probe relatively to the sample in order to measure surface properties and topography. With only few exceptions [31, 32], SPMs rely on raster scanning: this is a sampling procedure for generating a surface map, based on a line-by-line sweep of parallel profiles. In order to obtain high lateral resolution, raster scanning is performed with actuators whose motion can be incremented and controlled in nanometric steps. Such actuators are normally made by taking advantage of piezoelectric (PZT) technology. PZT materials can be shaped into the form of hollow tubes [33], or coupled to mechanical flexures [34], or a hybrid of the two [35, 36]. Voice coil actuators are also implemented, allowing the movement of the probe with good accuracy [34]: such electromagnetic actuators usually have a larger scan range and are cheaper than piezoelectric scanners. Both piezoelectric and electromagnetic actuations provide very good performance in terms of resolution (down to 0.1 nm), range (up to 500 μm) and speed (larger than 500 $\mu\text{m/s}$, and more than 50 Hz); on the other hand, some limitations are present and distortions can reduce the positioning accuracy of such systems. In particular, nonlinearities of the actuation are introduced, due to hysteresis, creep, drift or aging effects, causing spatial and temporal distortions of the measuring volume [37]. For this reason, the so called closed-loop SPMs incorporate sensors that can perform a partial linearization and compensation of the displacement. Linear variable differential transformer (LVDT) or capacitive sensors, are used to control the positioning of the probe and

to perform the correction through a feedback circuit [36]. Software compensation can be implemented as well, for instance using learning control algorithms that take advantage of the systematic component of distortions, as proposed by Kam et al. [37]. Furthermore, the design can be improved in order to reduce noise and eventually optimize the overall stability of the instrument [38, 39]. Closed-loop systems and software compensations allow only a partial reduction of distortion effects. This is particularly true for drift, which is an uncontrolled time dependent movement of the tip relatively to the sample surface, resulting in apparent relative misalignments of scanned profiles both on x (or y) and z direction. Drift distortions are particularly evident when measurements are performed:

- at high resolution, since dense sampling normally requires longer scan times;
- on small scan ranges, when drift distortions are larger than the pixel size.

Drift distortions are often regarded as temperature dependent phenomena, caused by temperature gradients and transients that occur within the instrument and in the measuring volume. However, there is no experimental evidence of such dependency in literature, and it is not clear if the causes of drift are referable only to temperature (“thermal drift”). Additionally, it is known that piezoelectric elements (the most used solution for SPM actuation) exhibit a behaviour that is mainly capacitive: having very high resistance, under static operation, in theory, no current is drawn nor power consumed to maintain a state of activation. As a consequence, the only power needed is that used to change the voltage on the PZT element. However, due to mechanical deformation, piezoelectric ceramics dissipate energy in the form of heat, proportionally to the dissipation factor $\tan \delta$, the tangent of the loss angle for the material [40, 41]. The power dissipated by a piezoelectric element with a capacitance C , driven at a voltage V and frequency f is normally calculated from equation (4.10):

$$P = 6.28 \cdot f \cdot C \cdot \tan(\delta) \cdot V^2 \quad (4.10)$$

However, the resultant temperature rise will not depend only on dissipated power, but also on the specific geometry and casing of the used piezoelectric element, and on specific factors such as the heat capacity and heat transfer (by convection, conduction or radiation). Therefore, it is not clear a priori how the scanner settings influencing power dissipation are correlated to the thermal behaviour of the scanner itself.

4.2.2 Experimental Set up

A set of experiments was performed to investigate and quantify the long term drift behaviour during AFM actuation, in order to verify correlation with temperature and with the most significant scan parameters. Investigations were carried out using an open-loop AFM (Dualscope DME 95-200), actuated through a piezo-tube scanner. This is a compact stand-alone instrument, which can be easily implemented in industrial manufacturing environment. The scanner was screwed to a steel support and fastened to a 40 mm column with thread and setting ring for height adjustable positioning; the scanner stands over a large x - y positioning stage which allows measurements on a volume X - Y - Z of $200 \times 200 \times 300$ mm (Figure 4.6). The microscope can operate both in AC and DC mode (contact and non-contact mode) on a scan range X - Y - Z of $200 \times 200 \times 15$ μm with a lateral resolution below 1 nm and a vertical resolution below 0.1 nm.

In order to quantify the drift, measurements were done on three reference samples:

- a (100)-oriented silicon wafer, with deviations from planarity of less than 1 nm within the measured area;
- two calibration gratings (Nt-Mdt TGZ02 and TGZ03) featuring a 1-D array of rectangular SiO_2 steps on a Si wafer; step height nominal values are respectively 104 nm and 540 nm, with a pitch of 3 μm .

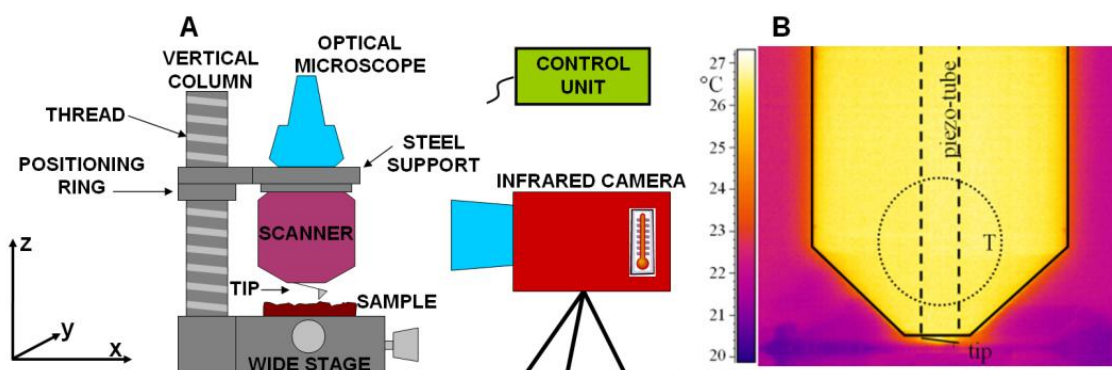


Figure 4.6: Schematic view of the experimental set up; B) Thermographic image of the AFM scanner after one hour of operation; the dotted circle indicates the region where temperature is averaged and monitored.

The experimental set up was provided with a temperature control system: an infrared-camera was positioned in the close proximity of the scanner to measure its temperature during

operation and in particular to generate a thermal map of the measurement volume. The infrared-camera can provide non-contact measurements; thus the interference with the instrument was minimized and the transmission of external vibrations to the instrument was avoided. The instrument used within these experiments (FLIR Systems ThermoVision™ A40-M) has an un-cooled microbolometer IR FPA sensor with a thermal sensitivity of 0.08 °C and operates over a 7.5-13 μm spectrum, with a maximum frame rate of 60 Hz and a resolution of 320×240 pixels in the field of view. A control unit was responsible for acquiring and synchronising signals.

The use of the infrared-camera allowed identifying temperature gradients and transients in a relatively large area. Then, a set of preliminary experiments at different scanning conditions was carried out in order to recognise the most critical components within the instrument volume, and eventually to define an optimal positioning of the camera. Such experiments evidenced how the scanning head, i.e. the part where the piezoelectric scanner is housed, is the primary heat source generation. During preliminary experiments, the infrared-camera response was also calibrated and eventually corrected in an indirect way, by analysing the signal from an NTC general purpose disc thermistor (with a resolution of 0.05°C) attached to the scanner.

All experiments were carried out in a laboratory with controlled temperature at 20 ± 1 °C and relative humidity within 45 ± 5 %.

Estimation of drift was based on measurements on the reference samples. In particular the instrument was programmed in order to scan repeatedly the same single profile on a sample, with fixed measuring settings, throughout the whole duration of each experiment (from 2 to 10 hours). The range used in slow scan direction was nought: all scans were made on the same x - y trajectory in order to avoid additional systematic distortions due to possible installation rotational errors of the reference samples. Drift appears as a misalignment between subsequent profiles (Figure 4.7). Quantification of drift was based on own developed software coded in C++, freely available for download [42] as a plug-in for commercial software for image processing (SPIP™, by Image Metrology A/S). The technique allows sub-pixel relocation, with a resolution better than one eighth of the pixel size. For each data set, a cross-correlation algorithm was used to define the most probable relative x -shift (or y -shift) and z -shift between a scanned profile and subsequent one. Repeating the operation profile by profile throughout the whole set of profiles, x -shift (or y -shift) and z -shift of the probe

relatively to the sample are mapped, for each profile.

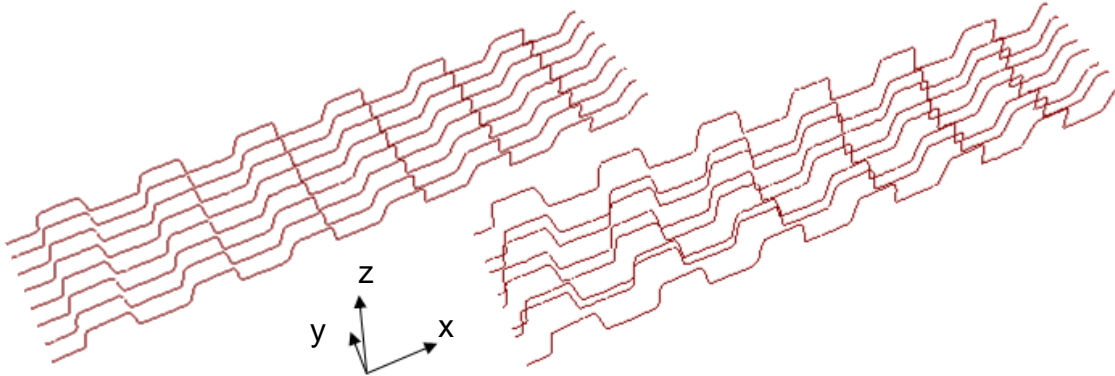


Figure 4.7: An example of a 20 μm long set of 8 profiles: on the left image how it appears for a drift free instrument; on the right image drift results in apparent shifts in x -direction and z -direction.

4.2.3 Experimental plan

The most relevant influencing factors for an AFM scanner can be ascribed mainly to the total applied voltage and its variations. The total applied voltage is directly proportional to the scan range. On the other hand, variations of voltage are associated to inversions in scanner movement direction, i.e. the number of cycles, or in other words the change from trace (forward scan) to retrace (back scan). Also, variations are associated to the number and entity of vertical movements of the probe, which are associated through the feedback system to the vertical range of the sample and its roughness. Then, different measurement ranges and speed can deviate from linearity the behaviour of the piezoelectric elements, determining heating gradients and transients. A set of experiments was designed to investigate the effect of such parameters (Figure 4.8). Measurements were performed with a sampling of 1024 points per line (corresponding to a resolution of respectively 5 nm, 20 nm and 49 nm). Thanks to sub-pixel computation, drift was then estimated with a resolution of less than 7 nm. The experimental plan included different AFM settings with regard to scan range R_{xy} (5 μm , 20 μm , 50 μm), vertical range R_z (0 μm , 0.10 μm , 0.54 μm) and scan rate ν (0.1 Hz, 0.5 Hz, 1 Hz). The AFM was operated in contact mode: three repetitions with different probes were done for each setting. Such range of configurations was defined in order to adequately include instrument setting applied in common practice.

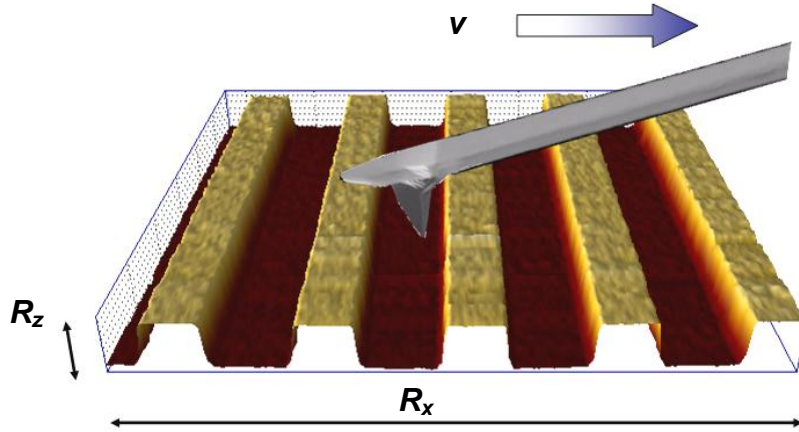


Figure 4.8: Representation of the main scan parameters considered within the investigations.

Additionally, to verify the symmetry of drift behaviour in x and y direction, measurements were repeated rotating the sample by 90 degrees about the z -axis and modifying fast scan direction to take measurements at relative angles of 0 and 90 degrees. This means that to actuate the scanner, the voltage is applied to perpendicular positions of the piezo-tube. Temperature was monitored with a frequency of 0.017 Hz over 150 minutes. Additional measurements were taken over 600 minutes to evaluate long time stability.

4.2.4 Results and discussion

The whole set of experiments was firstly analysed in order to evaluate the thermal effects on the scanner. Results are reported in Figure 4.9, where each value of temperature $\bar{T}(t)$ at a given time t from the beginning of the measurement was evaluated as follows:

$$\bar{T}(t) = \sum_{i,j,h,k=1}^3 T_{i,j,h,k}(t) / (i \cdot j \cdot h \cdot k) \quad (4.11)$$

In equation (4.11), the index i refers to the three z ranges, j to the three x - y ranges, h to the three scan rates, and k to the three repetitions with three different probes; $i \cdot j \cdot h \cdot k$ is the total number of measurements performed for the experiment.

Before the experiment the scanner was in thermal equilibrium in a measuring room at the reference temperature of 20 °C.

At different scanning conditions, the instrument exhibited the same behaviour, with an initial temperature gradient of about 0.18 °C/min followed by a logarithmic decrease, eventually stabilising after about 90 minutes at a constant value of about 5 °C over the initial temperature

of the scanner. In order to evaluate the variability of temperature at different scanning conditions, two additional curves representing standard deviation were added to the average temperature curve in Figure 4.9. Standard deviation $\sigma(t)$ at a given time t was evaluated as the standard deviation of temperature measured at different scanning conditions $T_{i,j,h,k}(t)$. Values of $\sigma(t)$ below 0.2 °C were observed throughout the duration of the experiment (150 minutes).

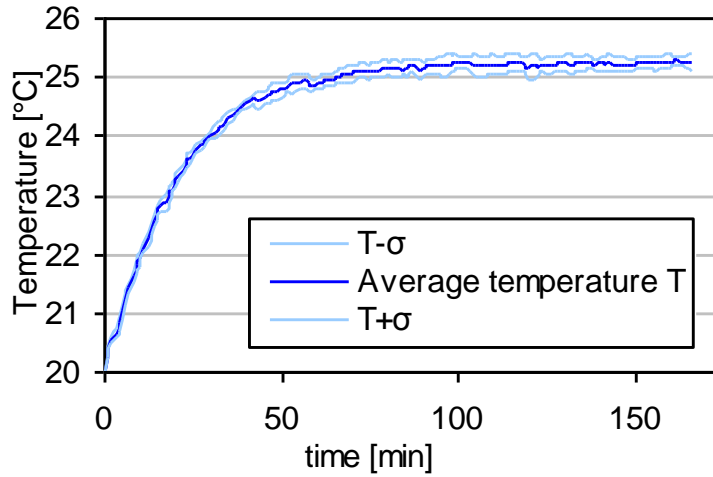


Figure 4.9: Average scanner temperature (mean of measured values at different scanning conditions) versus time.

The effects of single parameters were studied, to quantify how they influence temperature gradient and transient of the AFM scanner. Main results as summarized in Figure 4.10, where the first diagram is relative to the effect of z -range (Figure 4.10 A)), the second to the effect of x - y scan range (Figure 4.10 B)) and the third one to scan rate (Figure 4.10 C)). Each diagram reports the deviations from the mean temperature; values are calculated as the average of deviations measured on three repetitions, according respectively to (4.12), (4.13) and (4.14):

$$\Delta T_z(t) = \sum_{i,k=1}^3 (T_{i,k}(t) - \bar{T}(t)) / 9 \quad (4.12)$$

$$\Delta T_{xy}(t) = \sum_{j,k=1}^3 (T_{j,k}(t) - \bar{T}(t)) / 9 \quad (4.13)$$

$$\Delta T_v(t) = \sum_{h,k=1}^3 (T_{i,k}(t) - \bar{T}(t)) / 9 \quad (4.14)$$

One of the three curves in each diagram refers to standard scanning conditions (height

0.1 μm , range 20 μm and scan rate 0.5 Hz), the other two curves refer to results achieved with one of the scan parameters respectively at low and high level. Each curve is drawn with a shadowed band representing the temperature sensor resolution (0.08 $^{\circ}\text{C}$). Analysing the diagrams, it comes clear that during the main temperature transient (the initial 90 minutes) there is no evidence of difference between different scanning conditions. For z - and x - y range variations there is a slightly smaller average temperature at extreme conditions than at standard ones. For scan rate variations there is evident overlapping of curves, with a maximum difference of 0.3 $^{\circ}\text{C}$.

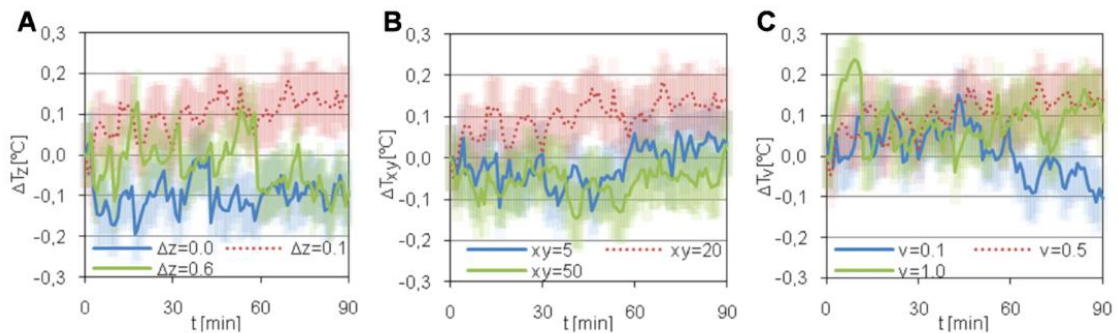


Figure 4.10: Effects of vertical z -range (A), horizontal x - y range (B) and scan rate (C) on scanner thermal behaviour. Values were calculated according to respectively (3), (4) and (5). Shadowed bands are representing the temperature sensor resolution (0.08 $^{\circ}\text{C}$).

Experimental investigations demonstrated that the temperature transient reported in Figure 4.10 is independent from the most important scanning settings, and that variations among different scanning conditions are within temperature measurement repeatability. Also, independently from scan settings, the instrument stabilizes after about 100 minutes to constant drift, exhibiting a systematic behaviour. In such condition, short-time temperature oscillations are present: i.e. considering 10 minutes intervals stochastic variations comprised within ± 0.05 $^{\circ}\text{C}$ are recognisable.

This is apparently in contradiction with equation (4.10). As discussed in previously, this is due to the fact that thermal behaviour is also strongly influenced by other important factors such as heat capacity and heat transfer. Therefore, even if different scanning conditions cause different power dissipation, its effect is attenuated by the heat conductivity of the instrument shield. This suggests that drift behaviour can be studied considering the SPM as a unique system rather than an assembly of separated parts; drift minimization can therefore be

achieved by optimization of the whole instrument rather than focusing on the scanner itself. Both horizontal (x and y) and vertical (z) drift evaluated at different instrument settings were studied and correlated to temperature ramp during the transient. The investigation indicated a strong correlation between temperature variation and average drift distortion: after linear regression, an R -squared value > 0.95 was constantly detected at different setting conditions. This is of the highest importance, since it clearly indicates that to reduce drift, measurement operations have to focus on thermal stability only.

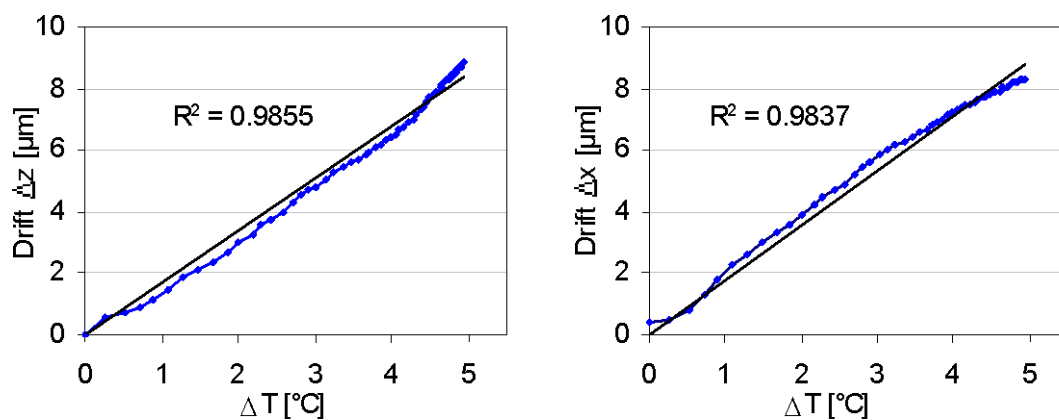


Figure 4.11: z -direction (left) and x -direction (right) drift distortions vs. temperature increase during the first hour operation: high correlation is demonstrated by high R^2 values.

In particular, in Figure 4.11 the case at standard scanning conditions (range $20 \mu\text{m}$, height $0.1 \mu\text{m}$, scan rate 0.5 Hz) is reported. Such dependency is very important: indeed it demonstrates that the scanner drift is strongly influenced by instrument thermal behaviour. Other sources (like electronic noise or vibrations), here not yet studied, can be of influence for drift distortion, but certainly thermal instability plays the most important role. After stabilization, i.e. after two hours of operation, the correlation between temperature residual oscillations and, as discussed in the following paragraph, drift distortions becomes insignificant. This is due to the fact that after two hours, stochastic temperature effects prevail on systematic behaviour, while other sources (such as vibrations) contribute to scanning instabilities and eventually on drift. In such conditions, second order factors determines drift behaviour, however their determination is out of the scope of the present paper.

4.2.5 Long and short time stability

Experimental results demonstrate how significant can be long term thermal distortions, with a drift amount of over 8 μm after a temperature variation of a few degrees. The effect is fortunately different when short term stability is considered. Indeed, as reported in Figure 4.10, short term temperature variations oscillate within a range of 0.1-0.3 $^{\circ}\text{C}$: according to the trend reported in Figure 4.11, such oscillation should cause significant short term distortions, in a range of 200-500 nm. But this is not confirmed by actual experiments, where smaller horizontal and vertical distortions occur. This was associated to the thermal inertia and the consequent slow response of the instrument. An experiment was done in order to verify the hypothesis. After stabilization of the instrument, an external source, a radiating heater with a constant temperature of 70 $^{\circ}\text{C}$, was brought in close proximity to the instrument for ten seconds. The distance of the heater from the scanner and from the main steel column was similar to the distance between the scanner and the column. The response of the instrument after the thermal impulse was studied, monitoring the thermal drift of the instrument. Results from two consecutive tests are reported in Figure 4.12. Even with such a large thermal input, in the heating phase the system response has a delay of about 20 seconds, and of few minutes in the cooling phase. Such thermal inertia is helpful for measurement stability, allowing a sort of self-compensation (due to averaging) which minimizes short term drift distortions.

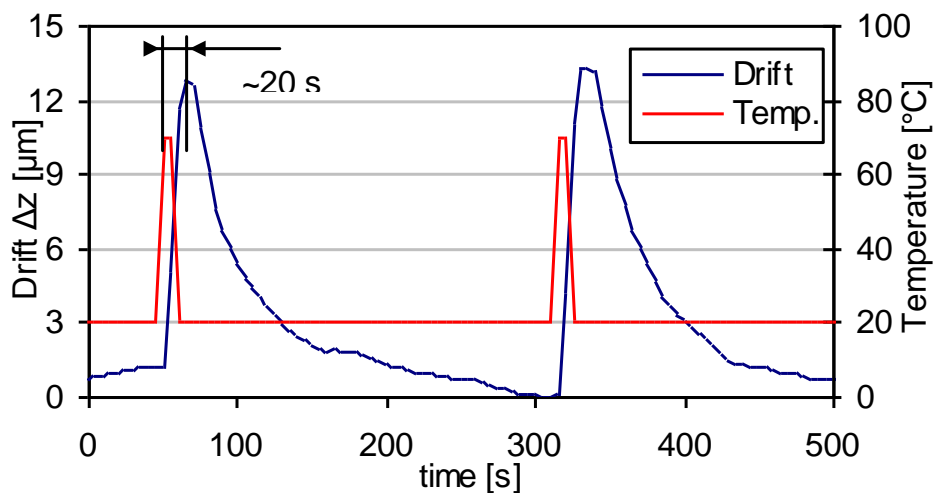


Figure 4.12. Effect on thermal drift (measured on vertical direction) of a thermal impulse (10 seconds exposition to a heated source at 70 $^{\circ}\text{C}$).

4.2.6 Finite Element Method simulations

Finite Element Method (FEM) simulations were carried out to better understand the deformation behaviour of the instrument. Thermo-mechanical simulations were performed with the software ANSYS Workbench. A fine mesh was generated (Figure 4.13). As initial conditions, the temperature of the instrument and of the environment was set homogeneous at 20°C, while natural convection between instrument and air was considered during the transient.

Taking advantage of information from the infrared-camera analysis, a concentrated heat source was set in correspondence to the scanner head. FEM allowed simulating the thermal behaviour of the instrument: as reported in Figure 4.13 B), the scanner support and the column are the parts that are most influenced by the scanner heating, with a temperature variation progressively diminishing from 25°C to 22°C.

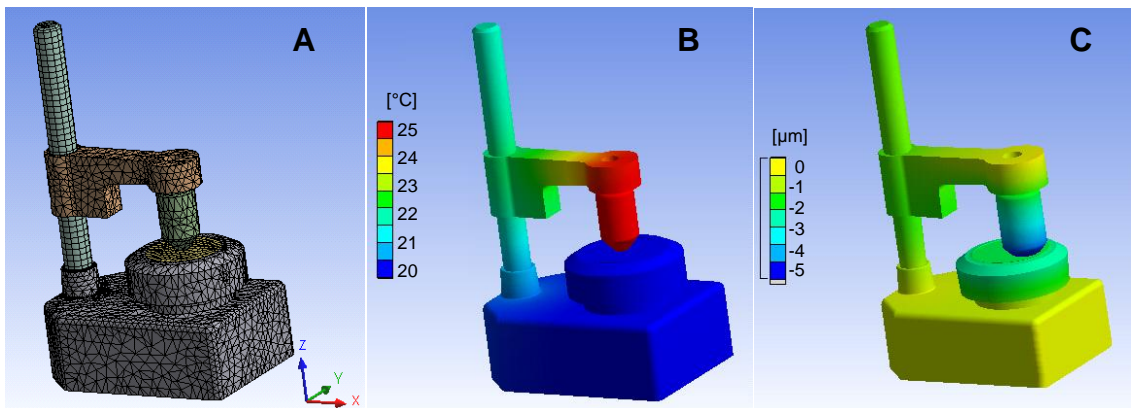


Figure 4.13: Three-dimensional rendering of the instrument for the thermo-mechanical simulation: A) the mesh; B) temperature distribution; C) deformation along z -axis.

The FEM simulation also allowed correlating the temperature behaviour to the system deformation. The position of the sample surface was set locked in all directions, while for the other parts of the system the movement was calculated relatively to the same sample surface. In particular in Figure 4.13 C) the z -axis deformation is reported: it can be noticed how due to the temperature variation, the scanner head has a relative z -shift with respect to the x - y stage of about 3 μm , therefore less than the 9 μm evidenced by experiments. Then, the overall deformation is only partially due to the deformation of the metrology loop: in agreement with literature [43], the residual deformation can be attributed to a deformation of the piezoelectric

transducer and to a variation of its properties and therefore of its transfer characteristic. Similar results and considerations are for the deformation in the x - y plane, were the simulation evidenced a displacement of the scanner head relatively to the positioning stage due to the metrology loop distortion of about 5 μm . Also in the case of deformation in the x - y plane the residual deformation can be attributed to a deformation of the piezoelectric transducer and to a variation of its transfer characteristic.

4.2.7 Instrument optimization

Finite elements simulations were used to study also the effect of the metrology loop length (i.e. the total length of structural elements that are required to hold the probe at a fixed distance from the sample) on total drift distortions. In particular, these analyses confirmed that a modification of the instrument set up, including a reduction of the stage height and a lowering of the arm supporting the scanner, allows a reduction of the distortions (Figure 4.14).

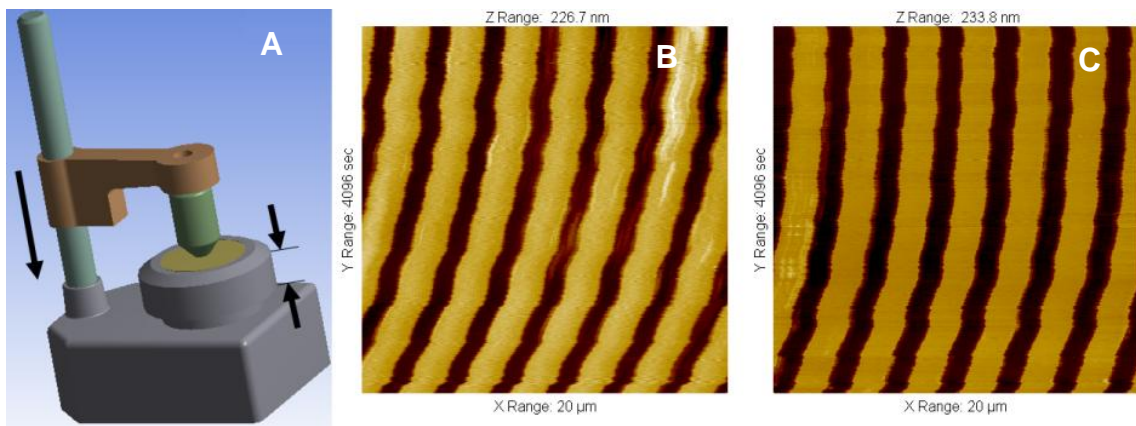


Figure 4.14 A) With the used instrument, a more compact instrument set up is possible lowering the arm supporting the scanner or reducing the height of the stage (see arrows). With respect to the results obtained using a long metrology loop (B), the results obtained using a modified instrument set up with a 30% shorter metrology loop (C) allows a reduction of drift distortions higher than 25% (as visible from reduced lines bending).

Experimental tests were performed to confirm what extrapolated from the simulations. Tests were performed using the procedure described previously, firstly on the instrument with a long metrology loop, and then with a more compact set up with a total length reduced by

30%. Two scans corresponding to these two setups are reported in Figure 4.14 B) and Figure 4.14 C) respectively: here the horizontal drift after about 70 minutes is demonstrated by the bending of the measured lines (while vertical drift was compensated by vertical alignment of the single profiles, in order to make the figure more clearly readable). The lines bending, i.e. the total horizontal drift, is higher than 6 μm in the case of the long metrology loop (Figure 4.14 B)), but decreases to less than 4 μm for the compact set up (Figure 4.14 C)). A further reduction of the set up would certainly decrease the total distortion and therefore improve the quality of the measurements; however the present scanner configuration does not allow a further reduction of the set up dimensions.

4.2.8 Conclusion

A study was conducted to correlate long term thermal phenomena to drift distortions in an SPM scanner. Drift estimation was then cross-correlated to thermal analyses carried out in parallel by means of an infrared-camera. The approach here applied for a single instrument, is of general interest to study also other specific scanners and set up, in order to define good laboratory practice. Mapping of long term drift distortions and temperature allows some important conclusion.

- 1) The study proves the strong correlation between long term temperature variation and average drift distortion, with reported $R^2 > 0.95$. This is of the highest importance, since it indicates that to reduce drift, operations have to focus on thermal stability.
- 2) Scanning parameters (scan range and scan rate) have a negligible influence on the long term thermal behaviour of the scanner, with a maximum difference of 0.3°C among different scanning settings.
- 3) Mapping of drift distortions and temperature in particular allows identification of the temperature transient and also characterization of the residual short time instability.
- 4) The identification of the warm up time is needed to stabilize the scanner. This can be evaluated recognizing the period of time after which thermal effects converge to a quasi-constant value with limited variability (see diagram of Figure 4.9). For example, it can be determined as the time after which temperature variation, calculated on data measured in 10 minutes, is within $\pm 0.05^\circ\text{C}$ standard deviation.
- 5) The characterization of the residual short term instability in terms of size and frequency help to define scan time (i.e. velocity) and scan range that minimize the short time drift,

therefore minimizing uncertainty contribution.

6) The optimization of instrument set up is possible. Thermographic maps allow recognizing temperature gradients within the instrument, the stage and the sample: this can help optimization of instrument set up, by insulating heat sources, or conditioning critical components.

4.3 Comparison of different commercial scanning probe microscopes

As result of the work described in the previous paragraph drift distortion is caused by temperature variation within the instrument structure. A way to optimize the instrument performances is modify the instrument set up for example insulating heat sources or conditioning critical components. For these reasons commercial SPMs with different set up have been analysed in order to study their thermal drift behaviour.

Commercial SPMs are designed and manufactured with different approaches, e.g. combining different scanners' architectures, with selected hardware, software and materials, in order to optimize specific instrument performances such as accuracy and scanning speed. Hence, different SPMs on the market have different drift depending on instrument design and materials. In this work, a set of experiments was conducted on different instruments operating under varying controlled environmental conditions, for drift estimation, with particular reference to the initial warming-up phase. The experimental procedure for drift evaluation was based on repeated measurements on a structured reference grating. Temperature was monitored using an infrared camera. Six different SPMs were compared based on the analysis of the evolution of horizontal and vertical drift over time, allowing correlation of the drift trend with instrument architecture.

Different strategies have been proposed to reduce thermal drift. The instrument structure can have a symmetrical design in order to help self-compensation when thermal distortions are occurring [44]. Materials with very low thermal expansion coefficient or parts with large thermal masses together with systems for air temperature control are also used to insulate the microscope and to minimize the heat transferred to the sample [45, 46]. Indeed, thermal drift occurs not only within the microscope but also within the sample itself. For this reason specifically designed cases are often used to contain the instruments, and tight magnetic holders are implemented to keep the sample in position. However, an amount of drift is always present, and different post-processing approaches, mainly based on the vertical

alignment of profiles, have also been proposed [25, 47]. Despite its importance, correlation of drift errors with thermal phenomena has not been thoroughly documented in the literature up to now. Also much less information is available on the performance of different instruments with different set-ups with respect to drift behaviour. In the following, a comparison is proposed between six different scanning probe microscopes, with comments related to their design and set-up, and with analyses in particular referred to the initial warming-up phase.

Previously a set of experiments was performed in order to investigate and quantify the drift behaviour during AFM actuation, and to verify correlation with temperature and with the most significant scan parameters [48]. On the basis of that work, the most important scanning parameters were defined in order to properly quantify thermal drift behaviour. The same set of experiments is used here as the common basis for the estimation of the performance of six different instruments.

4.3.1 Experimental set up

The SPMs were operated as AFMs, actuated in the so-called contact mode, with a horizontal range of 20 μm and 1024 points per line sampling (corresponding to a resolution of 20 nm). Thanks to sub-pixel computation, drift was then estimated with a resolution of less than 7 nm. The reference sample was a calibration grating (namely TGZ02, by Nt-Mdt) featuring a 1D array of rectangular SiO₂ steps on a Si wafer; the nominal step height was 104 nm, with a pitch of 3 μm . Profiles were scanned always in the same position (i.e. null movement was set in the so-called slow scan direction) with a rate of 0.25 Hz (corresponding to a speed of 10 $\mu\text{m/s}$). Such parameters, chosen on the basis of the previous work [48], represent also typical working conditions for a standard SPM instrument. Additionally, the experiment set-up was completed with an infrared camera positioned in the close proximity of the scanner to measure instruments' temperature stability during operation. The instrument used in this work (FLIR Systems ThermoVision TM A40-M) is minimally invasive, being a non-contact device based on the detection of infrared radiation. It has an uncooled microbolometer IR FPA sensor with a thermal sensitivity of 0.08° C and operates over a 7.5–13 μm spectrum, with a maximum frame rate of 60 Hz and a resolution of 320 \times 240 pixels in the field of view. The infrared-camera response was also preliminarily calibrated indirectly, by analysing the signal from an NTC general purpose disc thermistor (with a resolution of 0.05°C) attached to the scanner. A control unit was specifically programmed for acquiring and synchronising

signals.

Drift evaluation has been performed as in the studies described in the paragraph 4.2 and presented in Figure 4.15.

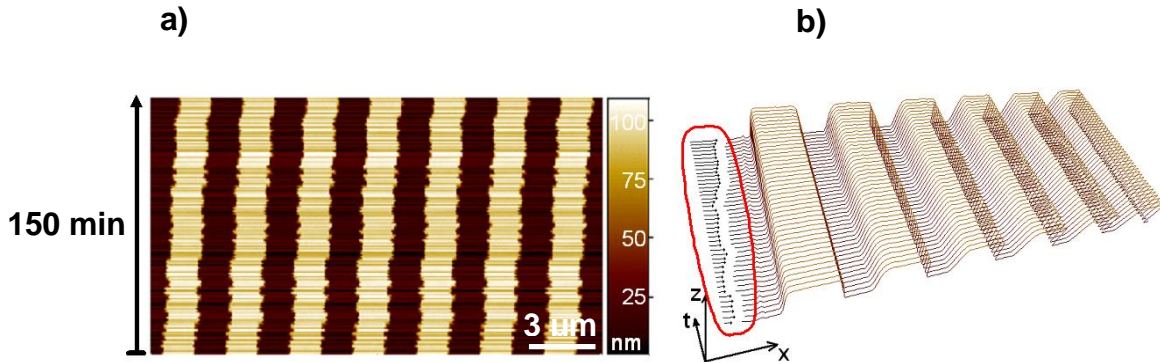


Figure 4.15: a) Image of a set of profiles obtained with a 150 minutes test, reporting evident drift distortions; b) after use of the cross correlation algorithm, vertical and horizontal shifts (circled in the figure) between profiles are computed.

4.3.2 Compared instruments

Six different scanners were involved in the investigation: two NT-MDT NTEGRA Prima with different configurations, a DME Dualscope DS 95–200, a Witec Alpha300 S, an APE Research A100 and a Veeco Dimension 3100. From here on, the six scanners will be identified anonymously as instruments A, B, C, D, E and F, with no mention and reference to the specific manufacturer and model (see Table 4.2).

(1) *Instrument A*. Instrument A is an AFM actuated through a piezo-tube, for scan-by-probe measurements. This is a compact stand-alone instrument that can be freely positioned on the surface of samples of almost any size. However, the scanner is fastened with proper fixture to a vertical column and a wide horizontal positioning stage allows measurements on a volume X–Y–Z of 200 mm × 200 mm × 300 mm with a scan range X–Y–Z of 200 μm × 200 μm × 15 μm. The instrument is not equipped with a closed-loop system to control the X, Y position of the probe so the instrument was operated only in an open- loop mode. Instrument A was installed on a granite table in a temperature- and humidity-controlled room and the vibrations are reduced through rubber dampers. There was no temperature insulation case present during measurements.

(2) *Instrument B*. This system is provided by two independent scanners: one for X, Y movements and one for the Z movement. The X, Y scanner consists of flexures that allow high linearity during scanning, accuracy and positioning reproducibility. The scan range is

$50\ \mu\text{m} \times 50\ \mu\text{m} \times 12\ \mu\text{m}$ and the working volume is $20\ \mu\text{m} \times 20\ \mu\text{m} \times 10\ \text{mm}$. Capacitive sensors and a feedback loop circuit control the X, Y position of the tip in order to reduce distortions due to creep and hysteresis. The instrument is isolated from vibration through bungee cords, while a specially designed acoustic hood reduces disturbance due to air flows and acoustic waves. Due to a problem with the capacitive sensor, the instrument was operated in open loop (with the capacitive sensors off during scanning).

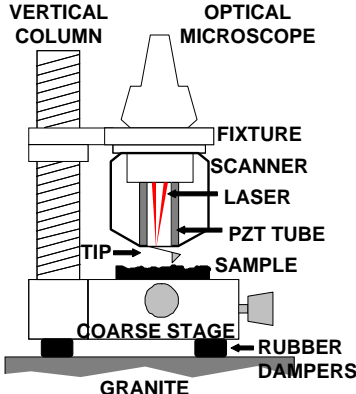
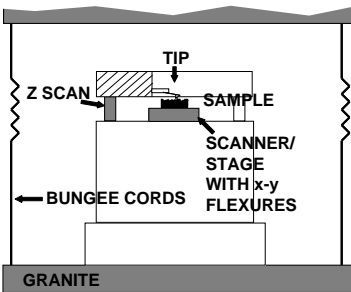
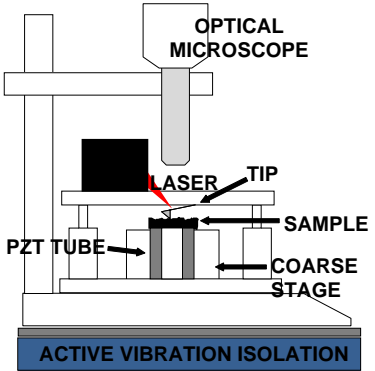
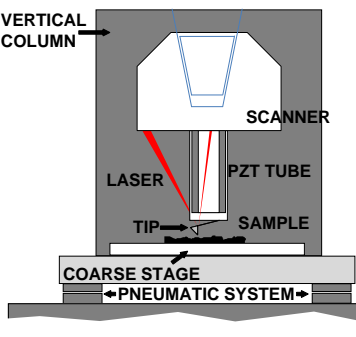
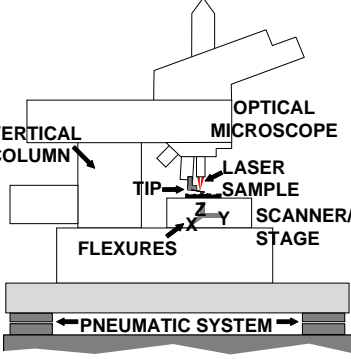
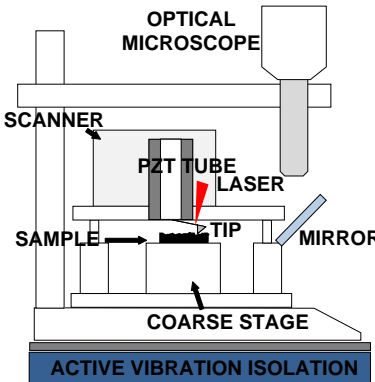
(3) *Instrument C.* This AFM is equipped with a PZT scanner working in scanning by sample mode. The maximum scanning range is $75\ \mu\text{m} \times 75\ \mu\text{m} \times 10\ \mu\text{m}$, and the working volume is up to $40\ \text{mm} \times 30\ \text{mm} \times 15\ \text{mm}$. The instrument is equipped with a three-axis closed-loop control with capacitive sensors that trace the actual displacement of the scanner and compensate piezoceramics nonlinearity, creep and hysteresis. The instrument is installed in an active dynamic vibration isolation system, while a metal cover protects the measurement volume from air flow or environment temperature gradients. The instrument was operated both in closed loop and in open loop (with the capacitive sensors off).

(4) *Instrument D.* This system is in a stand-alone configuration installed in a cleaning room. The AFM is equipped with a PZT scanner working in a scanning by probe mode. The X–Y coarse stage permits the micron-scale positioning of large samples beneath the tip with a $120\ \text{mm} \times 100\ \text{mm}$ travel range. The scanning range is up to $100\ \mu\text{m} \times 100\ \mu\text{m} \times 5\ \mu\text{m}$. The AFM is equipped with capacitive sensors, for closed-loop scanning. Instrument D is installed in a clean room, with a pneumatic system for the isolation from vibrations, while a specially designed acoustic hood protects the scan area. The instrument was operated both in closed loop and in open loop (with the capacitive sensors off during scanning).

(5) *Instrument E.* This AFM works with a scan-by-sample mode; the scanning range allowed by the piezoelectric actuation is $100\ \mu\text{m} \times 100\ \mu\text{m} \times 20\ \mu\text{m}$. Measurement can be performed on quite large (but not heavy) samples, the measuring volume being larger than $100\ \text{mm} \times 100\ \text{mm} \times 100\ \text{mm}$. The system is equipped with capacitive sensors for closed-loop scanning. Instrument E is positioned on a pneumatic system for isolation from vibrations, while only a thin polymer case partially protects the measuring volume from external disturbance sources.

(6) *Instrument F.* Instrument F works with a scan-by-probe mode; the scanning range allowed by the tube piezoelectric is about $70\ \mu\text{m} \times 70\ \mu\text{m} \times 10\ \mu\text{m}$, on a working volume of $40\ \text{mm} \times 40\ \text{mm} \times 30\ \text{mm}$. This AFM is equipped with capacitive sensors for closed-loop scanning.

Table 4.2: Schematic representations of different SPMs used within the experiment, with indication of main characteristics.

Instrument A	Instrument B	Instrument C
		
<p>Scan range: $200 \times 200 \times 15 \mu\text{m}$ Volume: $200 \times 200 \times 300 \text{ mm}$ Closed loop: none Scan mode: by probe Case: none Isolation: rubber dampers MCL: $>600 \text{ mm}$</p>	<p>Scan range: $50 \times 50 \times 12 \mu\text{m}$ Volume: $20 \times 20 \times 10 \text{ mm}$ Closed loop: capacitive sensors Scan mode: by sample Case: None Isolation: bungee cords MCL: $>200 \text{ mm}$</p>	<p>Scan range: $75 \times 75 \times 10 \mu\text{m}$ Volume: $40 \times 30 \times 15 \text{ mm}$ Closed loop: capacitive sensors Scan mode: by sample Case: None Isolation: active electronic system MCL: $>100 \text{ mm}$</p>
Instrument D	Instrument E	Instrument F
		
<p>Scan range: $100 \times 100 \times 5 \mu\text{m}$ Volume: $120 \times 100 \times 50 \text{ mm}$ Closed loop: capacitive sensors Scan mode: by probe Case: None Isolation: pneumatic system MCL: $>300 \text{ mm}$</p>	<p>Scan range: $100 \times 100 \times 20 \mu\text{m}$ Volume: $100 \times 100 \times 100 \text{ mm}$ Closed loop: capacitive sensors Scan mode: by sample Case: plastic cover Isolation: pneumatic system MCL: $>600 \text{ mm}$</p>	<p>Scan range: $70 \times 70 \times 10 \mu\text{m}$ Volume: $40 \times 40 \times 30 \text{ mm}$ Closed loop: capacitive sensors Scan mode: by probe Case: metal cover Isolation: active electronic system MCL: $>100 \text{ mm}$</p>

Vibrations are dampened by means of an active dynamic isolation system; a metal case provides a good insulation of the measurement volume from the external environment. The instrument was operated both in closed loop and in open loop (with the capacitive sensors off during scanning).

A schematic representation of the different instruments with a summary of the most relevant properties is reported in Table 4.2. The table also reports the metrological chain length (MCL). Such a value represents an approximate estimation of the total length connecting the scanning tip with the sample, through the instrument structure (probe–scanner–column–base–stage–sample). It is worthy of note that unfortunately only instruments B, C and D were located in the same room, while the others were placed in different rooms under different environmental conditions. Additionally the instruments had different probe and sample holders. Instruments A and E have magnetic probe holders, while for the others a clip spring secures the probe chip to the scanner or to the frame. Instruments B, C and F have magnetic sample holders; therefore, for these instruments the reference grating was attached through a polymer tape to a metal substrate; for the other instruments, the sample was secured through a polymer tape to a sample holder resting over the stage. Such different conditions are not the ideal base of comparison to analyse the drift due only to the scanners; however, they represent typical setting conditions and therefore provide an idea of the standard drift behaviour expectable for the same instruments.

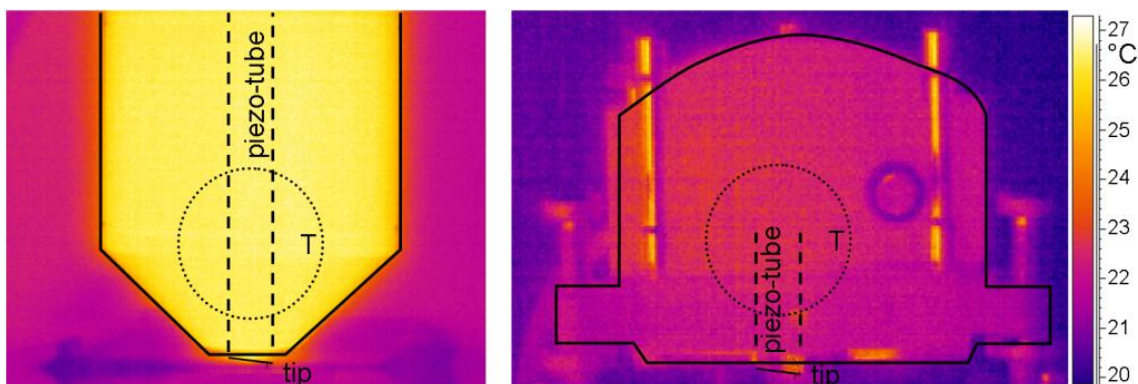


Figure 4.16: Thermographic images of two of the six SPMs after one hour of operation; the dotted circle indicates the region where temperature is averaged and monitored.

4.3.3. Results and discussion

In the following the analyses performed for mapping the thermal behaviour of the six

scanning probe microscopes and its influence on the overall stability of the instruments are reported. All the SPMs were analysed using the infrared camera.

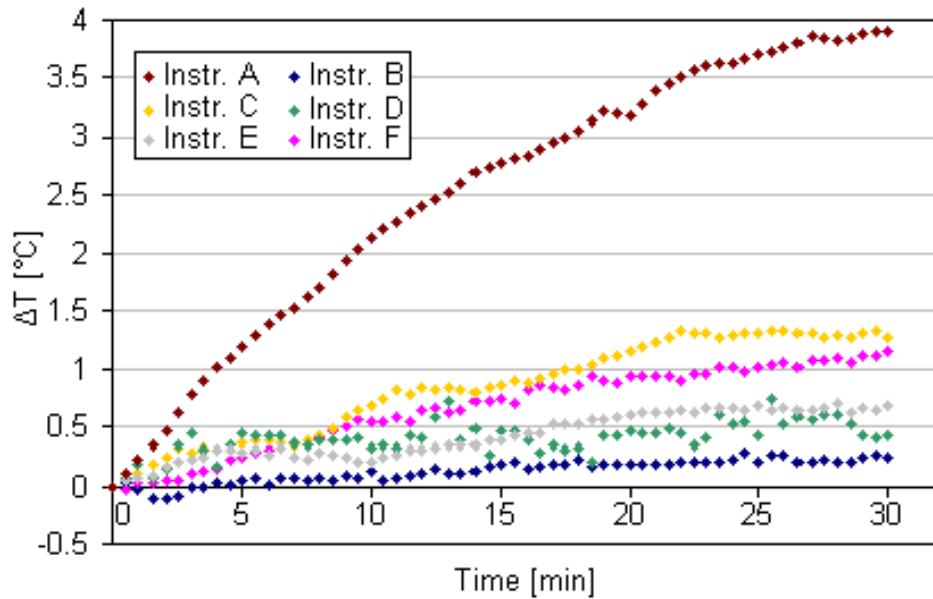


Figure 4.17: Average temperature variation measured in a lapse of time of 30 minutes, immediately after the instruments were turned on and actuated.

For the time period when each SPM was scanning the reference sample, the infrared camera, which was positioned in the proximity of the tested SPM, measured temperature gradients and transients of the instrument body. Indeed, a qualitative analysis of infrared maps allows the detection of heat sources within the instrument volume and in particular in the proximity of the measuring volume. Two examples, relative to two of the six SPMs, are reported in Figure 4.16. Average temperature measurements from the six instruments were compared in a diagram (Figure 4.17). Values are reported up to stabilization of temperature. In particular, the first 30 min, immediately after instruments were turned on and actuated, are the most critical lapse of time, when the most critical transient (i.e. the maximum temperature variation) can be expected. During the first 30 min lapse of time, temperatures were found to vary from 0.3 to 4 °C, with instrument B exhibiting the best performance and instrument A the worse performance (Table 4.3). Data sets were also fitted with a linear interpolation. Firstly, this allowed the estimation of temperature variation rates: accordingly with temperature variations, values were found to range between 0.9×10^{-2} and $16 \times 10^{-2} \text{ } ^\circ\text{C min}^{-1}$. Secondly, deviations of temperature from the best fitting line were used to quantify the stability of

temperature: fluctuations of temperature (measured through standard deviations) were found to range between 0.04 °C and 1.1 °C, with instruments B, D and E performing better than instruments C, F, A. It is worthy of note that for these analyses, the environment seems to have only a minor influence, since instruments B, C, D, E and F were located in rooms with temperature controlled by the same conditioning system; instruments B, C, F were located in the same laboratory room; instrument D was located in a class 100 laboratory room; instrument A was located in a room with a finely controlled temperature at 20 ± 1 °C and humidity $45 \pm 5\%$. Some consideration can be taken into account with regard to the higher temperature variation found for instruments C, F and A. Indeed, compared to the other instruments, these are more compact. In particular, instruments F and A feature the smallest shells (as small as 10 cm × 10 cm × 10 cm), containing the piezoelectric scanner, the laser and the photodiode with electrical connections and part of electronics. Therefore, the higher compactness, which is often an important factor in precision instrument design, is here among the most important causes of the worse temperature behaviour.

Table 4.3: Temperature variations during the instrument actuation in the first 30 minutes.

Instrument	B	D	E	C	F	A
Temperature variation [°C]	0.24	0.42	0.69	1.2	1.3	3.9
Temp. variation rate · 10 ⁻² [°C/min]	0.91	2.2	2.7	4.3	5.3	16
Standard deviation [°C]	0.04	0.11	0.12	0.27	0.33	1.1

Measurements from different scanner systems are reported in Table 4.4. For each instrument the following parameters are reported:

- Initial drift rate. It is the drift speed during the first 5 min, measured through the best fitting linear interpolation of drift versus time, both in the fast scan direction x and in the vertical direction z. Such a parameter is an estimation of the systematic component of drift distortion.
- Initial short-time instability (STI). It is the deviation of drift values after the subtraction of corresponding values in the linear fitting. Such a value is an estimation of the stochastic component of drift distortion.
- Stabilization time. It is the time after which the instrument can be supposed to work with

null systematic drift. It was measured as the time after which, in a lapse of time of 5 min, the systematic drift distortion was less than half STI, estimated in the same lapse of time. Such a value is larger than the temperature stabilization time, measured in the proximity of the measuring volume, meaning that even after the temperature has stabilized, the scanner is not completely stable.

- Total drift. It is the total drift distortion, measured from the beginning of the measurement to the stabilization time.

- Regime short-time instability. It is the deviation of drift values after the stabilization time. Such a value is an estimation of the stochastic component of drift after instrument stabilization, which cannot be compensated and therefore constitutes an uncertainty contribution.

Table 4.4: Horizontal drift measurement results.

	Feedback	Stabilization time [min]	Dir.	Initial drift rate [nm/min]	Initial STI [nm]	Total drift [nm]	Regime STI [nm]
A	open	100	x	212	35	9200	36
			z	231	58	11300	46
B	open	24	x	39	12	79	8
			z	61	16	132	14
C	open	21	x	68	25	358	17
			z	46	23	430	14
C	closed	21	x	47	24	243	21
			z	34	26	265	20
D	open	19	x	42	12	186	8
			z	53	17	124	5
D	closed	19	x	36	14	106	10
			z	49	33	114	13
E	closed	130	x	116	42	2240	22
			z	56	37	3250	27
F	open	26	x	61	16	263	10
			z	41	21	255	8
F	closed	18	x	34	22	188	18
			z	29	25	230	23

Average x–z drift measurements from the six SPMs are also given in a diagram, as a function of temperature (Figure 4.18). Values are reported up to stabilization of drift, plotted in a log–

log scale in order to help readability. As discussed in the previous paragraph, the first 30 min are the most critical lapse of time: correspondingly, most of the drift distortion is concentrated in the same lapse of time, when most thermal variation takes place. Some comments can be made with regard to different instruments and different reported parameters. One important term of comparison is the total stabilization time. Instruments A and E exhibit a very long stabilization time, definitely much larger than that for the other instruments. This can be related to their particular architecture. Indeed these two instruments have a very long MCL, which surely influences the overall stability: statistically a longer time is needed before the whole set-up converges to stable conditions. Additionally instrument A, differently from E, reports very high initial drift rate and high total drift distortions, in the order of several microns. The difference between instrument A and E is most probably due to the fact that, in order to increase positioning flexibility, instrument A was only mounted on a relatively high and thin steel column, very sensitive to the high thermal gradient generated by the scanner. On the other hand, instrument E has a lower temperature transient (see Figure 4.17) and also a larger column which provides better stability.

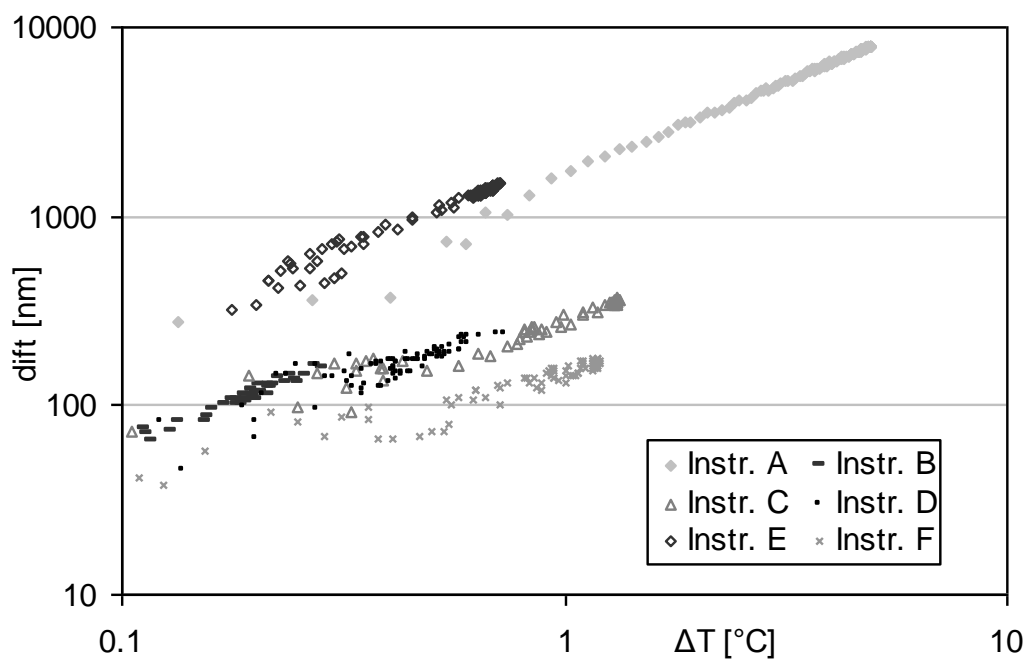


Figure 4.18: Average x-z drift reported as a function of the temperature variation, represented with a log-log plot in order to help readability. For instruments C, D and F, data refers to the closed loop configuration.

According to Figure 4.17, instrument D has a temperature variation very similar to instrument E, but due to a better column design and to a shorter MCL, the overall stability of the instrument is reached in only 20 min, and with a minor amount of drift distortion (see Figure 4.18). Compared to instrument D, instruments B, C and F have a more compact design with an even shorter metrological chain, and with a comparable thermal transient; however, the overall stabilization time is almost the same. It should be noted that instruments should be considered as two separate components: the scanner and the rest of the instrument. The final stabilization time for an instrument is then the higher of the stabilization times of the two components. It is difficult to distinguish which of them is the determinant factor; however, for a well-designed commercial instrument, it is difficult to reduce the overall stabilization to values less than 10 min. Instruments C, D and F were operated both in open and in closed loop. This possibility helps with some considerations. Firstly, the initial drift rate is apparently higher in the open-loop case than in the closed-loop case. This is just a wrong conclusion: indeed open-loop systems based on PZT technology are commonly affected by creep. Difference in drift rate values should then be considered as uncompensated creep in the open loop rather than drift compensated with the closed loop. Creep was not taken into account for instruments B and E, where flexure actuation guarantees creep free motion. For instrument A, due to very high drift distortion, creep constitutes only a secondary contribution to the whole distortion. Secondly, an analysis of initial and regime short-time stability indicates that use of feedback sensors in a closed-loop configuration causes higher instability (i.e. higher STI values). This is something that is well known from the literature, which often reports higher noise values connected to the implementation of feedback sensors [49]. Apart from instruments A and E, all of the other instruments have initial drift rates between 30 and 70 nm min⁻¹: such values should be distinguished separately with regard to horizontal and vertical drift. Indeed horizontal drift is not acceptable whenever geometrical measurements have to be performed on the horizontal plane, such as wavelength, width, area, volume, etc. Whenever, measurements are to be taken in the vertical direction, as in the case of amplitude roughness parameters or height distribution, horizontal drift has only a minor contribution. Similarly, vertical drift is normally not acceptable mainly whenever measurements have to be taken in the vertical direction. But differently from the horizontal drift, post-processing operations, normally known as line-by-line levelling, can be performed to compensate drift distortions between subsequent profiles. These rely on the fact that all the profiles have the same average

vertical elevation. Other techniques have also been proposed for compensation in the case of structured or curved surfaces [25]. If compensation is possible, the residual error only affects a single profile: in such a case, drift should be considered as a relevant uncertainty contribution mainly in the case of slow scan operations. By way of an example, a long scan carried out at a low scanning speed (say as low as $s = 10$ s per forward profile) with a relatively high drift rate (say $d z = 100$ nm min⁻¹) affects each profile by an amount $d z \cdot s = 100 \times 10/60 = 16$ nm. Normally recognition and compensation of systematic behaviour of drift within single profiles are very difficult and often not possible: such residual distortion is then to be treated as an uncertainty contribution in the estimation of quantitative measurements. Additionally, also the regime short-time stability has to be treated as an uncertainty contribution. Commercial instruments exhibited residual short-time instability comprised between 10 and 50 nm: this is the most critical uncertainty contribution. Any improvement in instrument design, measurement set-up and scanning parameter optimization should be focused towards minimization of such values, which normally constitute one of the highest uncertainty contributions in SPMs nanometrology.

4.3.4 Conclusions

A study was conducted to estimate how much drift distortions affect SPM measurements with different set up configurations. To this end, six different instruments were compared on the basis of the same experimental analysis, based on a step height sample measured under standard scanning conditions. For commercial instruments, average thermal drift as large as 50 nm min⁻¹ can be expected both in the horizontal and vertical planes, unless the instrument converges to a stabilized state. Stabilization time for the scanner to converge to a drift rate below the short-time stability is normally less than 30 min. Residual short-time instability as large as 15 nm can be expected for an instrument after stabilization. Analysis of the evolution of horizontal and vertical drift over time evidenced how a compact instrument architecture combined with low thermal gradient is important to keep drift at low values. On the other hand, large metrological chain lengths are accompanied with higher drift values and higher stabilization times.

Chapter 5

3D optical microscopy for coordinate metrology measurement of microfluidic channels

In this work an innovative method is proposed for the geometrical and dimensional characterization of micro fabricated parts through 3D optical microscopy. The measurement of microfluidic channels is reported as example.

5.1 Soft channels for push-down microfluidic valves

The specific type of channel investigated in this work is made of soft materials (typically, polydimethylsiloxane - PDMS) and is used as a component of “push-down” valves [50, 51], such as the one depicted in Figure 5.1. In the figure, the channel subject to investigation is the *main channel*: the increase of fluid pressure in the actuation channel located above leads to the collapse of the ceiling of the main channel and to the interruption of fluid flow (Figure 5.1 b). The size of a single push-down device such as the one depicted in Figure 5.2 is approximately $200\ \mu\text{m} \times 200\ \mu\text{m} \times 20\ \mu\text{m}$. A sequence of three or more of such devices, actuated in the correct sequence, realizes a peristaltic pump. Given the small sizes, minimal control pressures are needed to operate such devices. Being made of biocompatible materials, they are really useful in biotechnology when managing live cells and pharmaceutical substances.

5.2 Critical geometric properties

The cross-section *shape* and the *aspect ratio* are critical for the soft channel here considered. For high aspect ratio channels, the ceiling may not reach the base surface when collapsed. Cross-sectional shape is also important: while round cross-sections, analysed in this work, allow for a complete closure of the channel, other shapes (e.g. rectangular/trapezoidal cross-section, see Figure 5.1 c) may not be completely collapsed under pressure, even for appropriate aspect ratios (e.g. Figure 5.1 d) [51].

For round cross-sections, both aspect ratio and regularity of the curvature radius must be

carefully controlled. The typical envelope size of a main channel is $200\ \mu\text{m}$ (width) \times $20\ \mu\text{m}$ (height), with an aspect ratio of 0.1.

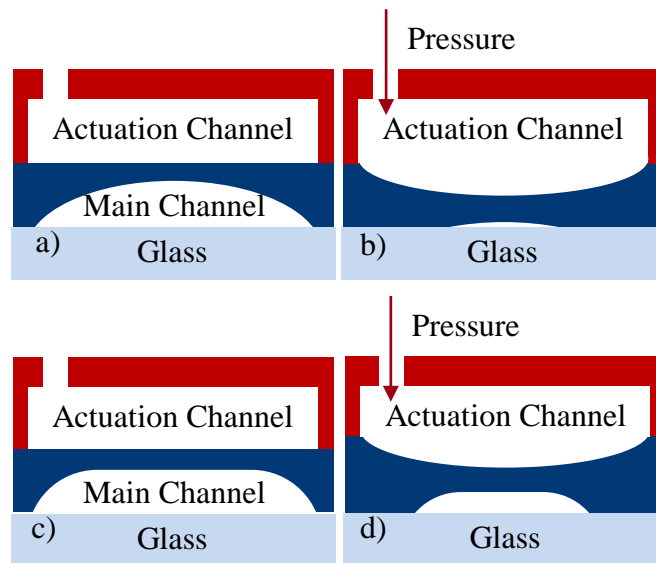


Figure 5.1.: Architectures and working principles of push down valves. a) soft main channel with cylindrical cross-section; b) channel collapsed under pressure closing the valve; c) soft main channel with rounded-rectangular cross-section; d) channel collapsed under pressure without closing the valve.

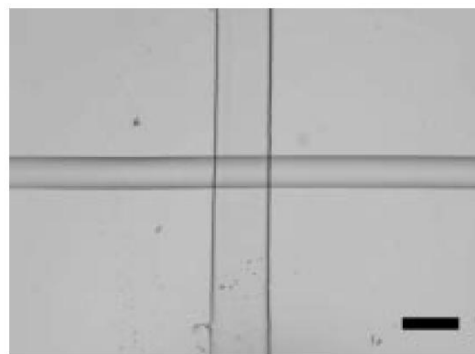


Figure 5.2: Optical micrographs of a valve with $200\ \mu\text{m}$ control line and $100\ \mu\text{m}$ flow line. Control line is oriented vertically. Extracted from [51].

5.3 Soft channel manufacturing

The channel geometry is obtained by letting liquid PDMS solidify over a mould (the master), shaped as the negative of the channel. To produce the master, *multilayer soft lithography* is used. A layer of SU-8 photoresist is first deposited on a flat silicon substrate by spin coating (layer thickness controlled by rotational speed of the spin coater and by the duration of the coating process). Then a mask is laid on top of the SU-8 surface (the mask is produced by

high-resolution printing on film), and the masked workpiece is exposed to UV light. UV intensity and time of exposure influence the quality of the final mould and in particular the quality of the channel edges. Then SU-8 layer is etched, to obtain the protruding negative of the channel. Since the negative has an approximately rectangular cross-section, the master is baked to allow some reflow of the SU-8 photoresist, so that an approximately rounded cross-section is obtained. This is the final master shape which is used for producing the final channel, by solidification of liquid PDMS.

Evidently, the critical step for obtaining the final geometry of the channel cross-section is the baking of the master, since only an approximate, indirect control can be exerted on the reflow of the SU-8 photoresist. Thus it is hard to achieve good accuracy and good repeatability on the channel geometry, which leads to high scrap rates of not devices not functioning properly.

5.4 Current practice of quality inspection

Quality inspection addresses first the individual part (PDMS soft layer containing the channels) and then the whole assembled valve device. The individual part is controlled mainly through visual inspection by means of conventional 2D optical microscopy and SEM imaging; most of this inspection is devoted to the identification of localized defects in the material (bubbles, inclusions, lack of material). Later, the final assembled device is subjected to functional verification. Two are the main identified causes for the valve failing the verification process: incomplete bonding between layers at assembly (which can be detected at functional testing, when fluid is observed leaking out of the channels sides, and into the gaps between the valve layers), and incomplete closure of the main channel (which can be detected by observing fluid flowing through the main channel despite applying the correct closing pressures and in absence of lateral leaks). The second type of functional failure can be safely ascribed to an imprecise realization of the channel cross-section geometry and/or aspect-ratio. The benefits of adopting a procedure for quantitative characterization of channel geometry, such as the one proposed in this work, are immediately evident: a better awareness of the mechanisms that lead to a channel not being able to fulfil its functional requirements, an improved understanding of manufacturing process capability (which in turn leads to the possibility of optimizing process parameters and designing improved process-aware product geometries), an overall reduction of scrap rate, and ultimately, the development of increasingly more performing and reliable product evolutions.

5.5 Foundations of the proposed approach for the assessment of channel geometry

Analogously to the typical approach followed in dimensional metrology of regular-size geometry, the proposed approach is based on the adoption of a coordinate metrology solution for acquiring a set of points from the specimen under investigation, reconstructing the geometrical features from such points and assess whether their deviations from nominal geometry are compatible with specifications.

At least two major aspects, specifically arising from the small size of the microfluidic channel, make the whole process peculiar: the first is related to the selection of *3D profilometers* and *3D microscopes*, operating as range imaging devices, over CMMs (micro and nano-CMMs) as the instruments of choice for acquiring point sets at such small scales, which leads to a series of issues to be dealt with in terms of measurement execution and data processing. The second is the need to adapt the overall geometric verification procedure, as defined by several ISO standards and in particular by ISO 17450-1, to operate on data which was not generated by a CMM, and therefore presents a whole series of challenges which are not commonly dealt with.

5.5.1 Micro and nano CMMs vs. 3D optical profilometers

CMMs are the most widely adopted solution for the dimensional metrology of standard-sized parts. Their advantage resides in the possibility of planning the sampling strategy optimizing the verification processes. The disadvantage resides mainly in measurement times, as point acquisition is intrinsically sequential. As a consequence of their widespread adoption, most standards on geometric verification more or less implicitly assume CMM measurement, and a large amount of information exists to ensure full characterization of metrological performance, especially in terms of measurement uncertainty and traceability.

Range imaging solutions, such as structured light scanners, are increasingly gaining popularity as an alternative to CMMs for standard-sized parts, given their ability to acquire a very large number of points in extremely short times. The main disadvantage is the lack of established procedures for assessing metrological performance. In particular, measurement uncertainty and traceability are still open issues.

Typical aspects of range imaging should also be considered: *unidirectional observation* (no vertical surfaces or undercuts can be acquired), *uniform sampling density* with *gridded layout*

(which may be suboptimal since it may not comply with the requirements of localized features), and *rectangular acquisition area* (again potentially suboptimal with respect to measurand projected boundaries).

A parallel to the illustrated scenario can be drawn for the metrological characterization of very small parts. On one hand, micro and nano-CMMs are increasingly becoming available, sharing some of the same advantages and disadvantages of the conventional CMMs.

On the other hand, instruments such as optical 3D profilometers and microscopes are already available in the neighbour domain of surface metrology, where they have been primarily developed for the characterization of three-dimensional surface finish [52]. They provide the main advantage of acquiring dense point sets in very short times, although with the same intrinsic disadvantages of range imaging devices illustrated above. It should be pointed out that, when specifically addressing the micro and sub-micro worlds, sampling strategies based on a gridded layout may not necessarily be a disadvantage: as a matter of fact, not enough knowledge may be available to plan a dedicated sampling strategy, in particular when little control can be exerted on the features of the surface being manufactured.

In the micro world, between CMM and optical 3D profilometers and microscopes, an intermediate class of instruments can be identified, represented by stylus-based 3D profilometers and atomic force microscopes (AFMs). Both adopt a sequential, point-by-point acquisition strategy, like CMMs, but acquire points according to raster scanning strategies, so that the resulting point set is topologically organized into a gridded layout, making the result essentially equivalent to a range image. This category of instruments can be considered an attractive option in specific circumstances, given the high-resolutions achievable (especially with the AFM), and the reliability of contact measurement (with the stylus-based profilometer) at least for specific types of surfaces. Efforts have been made, to make AFM-operation in dimensional verification more similar to CMMs, through the implementation of non-raster sampling strategies [32].

Given the described scenario of commercially available measurement instruments, in this work a specific class of optical 3D microscopes has been selected: the optical 3D confocal microscopes. These are a range imaging devices, with very fast measurement times, a non-contact measurement technology (which is essential for soft materials such as the PDMS), and measurement specifications (range and resolution) compatible with the specific microfluidic channel geometry.

5.6 ISO 17450-1 work flow

ISO 17450-1 define the work flow for the verification of manufactured workpieces. The standard considers three main steps necessary to perform a verification and comparison for conformance.

The first step is the definition of a nominal model of the sample. The information contained in the nominal model specified which ideal features compose the sample. Every single feature is described through dimensions, positions and tolerances. These information are the nominal requirements.

The second step is the definition of a non-ideal surface model called “skin model” that is the geometrical representation of the real workpiece using an infinite set of points. In this step a set of operation such as partition, extraction, filtration, association, collection, construction and evaluation are designed. These operations will be physically performed on the real sample during the measurement procedure, so the second step can be considered the design of the measurement procedure that will be performed on the manufactured workpiece. The third step is the verification of manufactured workpiece for compliance with design intent. In this step, the operations defined in the previous step are physically performed, i.e. the measure is performed. Measurement results are calculated as defined in the second step and compared with the nominal characteristics. ISO 17450-1 has been considered as reference for this work [13].

5.7 Nominal model and measurand definition

In the case considered in this work, a nominal model of the sample is not provided. The geometries and dimensions of the samples are defined without tolerances specifications.

During the manufacturing of the sample two parameters are defined:

- the width of the tracks printed in the mask used during photolithography,
- the thickness of the photoresist deposited through spin coating on the silicon substrate.

Dimensions of the channels results from the manufacturing process and are not taken into account when producing channels for normal application of fluid transport.

In order to define features and measurands, the sample has to be roughly modelled (Figure 5.3) considering the manufacturing process and information derived from optical and scanning electron microscopy.

The proposed model of the sample is constituted by two surfaces, a plane indicated as “top plane”, and a cylindrical surface that represent the channel. The model is based on the hypothesis that the channel surface is part of a cylinder, with the axis parallel to the top plane.

The measurands defined are:

- width of the channel defined as the distance between the lines obtained intersecting the top plane and the cylinder,
- depth of the channel defined as the distance between the bottom generatrix of the cylinder and the top plane,
- radius of curvature of the channel, i.e. radius of the cylinder.

This is a first modelling step necessary to define a measurement procedure.

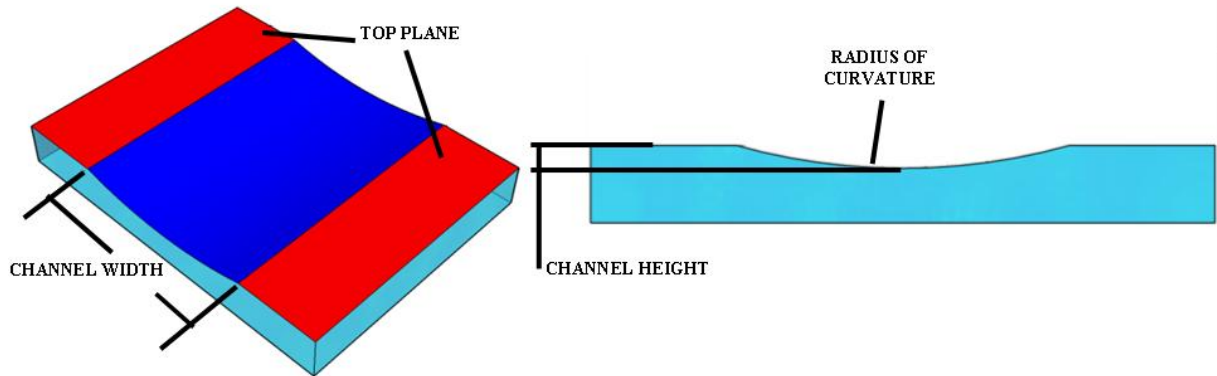


Figure 5.3: Representation of the nominal model constituted of a plane (red) and a cylindrical surface (blue).

5.8 Data acquisition

The channel topography has been acquired using a state-of-the-art 3D optical profilometer (Sensofar Plu Neox) [53] operating in confocal mode with blue light ($\lambda_{\text{blue}} = 460 \text{ nm}$). The proper objective has been selected considering two aspects:

- the field of view in order to acquire the whole channel topography without introducing stitching and consequent stitching errors.
- the capacity to acquire sloped surfaces in order to characterize the sides of the channels.

A Nikon CFI LU EPI P 20x magnification objective has been used. Main instrument data are summarised in Table 5.1. Instrument and objective have been calibrated using a flat mirror standard to correct the aberration and using a step height standard for vertical calibration. The

standard is provided by SiMetricS. It is a Silicon Depth Standard Type A1 (ISO 5436-1). The calibrated value of depth is $10.24 \mu\text{m} \pm 0.03 \mu\text{m}$ ($k=2$).

Table 5.1: Main instrument data.

	20x
NA	0.45
Maximum Slope	21°
FOV(μm)	636 x 477
Spatial Sampling	$0.83 \mu\text{m}$
Optical Resolution	$0.31 \mu\text{m}$
Vertical Resolution	$< 20 \text{ nm}$

A reference system is considered when measuring. The directions x , y are the axis of the plane perpendicular to the optical axis of the instrument. The sample surface is parallel to this plane. The optical axis of the instrument is the z axis. The result of a measurement is a set of data representing the surface topography of the sample. Data are organized in a $m \times n$ matrix that can be expressed as $I(i,j)$, $i=1,m$, $j=1,n$ where m and n are the number of pixels of the CCD sensor i.e. 768×576 . $I(i,j)$ value is the value of the z coordinate of the point measured on the corresponding i,j pixel. The value of the x,y coordinates of the i,j point are not directly measured.

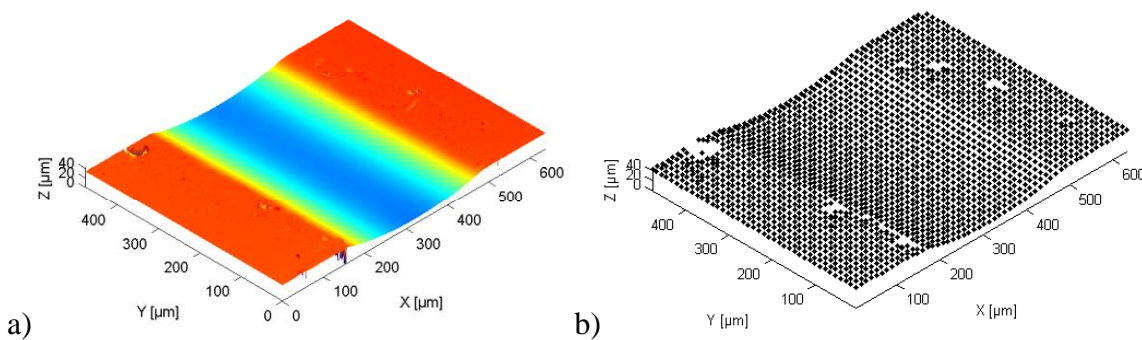


Figure 5.4: Representation of the acquired raw data as image/topography with height based colouring (a) and as point cloud (b). Data are distributed in a regular grid of: 768×576 points. The field of view is $636.61 \mu\text{m} \times 477.25 \mu\text{m}$. Pixel spacing results in $0.83 \mu\text{m} \times 0.83 \mu\text{m}$.

They can be associated to the pixel using information on measurement field of view and number of pixels. A grey scale image can be represented similarly using a matrix $I(i,j)$, but

while in an image the pixel value is the grey value, in this case the pixel value is the z value of the point. Associating x,y to I(i,j) pixels it is possible to export a point cloud, so every measured point is defined by three coordinate values. The output obtained from the instrument allows considering the data as image or point cloud (Figure 5.4) taking advantage of both image processing techniques and point cloud analysis.

5.9 Data analysis

Data analysis and processing are operations that allow obtaining quantitative information from the acquired topography. The results of data analysis are the measurement results of the measurands defined in the nominal model. The data analysis process followed in this work is based on the coordinate metrology. The data can be considered 2D ½ data, allowing the application both of image processing techniques and point cloud analysis.

The main steps followed for data analysis are:

- pre-processing
- points extraction and association
- measurements evaluation

5.9.1 Pre-processing

Optical profilometers are instruments dedicated to the surface characterization. Output data resulting from measurement are ready to be analysed with software dedicated to the calculation of the typical parameter for surfaces and profiles characterization. Output data has to be processed in order to allow the use of software dedicated to the point cloud analysis and coordinate metrology. The problem of management of files with different format is a mere computer science problem and it can be ignored. The main characteristic of the output data that must be considered for pre-processing are two:

- the presence of “void pixels”
- the presence of artefacts

5.9.2 Void pixels

When measuring with optical profilometers, in some points of the field of view, no measured

values are calculated. This happens when no light signal is reflected in the sensor. For example, when measuring deep holes or deep channels, the bottom surface is not illuminated and no signal is detected. Moreover, optical profilometers are limited in the acquisition of sloped surfaces. The maximum detectable slope depends on the numerical aperture of the objective, on the optical properties of the sample and on the surface roughness. Measurements of surfaces overcoming the maximum detectable slope result in signal absence, so in void pixels. In the output data, the value present in a “void pixel” is a conventional value, equal for every void pixel. The value can be a string indicating the absence of a numerical value or a conventional number. In both cases, but in particular in the second, calculation may be affected by errors. Hence, void pixels must be taken into account because they affect the data analysis in every calculation step. In this work the void pixels present on the measurement data have been identified and tracked. The position of the void pixels is registered in a logical matrix (i.e. an image as represented in Figure 5.5 b)) where boxes with the value 1 indicate the position of valid values and boxes with the value 0 indicate the position of void pixels.

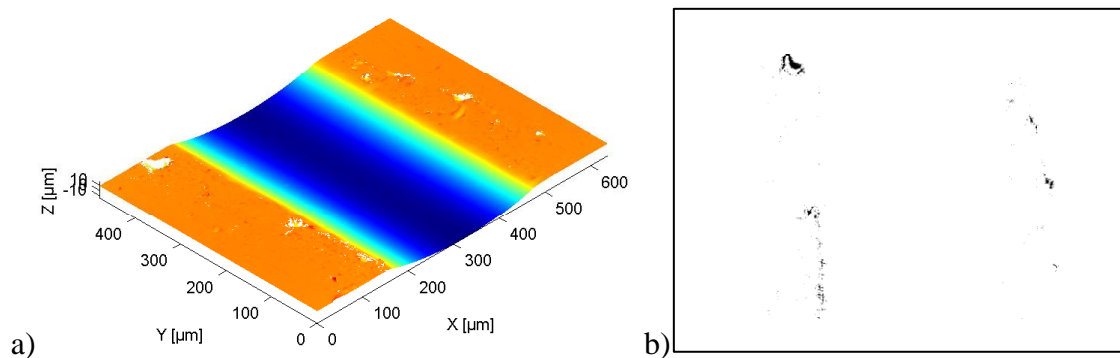


Figure 5.5: Representation of the acquired raw data as image/topography with height based colouring (a) and representation of the map of void pixels (b) with black pixels in correspondence of void pixels.

5.9.3 Artefacts

Other defects that can be present in the output data are the artefacts. The bad light reflection and detection, caused for example by dust or surface contaminations, can result in artefacts such as spikes. Spikes are visible as peaks that interrupt the continuity of the surface. The pixels interested by this phenomenon contain numerical values that are affected by large errors. Artefacts have been tracked through a custom filtering process (depicted in Figure 5.6) taking advantage from image processing techniques [54].

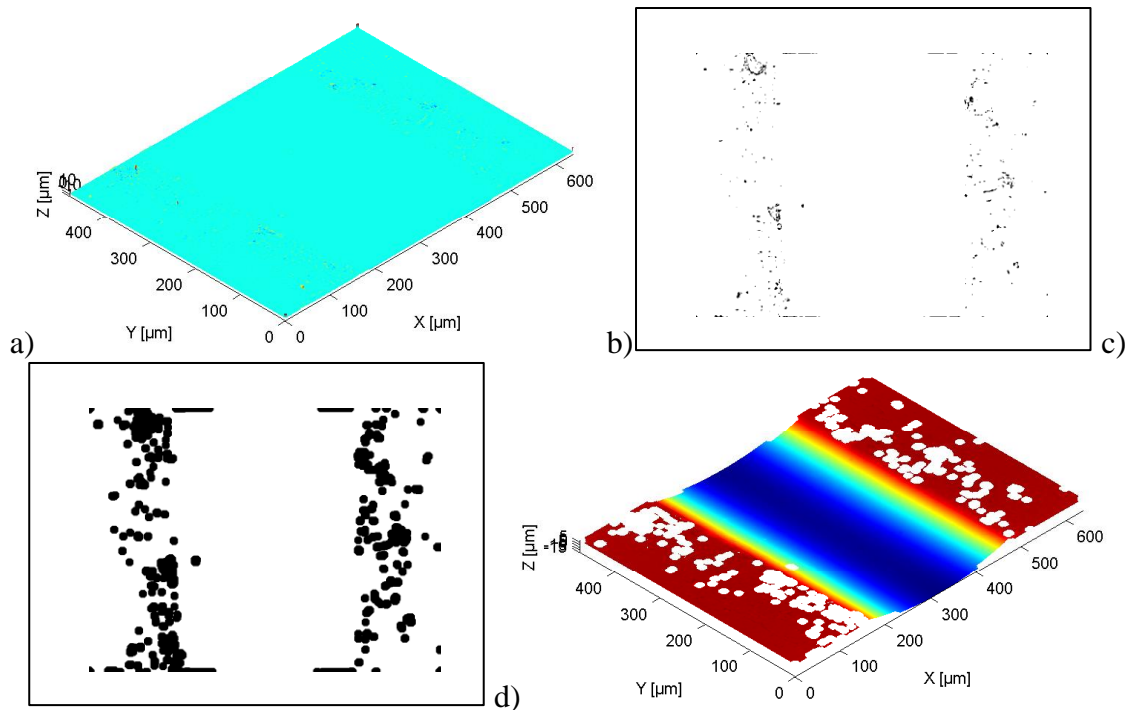


Figure 5.6: Representation of the filtering process. Sub image (a) and map of artefacts (b). Artefact maps after erosion of (c) and resulting filtered topography (d).

A modified version of the original image (I_{int}), where void pixels has been interpolated, is used in the procedure. The reason is that image filtering operations can cause distortion when encountering discontinuities on the image, so it is necessary to work with images that don't present void pixels. A median filtering operation has been applied and a smoothed version of I_{int} is obtained. The smoothed version has been subtracted from the starting image I_{int} obtaining a new image (Sub) where the differences between the two images are represented by spikes. Spikes are present where artefacts are present in the starting image. The median value and the standard deviation of Sub have been calculated. Artefacts positions have been identified imposing a threshold on the image Sub. The threshold is based on the pixels values. A zone of values between the median value plus and minus n times the standard deviation is considered. Pixels with values outside this zone are considered pixel where artefacts are present. A logical mask is created to map the artefacts. A morphological operation of erosion is applied on the logical map in order to map neighbour pixels around artefacts as pixels affected by errors. This map has been combined with the map of void pixels creating logical image that tracks the pixels that don't have to be considered in measurement calculation.

In this process several parameters must be established. In the specific case the kernel of median filter is 9×9 , the number of standard deviations around the median value for threshold is ± 4 and the structural element for image erosion is a disk with $R=13$.

5.10 Levelling

During image processing two steps of levelling are introduced. Levelling is necessary to identify a height reference when performing for example threshold operations. A first rough levelling is performed on the raw data after the void pixel mapping. A selective fine levelling is then performed in preparation to the measurement process. Plane levelling consists in calculate the z least-squares mean (z -LSM) plane for the image points, and subtracting the height values of the calculated plane from the height values of the original data points (z subtraction, also known as projection onto the x, y plane). Levelling procedures modify z coordinates of points while x, y coordinates are not recalculated. The cosine error in the position of the x, y coordinates of the points is introduced. A simplified model of two dimensions is presented in Figure 5.7.

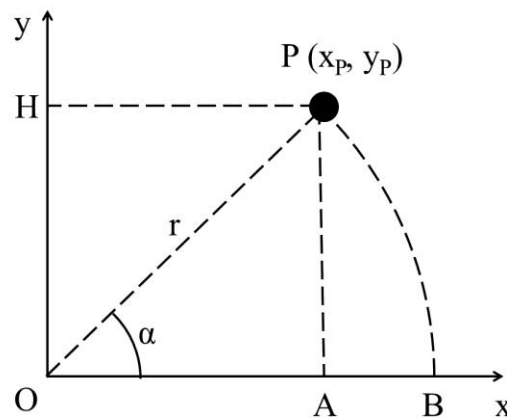


Figure 5.7: rotation of a point in two dimensions.

The point P after rotation is coincident to the point B and the x coordinate is equal to the length of the segment \overline{OB} , so it is equal to r (5.1). Plane levelling through plane subtraction move the point P to the point A and the x coordinate is equal to the length of the segment \overline{OA} expressed by (5.2). The error in the coordinate calculation is given by the length of \overline{AB} (5.3).

$$\overline{OB} = r \quad (5.1)$$

$$\overline{OA} = r \cdot \cos \alpha \quad (5.2)$$

$$\overline{AB} = r - r \cdot \cos \alpha = r \cdot (1 - \cos \alpha) \quad (5.3)$$

Considering the centre of the topography as centre of rotation the maximum value of r is 318 μm (instrument configuration as expressed in Table 5.1). The maximum value of permissible error is half the spatial resolution that is 0.415 μm . This result in a maximum value of $\alpha = 2.93^\circ$. With an accurate positioning of the sample the angle of tilting is lower than the limit value. Therefore the tilting correction through plane subtraction is not influencing the topography because the introduced error is lower than half the spatial resolution. A more accurate procedure of levelling consists in calculating the normal vector of the z-LSM plane and rotating the topography in order to obtain that the normal vector is parallel to the vertical axis. The rotation works correctly considering point cloud, but errors can introduced when considering images. For example rotation can causes that two value of height are associated to a single pixel. Moreover, when processing images, a matrix where surface is described by a grid is necessary, so a resampling of the topography would be necessary after rotation. A resampling is based on interpolation of values so errors are introduced in the topography. Considering that errors are introduced in both levelling procedures and taking into account the computational time required for resampling, the levelling based on plane subtraction has been preferred in this work.

5.11 Feature extraction and association

As discussed previously and represented in Figure 5.3, the sample is modelled considering two geometrical features: a plane and a cylindrical surface. Extraction feature operation used to identify specific points from a non-ideal feature. Usually the extraction is based on the identification of the edges between the features. In macro scale edges are portions of sample smaller respect to the dimensions of the features resulting in sharp and defined zones. In the case proposed in this work edge identification is not possible because the connection between the features results in rounded surfaces. Moreover, the dimensions of features are comparable to the dimensions of edge. A procedure based on the use of threshold has been used.

5.11.1 Extraction of the plane, association and levelling

For the extraction of the points belonging to the top plane two threshold criteria have been considered.

The first criteria take into account the gradient of the surface. Top plane is a flat part of the sample where the gradient is approximately zero. A gradient image is calculated starting from I_{int} and points with a gradient value lower than the established value of threshold have been considered. Even if this is an effective way to consider only the points belonging to the plane, some points that lay on the bottom region of the channel, that is a flat region, are mapped. A second threshold criteria based on the value of height is necessary and takes into account that the points of the plane have high values of height while the points on the bottom of the channel are at the bottom of the topography. A logical image is defined in order to map the points belonging to the plane. Applying the map to the filtered topography the points belonging to the plane have been identified and then fitted with a z-LSM plane, for the association step (see Figure 5.8 a)). Whole topography has been levelled. Hence, the top plane is also the plane of alignment for coordinate measurement.

5.11.2 Extraction of the cylindrical surface and association

The criteria followed for the extraction of points belonging to the cylindrical surface, so to the channel, is based on threshold of height. Considering the z range of values of the topography, points under the 50% of the range value are considered part of the cylindrical surface. Two features, a plane and a cylinder, are considered as feature. Even if points that can be associated to the plane have been extracted, this does not mean that remain points must be associated to the cylinder. The steepest zone of the channel is affected by acquisition errors. In fact, confocal microscopy suffers of error acquisition when measuring sloped surfaces due to bad optical reflection. For this reason the selected threshold value is 50% (see Figure 5.8 b)).

The association of the selected points with a cylinder, so the fitting operation, has been performed through a least square geometric elements fitting of cylinder [55] developed by NPL. The fitting has been performed considering different weights for the points. Considering the error of the instruments measuring sloped surfaces, weights have been calculated on the base of the vertical distance of the point from the threshold value. In this way points with bigger weight are the points at the bottom of the channel so the points that are affected by a

lower acquisition error.

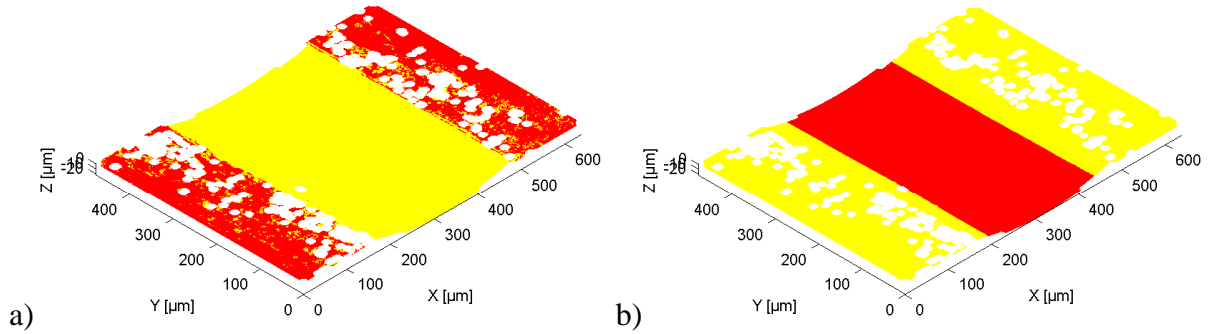


Figure 5.8: Representation of the extraction. Extraction of the points associated to the top plane (a) and extraction of the points associated to the cylinder. Extracted points are red.

5.12 Evaluation

During the definition of the nominal model, three measurands have been defined: the radius of curvature of the channel, the height of the channel, the width of the channel. These characteristics are easy to be defined in the nominal model where the axis of the channel is parallel to the top plane. Except for the radius of curvature that is evaluated through the radius of the cylinder associated to the channel, more consideration has to be done for the definition and evaluation of the width and the height of the channel.

5.12.1. Evaluation of the width of the channel

In the nominal model the width of the channel is defined as the distance between the lines obtained intersecting the two features, cylinder and plane. In the case of the nominal model the axis of the cylinder and the plane are parallel so the lines obtained by intersection are straight and parallel. The distance between the lines is unique. Moreover, the lines of intersection correspond to the channel edges. Considering the associated features, the axis of the cylinder is not parallel to the top plane and their intersection results in an ellipse. The lines that have to be used for the calculation of the distance are portion of an ellipse, so the definition of distance is not unique (see Figure 5.9). Two points on the elliptic lines are calculated intersecting a second plane, perpendicular to the axis of the cylinder and perpendicular to the top plane. The distance between the two points is a distance vector normal to the axis of the cylinder. Theoretically, an infinite number of distances between

intersection points can be calculated. In this work a finite number of distances have been calculated for computational reasons. The width of the channel has been calculated as the mean of all the calculated distances.

5.12.2 Evaluation of the depth of the channel

Again, considering the nominal model, the depth of the channel is defined as the distance between the bottom of the channel and the top plane. The bottom of the channel is calculated intersecting a plane perpendicular to the top plane and containing the axis of the cylinder.

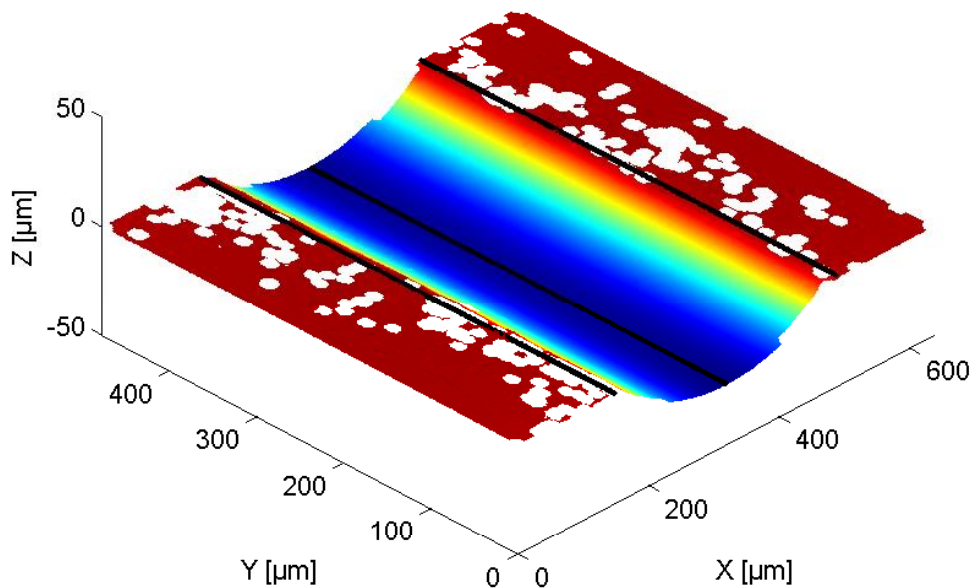


Figure 5.9: Representation of the topography and lines of intersection (black) between the associated features: edges and bottom.

In the nominal model this result in a straight line that is a cylinder generatrix, parallel to the axis of the cylinder and parallel to the top plane. Hence the channel depth, defined as the distance between the intersection line and the top plane, result in a unique value. Considering the associated feature the intersection result in a generatrix of the cylinder, but the line is not parallel to the top plane. This means that there are several values of depth, theoretically an infinite number. The depth of the channel has been calculated considering a finite number of points of the line of intersection and calculating the average distance between the top plane and the points.

5.12.3 Results

Five data sets have been acquired from the sample at the same measurement conditions. Data set have been processed as explained in the paper without changing the processing parameters (thresholds, kernel size, etc.). Results are reported in Table 5.2.

Table 5.2: Results of the evaluation. Results are expressed in μm .

	Width	Depth	Radius
1	342.178	22.703	656.004
2	343.023	22.704	659.166
3	342.197	22.677	656.812
4	340.880	22.703	651.125
5	344.143	22.694	663.682
Mean	342.484	22.696	657.358
St. Dev.	1.203	0.012	4.589

5.13 Discussion

In this paper it is shown that is possible to perform 3D dimensional measurements of specimen at micro scale. Even if the specimen are not adapt to be measured using the conventional instruments for topography characterization at micro scale, such as stylus profilometers and scanning probe microscopes, it is possible to obtain quantitative results using the optical microscopy. Confocal microscopy or white light interferometry provides 3D surface topography of a specimen with high precision. These techniques were mainly developed for surface characterization [56, 57] but through an innovative data processing technique they resulted applicable also for coordinate metrology. The developed data processing method is obtained merging surface analysis, image processing and point cloud analysis techniques. The approach here proposed is one of the first steps of dimensional metrology at micro scale [58–60] and it is believed that the several micro-fabricated parts can be characterized in the same way. By the way some general issues need further investigation.

5.13.1 Measurement limitations

Being 3D optical profilometers developed for surface characterization, they acquire the topography probing the sample from a single direction identified as the z-axis. This means that the acquired topography is not a real 3D geometry, but it is a 2½D, because undercuts,

but also tilted surfaces, are not acquired.

Stitching images taken changing the orientation of the sample can be a solution in order to have a full 3D topography. The vertical and lateral resolutions increase using objectives with high magnification. Usually objectives with large zoom present also high numerical aperture values increasing the maximum detectable slope. High magnification objectives present lower field of view and measurement range, so stitching can be necessary. Unfortunately stitching present some disadvantages. Errors are introduced by the stitching data processing, so the accuracy achieved through a best objective is lost. The acquisition time can be very long (hours for an area of few mm^2) and the amount of data is limited by computer memory capacities. The measurement technique would not be useful for in-line applications.

Stitching of images is an interesting evolution for fully 3D measurements but it requires further investigation on the effect on measurements. CT systems are alternative solution [61, 62], however they supply a huge size of data and the measurement time is long.

5.13.2 Sampling

3D optical profilometers provide a grid based sampling. Acquired points are equally spaced in x, y directions on the basis of the acquisition sensor. The lateral resolution can be limited by the pixel spacing. The lateral resolution depends on the number of pixel of the sensor and on the objective magnification. The choice of the objective magnification is limited by the sample sizes in order to acquire the entire sample in a single acquisition avoiding stitching. A “smart sampling” could be useful in order to improve the resolution where needed and in order to decrease the points density where high resolution is not required. This will result also in a reduction of the amount of data, increasing data processing time [63, 64].

5.13.3 Data processing

Data processing proposed in this work, merges techniques deriving from image processing, surface characterization and point cloud analysis. Image processing techniques are easily available and well known in the world of imaging and the application to the dimensional metrology as shown in this work is immediate. By the way, the effect of the algorithms, such as filtering, levelling or erosion must be considered when performing dimensional metrology. For example a median filtering should have been enough to reduce artefacts, but the

application of the median filtering cause distortion in geometries, smoothing the surface. For this reasons a custom filtering procedure have been developed. Hence, even if the application of algorithm of image processing is equivalent between grey scale images and topographies, it can result in measurement errors. Studies on the effect of the data processing on the dimensional measurement of sample are necessary.

5.13.4 Traceability and Uncertainty

Traceability and uncertainty assessment are fundamental for quantitative measurements. Even if the microscope used in this work has been calibrated through a certificated standard, the traceability of optical instruments is still an issue. ISO 25178 provide the state of the art in the field of surface characterization covering also the calibration of instruments for surface characterization. By the way currently there is only a draft of ISO 25178 covering the calibration of optical instruments for surface characterization. If traceability is an issue, uncertainty evaluation is a big problem. Using optical instruments, the measurements are affected by errors that are related to the properties of the samples. Surface finishing, surface colour, the material reflectivity or environmental illumination influence the measurement results and errors are difficult to quantify. Sources of uncertainty related to the instruments are:

- uncertainty due to the sampling strategy
- uncertainty due to the instrument resolution
- uncertainty due to the residual flatness and optical aberration
- uncertainty due to the z positioning through piezo or vertical linear scale
- uncertainty due to the nonlinearity of the z scale
- uncertainty due to the interaction of the surface, the light and the objective
- uncertainty introduced by the algorithms for the calculation of the z value of a points

Other sources of uncertainty are related to the data processing and are all the used software algorithms.

In this work authors are not able to quantify the uncertainty correlated to the performed measurements, however the scope of the work is to propose an innovative way for metrology at micro scale.

5.13.5 Application of ISO 17450-1

As stated in 5.6, the specification ISO 17450-1 has been a reference for the development of the measurement procedure. Moreover, ISO 17450-1 have been developed for macro scale metrology through CMM and its application at micro scale requires adjustment. Differences between macro scale and micro scale metrology are here reported.

Procedure described in the specification is based on the definition of a nominal model. Nominal model is the starting point for the definition of the geometrical features, dimensions and specifications; for the definition of the skin model and of the measurement procedure. In micro scale, real parts can result far from the ideal model because of the manufacturing process capabilities. The form error of the geometries of the real parts can be so high to result in different features. Moreover, the dimensions of the feature can result similar to the dimensions of the transition zones between features. Physical partition can result real complicated and affect the measurement results.

Directly connected to the partition is the extraction. In the macro scale world, points are acquired probing points on the desired feature, so acquired points are associated to the feature while they are acquired. Measuring with optical profilometers a grid of points is acquired. Physical extraction has to be performed through clustering and threshold algorithms that require several parameters to be set for the implementation. Following step of association, collection, construction and evaluation result equivalent both for macro scale and micro scale. Evaluation result more complicated in micro scale than in macro scale world. In fact, the problem is in the specification definition. As discussed in previous works [1, 65], while in macro world the tolerance zone is hundred or thousand times smaller than the dimensions of the workpieces, in micro world this could be impossible to realize and to control. This is still a big issue in micro metrology. The procedures necessary to perform 3D coordinate metrology at micro scale through optical profilometers need further investigation in order to understand their effect on measurement results.

5.14 Conclusions

In this work a method to perform 3D coordinate metrology at micro scale through the use of optical profilometers has been proposed. The method is based on the use of new algorithms for data processing that merge techniques deriving from dimensional metrology (e.g. point cloud analysis) and image processing (e.g. filtering process). The approach has been applied

to the measurement of a microfluidic channel realized by soft lithography and constituting part of a valve. Through the proposed approach it is possible to obtain quantitative information about the dimensions and geometries of the channel. It is reasonable to imagine to extend the approach here presented, to the characterization and quality inspection of similar micro fabricated parts and devices. Several issues have to be solved in order to obtain a fully metrological approach to the micro parts measurements. In particular problems related to metrological traceability and uncertainty assessment must be resolved.

Conclusions

The main conclusions of the research activities conducted during the Ph.D. period and described in this thesis are here summarised.

In Chapter 1 and Chapter 2 a review of the state of the art of micro engineering and in particular of metrology at micro scale is given.

The process of miniaturization of products started 30 years ago in the field of micro electronic technologies and today involves other fields such as medicine, biology or aerospace engineering. A small product means, less material, less weight, less manufacturing time, less logistic costs, less environmental impact, so less money for the production. From the study of the state of the art resulted that the quality control and the metrology in particular, is a fundamental part of the manufacturing process for two reasons:

- to guarantee products that respect the specifications,
- to give useful information to improve the manufacturing process.

Instruments for the inspection of defects and for quantitative 2D measurements are available at the state of the art and commonly used in industry. Instruments able to give a full 3D characterisation of the geometries are now commercially available and being introduced in industry, since they are more effective when investigating more complex components. Three categories of instrument for 3D coordinate metrology at micro scale have been studied: scanning probe microscopes (SPMs), optical profilometers (WLI and confocal microscopes), and micro and nano coordinate measuring machines. It has been decided to focus on two of these categories: the scanning probe microscopes and the optical profilometers. Atomic force microscopes are the instruments that can give the best resolution for the assessment of surface topography while the optical profilometers are the instruments that have the biggest working range, the easiest to be used and the fastest. Moreover, commercial optical profilometers for surface characterization are quite recent and their technological evolution is expected. The importance of this category of instruments is given also by the publication of some dedicate international standards (ISO 25178 series).

In Chapter 3 the use of these techniques for the quality control of parts realized through replication has been studied. The study considered the possibility to measure the surfaces of the parts present in a replication process (mould inserts and replicated parts) and to calculate a single parameter, able to describe and to map the quality of the replication process, both in

structured and unstructured surfaces. Artificial data sets were used to simulate replicated surfaces and to test their measurements through different instruments. The results were analysed in order to compare the quality of surface replication from the master to the final part. It resulted that simulations of replication can help to select the correct instrument and measurement settings. Roughness parameters related to the Abbot-Firestone curve resulted useful to monitor the quality of a replica if the part presents isolated features extended along a direction perpendicular to the surface. Cross correlation index can be used to provide a description of the similarity between master and replications and when combined with a Fourier analysis can also highlight the presence of distortions during demoulding. However, it is clear that the cross correlation is limited by the necessity to obtain two measurements of the same portion of the surface in the master and the replica.

On the basis of these results emerged that the quality of replication can be controlled through the measurement of a single parameter only in few cases. When the product presents structured surfaces with three dimensional features or complex geometries there is the necessity to perform 3D metrology to characterize geometries and dimensions. Surface metrology is not enough, but instruments for surface metrology can be used and adapted for 3D coordinate metrology at micro scale.

A category of instruments candidates to be adapted for coordinate metrology at micro scale are the Scanning Probe Microscopes (SPMs). SPMs are well-known instruments, but in order to perform accurate measurements it is important to study the sources of error affecting measurements. Many of the sources of error are well known except the thermal drift. In Chapter 4 it is presented a study conducted to correlate long term thermal phenomena to drift distortions in an SPM scanner. Drift estimation was cross-correlated to thermal analyses carried out by means of an infrared-camera. Mapping of long term drift distortions and temperature allows some important conclusion. The study proves the strong correlation between long term temperature variation and average drift distortion. It indicates that to reduce drift, operations have to focus on thermal stability. Scanning parameters have a negligible influence on the long term thermal behaviour of the scanner. Mapping of drift distortions and temperature allows the identification of the temperature transient and also the characterization of the residual short time instability. The identification of the warm up time is needed to stabilize the scanner. The characterization of the residual short term instability in terms of size and frequency help to define scan time and scan range that minimize the short

time drift, therefore minimizing uncertainty contribution. The optimization of instrument set up is possible. Thermographic maps allow recognizing temperature gradients within the instrument, the stage and the sample: this can help optimization of instrument set up, by insulating heat sources, or conditioning critical components. A second study was conducted to estimate how much drift distortions affect SPM measurements with different set up configurations. Six different instruments were compared on the basis of the previous experimental analysis. Results show that for commercial instruments, average thermal drift as large as 50 nm min^{-1} can be expected both in the horizontal and vertical planes, unless the instrument converges to a stabilized state. Stabilization time for the scanner to converge to a drift rate below the short-time stability is normally less than 30 min. Residual short-time instability as large as 15 nm can be expected for an instrument after stabilization. It is evident how a compact instrument architecture combined with low thermal gradient is important to keep drift at low values.

In order to perform 3D coordinate metrology using instruments developed for surface metrology such as scanning probe microscopes and optical profilometers a new approach to data analysis have been developed. In Chapter 5 the new approach is presented and applied to a case study of a microfluidic device measured through an optical profilometer.

The new method take inspiration from the procedures for coordinate metrology described in ISO standards and applied to meso and macro scale products. The micro dimensions of the geometrical features and the measurement technique required some adaptations of the conventional procedures. Dedicated algorithms of data management, filtering and points extraction have been developed to overcome these differences in order to define a semi-automatic and repeatable measurement approach. A calculation code has been developed. The code take advantage of the double nature of the data resulting from the measurements performed through the optical profilometers. Data can be considered as images or as point cloud. Dedicated procedures of filtering have been developed and adapted in order to reduce the artefacts presents in the data. Algorithms of thresholding of the data for the points extraction have been developed and implemented. Finally the extracted points have been associated to the feature for the evaluation of the dimensions and geometries.

Through the proposed approach it is possible to obtain quantitative information about the dimensions and geometries of micro components.

In conclusion the implementation of coordinate metrology at micro scale is still problematic.

Considering aspect such as geometrical product specification there is a lot of work to be done, however in author's opinion. The main issue is in connection to the evaluation of measurement uncertainty. In particular, optical instruments lack in terms of traceability and without traceability the measurements can be considered only in relation to other measurement performed in the same conditions. Future work should then regard the development of calibrated standards and procedures to give traceability to the measurement.

References

- [1] H.N. Hansen, K. Carneiro, H. Haitjema, L. De Chiffre, (2006), "*Dimensional micro and nano metrology*", CIRP Annals - Manufacturing Technology, 55, 721–743.
- [2] K.J. Stout, (1998), "*From cubit to nanometre - a history of precision measurement*", Press, Penton.
- [3] L. Alting, F. Kimura, H.N. Hansen, G. Bissacco, (2003), "*Micro engineering*", CIRP Annals - Manufacturing Technology, 52, 635–657.
- [4] G. Bissacco, (2004), "*Surface generation and optimization in micromilling*", Ph.D.Thesis, Supervised by Prof. Leonardo De Chiffre, Technical University of Denmark.
- [5] A. Weckenmann, T. Wiedenhofer, (2005), "*The use of the GPS-Standard in Nanometrology*", Proc. of 5th euspen international conference, pp. 169–172, Montpellier, France.
- [6] P. Bariani, (2005), "*Dimensional Metrology for Microtechnology*", Ph.D.Thesis, Supervised by Prof. Leonardo De Chiffre and Prof. Hans N. Hansen, Technical University of Denmark.
- [7] M. Reilly, S P, Leach, R K, Cuenat, A, Awan, S A, Lowe, (2008), "*NPL REPORT DEPC-EM 008 - Overview of MEMS sensors and the metrology requirements for their manufacture*".
- [8] G. Rodger, (2001), "*Measurement Good Practice Guide nr. 39 - Dimensional Measurements using Vision Systems*", NPL - National Physical Laboratory, Teddington (UK).
- [9] A. Voltan, (2010), "*Metrological performance verification of optical coordinate measuring systems*", Ph.D.Thesis, Supervised by Prof. Enrico Savio, Università degli Studi di Padova.
- [10] F. Marinello, P. Bariani, E. Savio, A. Horsewell, L. De Chiffre, (2008), "*Critical factors in SEM 3D stereo microscopy*", Measurement Science and Technology, 19, art. n. 65705.
- [11] L. Carli, (2010), "*3D-SEM metrology for coordinate measurements at the nanometer scale*", Ph.D.Thesis, Supervised by Prof. Leonardo De Chiffre, Technical University of Denmark.
- [12] F. Marinello, (2007), "*Atomic force microscopy in nanometrology: modeling and enhancement of the instrument*", Ph.D.Thesis, Supervised by Prof. Paolo F. Bariani and Prof. Leonardo DE Chiffre, Università degli Studi di Padova.

- [13] (2011), ISO 17450-1:2011 Geometrical product specifications (GPS) -- General concepts -- Part 1: Model for geometrical specification and verification, Iso, Geneva.
- [14] G. Tosello, H.N. Hansen, F. Marinello, S. Gasparin, (2010), "*Replication and dimensional quality control of industrial nanoscale surfaces using calibrated AFM measurements and SEM image processing*", CIRP Annals-Manufacturing Technology, 59, 563–568.
- [15] G. Tosello, H.N. Hansen, S. Gasparin, (2009), "*Applications of dimensional micro metrology to the product and process quality control in manufacturing of precision polymer micro components*", CIRP Annals - Manufacturing Technology, 58, 467–472.
- [16] R.K. Leach, (2010), "*Fundamental principles of engineering nanometrology*", William Andrew, Elsevier, 1st ed.
- [17] (2012), ISO 25178-2:2012 Geometrical product specifications (GPS) -- Surface texture: Areal -- Part 2: Terms, definitions and surface texture parameters, Iso, Geneva.
- [18] P. Pawlus, L. Galda, A. Dzierwa, W. Koszela, (2009), "*Abrasive wear resistance of textured steel rings*", Wear, 267, 1873–1882.
- [19] T. V. Vorburger, J.F. Song, W. Chu, L. Ma, S.H. Bui, A. Zheng, et al., (2011), "*Applications of cross-correlation functions*", Wear, 271, 529–533.
- [20] B. Mokaberi, A.A.G. Requicha, (2004), "*Towards automatic nanomanipulation: drift compensation in scanning probe microscopes*", Proc. of ICRA 04 International Conference on Robotics and Automation, pp. 416–421, Barcelona, Spain.
- [21] A.A.G. Bruzzone, H.L. Costa, P.M. Lonardo, D.A. Lucca, (2008), "*Advances in engineered surfaces for functional performance*", CIRP Annals - Manufacturing Technology, 57, 750–769.
- [22] H.N. Pishkenari, N. Jalili, A. Meghdari, (2006), "*Acquisition of high-precision images for non-contact atomic force microscopy*", Mechatronics, 16, 655–664.
- [23] F. Marinello, P. Bariani, S. Carmignato, E. Savio, (2009), "*Geometrical modelling of scanning probe microscopes and characterization of errors*", Measurement Science and Technology, 20, art. no 84013.
- [24] H.J. Hug, T. Jung, H.J. Guntherodt, (1992), "*A high stability and low drift atomic force microscope*", Review of scientific instruments, 63, 3900–3904.
- [25] F. Marinello, P. Bariani, L. De Chiffre, E. Savio, (2007), "*Fast technique for AFM vertical drift compensation*", Measurement Science & Technology, 18, 689–696.
- [26] B. Sahu, C.R. Taylor, K.K. Leang, (2010), "*Emerging challenges of microactuators for nanoscale positioning, assembly, and manipulation*", Journal of Manufacturing Science and Engineering, 132, 1–16.

-
- [27] Y. Zhao, D.L. Trumper, R.K. Heilmann, M.L. Schattenburg, (2010), "*Optimization and temperature mapping of an ultra-high thermal stability environmental enclosure*", Precision Engineering, 34, 164–170.
- [28] M.A. Donmez, M.H. Hahn, J.A. Soons, (2007), "*A novel cooling system to reduce thermally-induced errors of machine tools*", CIRP Annals-Manufacturing Technology, 56, 521–524.
- [29] H. Schwenke, W. Knapp, H. Haitjema, A. Weckenmann, R. Schmitt, F. Delbressine, (2008), "*Geometric error measurement and compensation of machines - an update*", CIRP Annals-Manufacturing Technology, 57, 660–675.
- [30] D. Huo, K. Cheng, F. Wardle, (2010), "*A holistic integrated dynamic design and modelling approach applied to the development of ultraprecision micro-milling machines*", International Journal of Machine Tools and Manufacture, 50, 335–343.
- [31] F. Marinello, E. Savio, P. Bariani, S. Carmignato, (2009), "*Coordinate metrology using scanning probe microscopes*", Measurement Science and Technology, 20, art. n. 84002.
- [32] E. Savio, F. Marinello, P. Bariani, S. Carmignato, (2007), "*Feature-Oriented Measurement Strategy in Atomic Force Microscopy*", CIRP Annals - Manufacturing Technology, 56, 557–560.
- [33] B. Bhikkaji, S. Moheimani, (2009), "*Fast scanning using piezoelectric tube nanopositioners: A negative imaginary approach*", Proc. of AIM 2009 International Conference on Advanced Intelligent Mechatronics, pp. 274–279, Singapore.
- [34] D. Kang, K. Kim, D. Kim, J. Shim, D.G. Gweon, J. Jeong, (2009), "*Optimal design of high precision XY-scanner with nanometer-level resolution and millimeter-level working range*", Mechatronics, 19, 562–570.
- [35] G. Schitter, P.J. Thurner, P.K. Hansma, (2008), "*Design and input-shaping control of a novel scanner for high-speed atomic force microscopy*", Mechatronics, 18, 282–288.
- [36] H.S. Kim, Y.M. Cho, (2009), "*Design and modeling of a novel 3-DOF precision micro-stage*", Mechatronics, 19, 598–608.
- [37] K.K. Leang, S. Devasia, (2006), "*Design of hysteresis-compensating iterative learning control for piezo-positioners: Application to atomic force microscopes*", Mechatronics, 16, 141–158.
- [38] S. Kuiper, G. Schitter, (2010), "*Active damping of a piezoelectric tube scanner using self-sensing piezo actuation*", Mechatronics, 20, 656–665.
- [39] A. Mesbah-Nejad, M. Moallem, (2010), "*A new actuation mechanism for an Interfacial Force Microscope: Design, implementation, and feedback control*", Mechatronics, 20, 640–647.
-

- [40] Noliac A/S, www.noliac.com, as it is on December 2012.
- [41] D. Thomas, D.D. Ebenezer, S.M. Srinivasan, (2010), "*Power dissipation and temperature distribution in piezoelectric ceramic slabs*", The Journal of the Acoustical Society of America, 128, 1700–1711.
- [42] Image Metrology A/S, www.imagemet.com, plugin for SPIP, as it is December 2012.
- [43] J. Sirohi, I. Chopra, (2000), "*Fundamental understanding of piezoelectric strain sensors*", Journal of Intelligent Material Systems and Structures, 11, 246–257.
- [44] Y. Kurisaki, H. Sawano, H. Yoshioka, H. Shinno, (2010), "*A newly developed XY planar nano-motion table system with large travel ranges*", Journal of Advanced Mechanical Design, Systems, and Manufacturing, 4, 976–984.
- [45] M. Lu, S. Gao, Q. Jin, J. Cui, H. Du, H. Gao, (2007), "*An atomic force microscope head designed for nanometrology*", Measurement Science and Technology, 18, 1735.
- [46] H.U. Danzebrink, L. Koenders, G. Wilkening, A. Yacoot, H. Kunzmann, (2006), "*Advances in scanning force microscopy for dimensional metrology*", CIRP Annals-Manufacturing Technology, 55, 841–878.
- [47] P. Rahe, R. Bechstein, A. Kühnle, (2010), "*Vertical and lateral drift corrections of scanning probe microscopy images*", Journal of Vacuum Science & Technology B: Microelectronics and Nanometer Structures, 28, C4E31.
- [48] F. Marinello, M. Balcon, S. Carmignato, E. Savio, (2011), "*Long term thermal drift study on SPM scanners*", Mechatronics, 21, 1272–1278.
- [49] A.A. Kuijpers, R.J. Wiegerink, G.J.M. Krijnen, T.S.J. Lammerink, M. Elwenspoek, (2004), "*Capacitive long-range position sensor for microactuators*", 17th IEEE International Conference on Micro Electro Mechanical Systems, pp. 544–547, Maastricht, Netherlands.
- [50] V. Studer, G. Hang, A. Pandolfi, M. Ortiz, W.F. Anderson, S.R. Quake, (2004), "*Scaling properties of a low-actuation pressure microfluidic valve*", Journal of Applied Physics, 95, 393–398.
- [51] M.A. Unger, H.-P. Chou, T. Thorsen, A. Scherer, S.R. Quake, (2000), "*Monolithic Microfabricated Valves and Pumps by Multilayer Soft Lithography*", Science, 288, 113–116.
- [52] R.K. Leach, (2011), "*Optical Measurement of Surface Topography*", Springer, 1st ed.
- [53] Sensofar-Tech S.L., www.sensofar.com, as it is on December 2012.
- [54] R.C. Gonzalez, R.E. Woods, (2008), "*Digital Image Processing*", Prentice Hall, 3rd ed.

-
- [55] NPL National Physical Laboratory, www.eurometros.org, LSGE lscylinder MatLab routine to find least-square fit of cylinder to data, as it is on December 2012.
- [56] (2010), ISO 25178-6 Geometrical product specifications (GPS) -- Surface texture: Areal -- Part 6: Classification of methods for measuring surface texture, Iso, Geneva.
- [57] (2010), ISO 25178-602 Geometrical product specifications (GPS) -- Surface texture: Areal -- Part 602: Nominal characteristics of non-contact (confocal chromatic probe) instruments, Iso, Geneva.
- [58] X. Jiang, P.J. Scott, D.J. Whitehouse, L. Blunt, (2007), "*Paradigm shifts in surface metrology. Part II. The current shift*", Proceedings of the Royal Society A: Mathematical, Physical and Engineering Sciences, 463, 2071–2099.
- [59] L. Blunt, S. Xiao, (2011), "*The use of surface segmentation methods to characterise laser zone surface structure on hard disc drives*", Wear, 271, 604–609.
- [60] N. Senin, L. Blunt, M. Tolley, (2012), "*The use of areal surface topography analysis for the inspection of micro-fabricated thin foil laser targets for ion acceleration*", Measurement Science and Technology, 23, art. n. 105004.
- [61] J.P. Kruth, M. Bartscher, S. Carmignato, R. Schmitt, L. De Chiffre, A. Weckenmann, (2011), "*Computed tomography for dimensional metrology*", CIRP Annals - Manufacturing Technology, 60, 821–842.
- [62] S. Carmignato, (2012), "*Accuracy of industrial computed tomography measurements: Experimental results from an international comparison*", CIRP Annals - Manufacturing Technology, 61, 491–494.
- [63] J. Wang, X. Jiang, L.A. Blunt, R.K. Leach, P.J. Scott, (2012), "*Intelligent sampling for the measurement of structured surfaces*", Measurement Science and Technology, 23, art. n. 85006.
- [64] J. Wang, X. Jiang, L.A. Blunt, R.K. Leach, P.J. Scott, (2011), "*Efficiency of adaptive sampling in surface texture measurement for structured surfaces*", Journal of Physics: Conference Series, 311, art. n. 12017.
- [65] H.N. Hansen, G. Tosello, S. Gasparin, L. De Chiffre, (2011), "*Dimensional metrology for process and part quality control in micro manufacturing*", International Journal of Precision Technology, 2, 118–135.